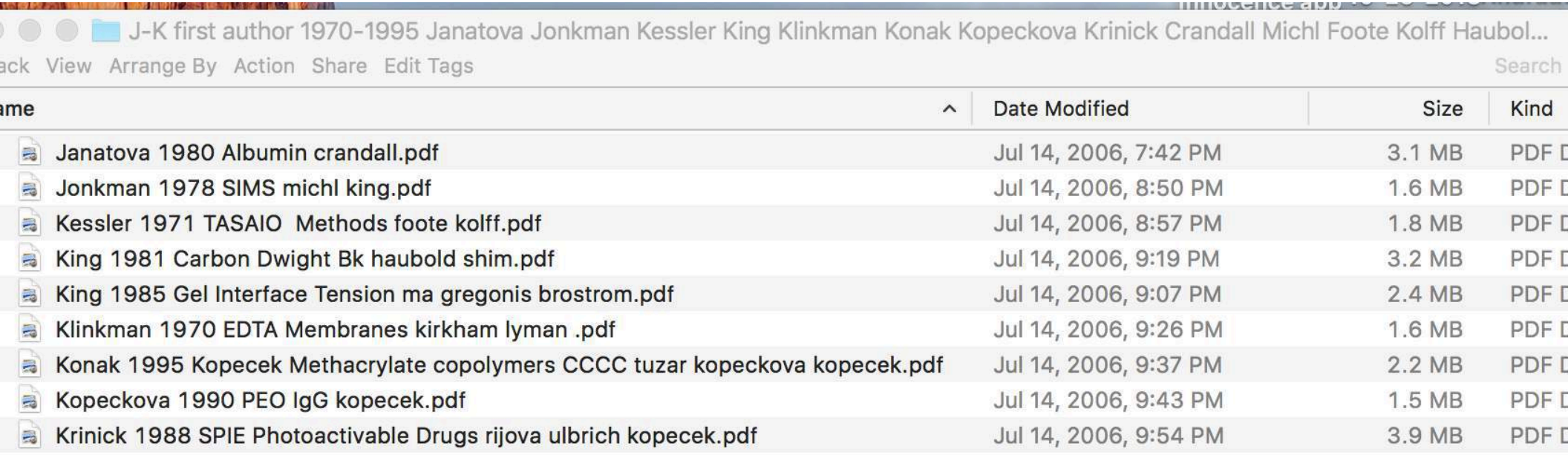
J-K first author 1970-1995 Janatova Jonkman Kessler King Klinkman Konak Kopeckova Krinick Crandall Michl Foote Kolff Haubol...
ack View Arrange By Action Share Edit Tags
Search
ame
Date Modified
Size
Kind
Janatova 1980 Albumin crandall.pdf
Jul 14, 2006, 7:42 PM
3.1 MB
PDF D
Jonkman 1978 SIMS michl king.pdf
Jul 14, 2006, 8:50 PM
1.6 MB
PDF D
Kessler 1971 TASAIO Methods foote kolff.pdf
Jul 14, 2006, 8:57 PM
1.8 MB
PDF D
King 1981 Carbon Dwight Bk haubold shim.pdf
Jul 14, 2006, 9:19 PM
3.2 MB
PDF D
King 1985 Gel Interface Tension ma gregonis brostrom.pdf
Jul 14, 2006, 9:07 PM
2.4 MB
PDF D
Klinkman 1970 EDTA Membranes kirkham lyman .pdf
Jul 14, 2006, 9:26 PM
1.6 MB
PDF D
Konak 1995 Kopecek Methacrylate copolymers CCCC tuzar kopeckova kopecek.pdf
Jul 14, 2006, 9:37 PM
2.2 MB
PDF D
Kopeckova 1990 PEO IgG kopecek.pdf
Jul 14, 2006, 9:43 PM
1.5 MB
PDF D
Krinick 1988 SPIE Photoactivable Drugs rijova ulbrich kopecek.pdf
Jul 14, 2006, 9:54 PM
3.9 MB
PDF D

PREPARATIVE BIOCHEMISTRY, 10(4), 405-430 (1980)

AN ANALYSIS OF THE HETEROGENEITY OF ALBUMIN

J. Janatova, R.E. Crandall, J.D. Andrade

Department of Bioengineering

University of Utah

Salt Lake City, Utah 84112 U.S.A.

ABSTRACT

A simple and rapid procedure for characterization of serum albumin samples and for the isolation of fractions from fresh serum or commercial sources has been developed, based on DEAE Sepharose CL-6B ion exchange chromatography. Characterization of the fractions included sulfhydryl analysis, gel electrophoresis, and immunoelectrophoresis. Both analytical and preparative procedures were used. It has been shown that the relative content of the fractions varies from individual to individual. It has also been shown that certain fractions found in commercial preparations are artifacts which should be removed before performing serious studies with serum albumin.

INTRODUCTION

Serum albumin (SA)[1] has often been regarded as a single homogeneous entity and has been used as a model protein. However, it has been shown that commercial SA preparations are heterogen-

20. J.M. Curling, J. Berglof, L.-O. Lindquist, and S. Eriksson, Vox Sang., 33, 97-107 (1977).

21. P.C. Kelleher, C.J. Smith, and R. Pannell, J. Chromatog., 173, 415-418 (1979).

22. Shaltiel, Methods Enzymology, 34, 126-140 (1974).

eous,[2-4] including differences in the content of various nonmercaptalbumins, dimers, higher oligomers, and in the content of mercaptalbumin itself. The heterogeneity of SA increases during isolation, concentration and storage. SA dimers and higher oligomers present in commercial SA preparations are mostly artifacts. Various nonmercaptalbumins make a major contribution to the heterogeneity of the SA monomer fraction isolated from commercial SA.[3] It has been suggested that the heterogeneity of SA, due to the presence of mercaptalbumin and at least two types of nonmercaptalbumins, is present in vivo;[5] this study confirms that supposition.

The fractionation of SA preparations, both human and bovine, on DEAE-Sephadex A-50 has been reported.[6,7] The present study uses DEAE-Sepharose CL-6B, which minimizes the problems inherent in other fractionation procedures.[6,7] The fractionation procedures described below serve to assess the heterogeneity of SA preparations and also enable one to obtain reasonable amounts of mercaptalbumin and nonmercaptalbumin fractions in a relatively short time, not only from commercial SA preparations but also from fresh serum either pooled or from individuals.

MATERIALS AND METHODS

Lyophilized bovine serum albumin, Fraction V, lots 280 and 283, was obtained from Miles Laboratories. Fresh BSA was isolated from bovine blood collected from the jugular vein of individual animals at the time of slaughter at the Jordan Meat Packing Co., Salt Lake City, Utah. 5,5'-dithiobis (2-nitrobenzoic acid) (lot 072677) was a product of the Aldrich Chemical Co. DEAE-Sepharose CL-6B (lots 3102 and 5717), Sephadex G150 (lot 0393) and Sephadex G25 coarse (lot 5115) were obtained from Pharmacia Fine Chemicals. Centriflo membrane cones, CF 25, and PM 10 membranes were products of Amicon. Activated charcoal type #517 was produced by the Witco Co.

Osmolarity measurements were performed on an osmometer (model 3L, Advanced Instruments, Inc.). Conductivity of buffers was measured using a General Radio impedance bridge, model 1650-B. Absorbance measurements were made on Hitachi Perkin Elmer 139, Gilford 240, and Beckman Acta II spectrophotometers using Beckman quartz 1.0 and 0.5 cm cells. A Corning Model 12 research pH meter and Corning glass electrode was used for pH monitoring of buffers. Color pHast pH indicator sticks from E. Merck Laboratories, Inc. were used to estimate the pH of protein solutions.

Protein concentration was determined routinely by measuring absorption at 279 nm. Absorption coefficient ($A^{1\%}_{1cm}$ at 279 nm) of 6.67 was used for bovine serum albumin.[7] The molecular weight of albumin was taken as 66,500.

Sulfhydryl group content was determined by spectrophotometric titration with 5,5'-dithiobis (2-nitrobenzoic acid) by the procedure of Ellman[8] as modified by Janatova, et al.[7] The method was performed in our laboratory using 0.06 M phosphate buffer, pH 7.00, in all reagent and protein solutions. Protein samples were tested for sulfhydryl content within 24 h of elution or immediately after dissolving the starting materials.

Polyacrylamide gel electrophoresis (PAGE) was performed at +5° on Gradipore® gels from Ortec (4-26% concentration gradient) in a vertical position using the Ortec 4200 Electrophoresis system. Gels were run in 0.065 M tris borate buffer, pH 9.0, according to the manufacturer's instructions. The gels were stained with commercial Ortec Amido Swartz Stain (Eastman) diluted 1:10 and destained in 10% aqueous acetic acid.

Protein solutions (volumes $\leq$ 20 ml) were concentrated by adding dry Sephadex G25 (1g per 4 ml solution) to the sample in a standard 30 ml Jelco disposable syringe with a porous polypropylene disk fitted in the bottom to support the gel bed. After ten minutes equilibration, centrifugation at 2,000 G was continued until the void volume of the Sephadex G25 was eluted (a Nalgene® centrifuge tube was used to collect the concentrated protein). The process was repeated until the desired concentration was reached, yielding 2-10% (W/W) solutions with a maximum loss of 20% after up to four repetitions. Small volumes were also concentrated over Centri-flo membrane cones (CF 25) by centrifugation at 1,000 G. Typical losses were about 5 to 10%.

Larger volumes (> 50 ml) were concentrated by ultrafiltration over a PM 10 membrane (Amicon) under N_2 (20 to 50 psi) using a 400 ml ultrafiltration cell.

Buffer changes of small volumes ($\leq$ 5 ml) were accomplished by centrifugation over Sephadex G25 coarse.[9] The Sephadex gel was supported in a 5 or 30 ml Jelco disposable syringe with a porous polypropylene disk. The protein solution was applied on

the top of the pre-equilibrated gel after its void volume had been removed by centrifugation (sample volume: gel volume, 1:5). After several minutes equilibration a repeated centrifugation yielded the protein in the new buffer. This procedure was generally repeated once to assure complete transfer.

For larger volumes (> 50 ml), a Sephadex G25 coarse matrix (4.8 x 25 cm, V_t = 450 ml) pre-equilibrated with the desired buffer provided a fast method for buffer exchange but also a dilution factor of 2.0 to 3.0. Ultradialysis yielded undiluted samples (a 400 ml ultrafiltration cell with PM 10 membrane and a 4000 ml Amicon Pressure reservoir were used).

DEAE-Sepharose CL-6B Chromatography

Isolation of SA fractions by chromatography on DEAE-Sepharose CL-6B at pH 7.0 was carried out at +4° to 6°. All buffers used were prepared by mixing monobasic and dibasic phosphate solutions of particular molarities in ratios to obtain pH 7.0 (measured at room temperature). Each new batch was checked for osmolarity and conductivity (Table I). All buffers contained 0.02% NaN_3 which

TABLE I

Osmolarity, Conductivity, and Molarity of Buffers

molarity	0.05	0.06	0.08	0.125
milliosmols	125	140	180	270
conductivity $X10^3$ (25°), Ω^{-1} cm^{-1}	6.21	7.14	9.09	13.42

had to be removed from some SA fractions over Sephadex G25 prior to further study.

SA samples in much larger volumes, e.g., 100 to 120 ml, could be applied provided the pH was 7.0 and corresponding ionic strength was $\leq$ 0.05 M phosphate.

Fractionation of BSA samples was carried out on a 2.5 x 58 cm gel bed of DEAE-Sepharose CL-6B in a 2.5 x 60 cm Glenco column using a combination of gradient and stepwise elutions. Ten ml per tube were collected, and flow rates up to 110 ml per hour were used. After the application of sample, the top of the column was rinsed, and elution with 0.06 M phosphate was started, followed by one of the elution protocols listed in Table II.

TABLE II

Elution Protocols

(a) For isolation of all SA chromatographic fractions (as shown in Figure 1 and Figure 4) 0.06 M (600 ml); 0.06 and 0.08 M (linear gradient; 1000 ml each). 0.08 and 0.125 M (linear gradient; 750 ml each); 0.125 M with 0.2 M NaCl (750 ml); re-equilibrate 0.05 M ($\geq$ 600 ml); total time at flow 100 ml per hour was about 52 hours.
(b) For isolation of MA, NMA-B1, and B2 fractions 0.06 M (600 ml); 0.06 and 0.08 M (linear gradient; 1000 ml each) 0.125 M with 0.2 M NaCl (750 ml); re-equilibrate 0.05 M ($\geq$ 600 ml); total time $\leq$ 44 hours.
(c) For isolation of MA (and eventually NMA-B1) 0.06 M ($\geq$ 1500 ml); 0.125 M with 0.2 M NaCl (750 ml); re-equilibrate 0.05 or 0.04 M ($\geq$ 600 ml); total time $\leq$ 30 hours.

The fractions were evaluated by measuring absorbance in a 0.5 cm UV cell at 279 nm. Determination of SH content was done directly on aliquots from tubes containing MA; material from tubes with smaller amounts of protein have been concentrated with dry Sephadex G25 (coarse) and centrifugation. PAGE has been run on aliquots, which had been, if necessary, concentrated prior to PAGE by using Centriflo membrane cones (CF25).

Isolation and Fractionation of BSA from Fresh Blood

Fresh blood was collected from adult Hereford males and females into 250 ml Nalgene® bottles by quickly exposing the jugular vein after shooting. Collection was complete within 3-6 minutes of bullet entry after which the blood was allowed to clot at room temperature and then chilled in an ice bath. Clotted blood was centrifuged by placing the Nalgene® collection bottles in pre-cooled centrifuge cups and centrifuging up to 1,750 G for 20 minutes in an IEC International centrifuge Model UV.

One hundred ml of the serum was equilibrated with sodium acetate buffer, pH 5.0, I = 0.25, 37 milliosmols by passing it through a Sephadex G25 coarse column (V_t of 450 ml). The column eluate was monitored by UV absorption at 279 nm using a 0.5 cm flow cell. The eluted serum in acetate buffer (300 ml) was clarified by centrifugation at 1,750 G for ten minutes.

Serum fractionation on DEAE-Sepharose CL-6B at pH 5.0 was done on DEAE-Sepharose CL-6B with a gel bed of 4.5 x 7.0 cm and V_t of 110 ml pre-equilibrated with acetate buffer (pH 5.0, I = 0.025, 37 milliosmoles). The column eluate was collected

into 20 ml fractions with a Buchler Fractomette 200 collector at 1000 ml/hr. The unretarded material was eluted by washing the column with the pH 5.00 acetate buffer ($\geq$ 500 ml). The bound albumin could be eluted with 500-700 ml pH 4.65 acetate buffer, I = 0.025 (until $A_{279nm} \leq 0.05$). Material still bound to the gel bed after the albumin had been eluted was removed by washing with 500 ml pH 4.0 acetate buffer, I = 0.010. Fractions from the peak of the pH 4.65 eluate containing BSA monomer were pooled (600 ml) and ultrafiltered to 50 ml over a PM 10 membrane. The albumin solution was then ultradialyzed with 0.05 M phosphate buffer, pH 7.00. The solution was centrifuged at 2,250 G for ten minutes to clarify it, removing a white precipitate. This supernatant was then ready for fractionation on DEAE-Sepharose CL-6B using eluation with phosphate buffers at pH 7.00 as described in Table II.

The elution sequence and conditions for DEAE-Sepharose CL-6B chromatography of BSA from fresh serum is summarized in Figure 6.

RESULTS AND DISCUSSION

Fractionation of Commercial BSA-Fraction V on DEAE-Sepharose CL-6B at pH 7.0

A typical elution profile of BSA Fraction V fractionated at pH 7.0 under the conditions of elution protocol (a) (Table II) is shown in Figure 1. The use of DEAE-Sepharose CL-6B has many advantages over DEAE-Sephadex.[7] The gel bed once prepared

can be used repeatedly and gives highly reproducible results. Whole fractionation, as shown in Figure 1, is achieved in 44 hours in comparison to 100 hours with DEAE-Sephadex.

The sulfhydryl contents (Figure 1) were obtained by analysis of individual tubes (or of two or three pooled adjacent tubes) very shortly after the elution of protein from the column. PAGE was performed on freshly eluted material from several tubes under every elution maximum after concentration in Centriflo cones (CF25). The results of PAGE have shown SA monomer with trace amounts of dimer to be present in MA (refer to Figure 1 for presentation of fraction names) NMA-B1, NMA-B2, and NMA-C fractions. Fraction D contained slightly more dimer(s) than monomer(s); fraction E also contained a small amount of trimer. Large amounts of trimer, a slightly smaller amount of dimer and tetramer and also the presence of monomer and pentamer were observed in the F fraction. When tested by immunoelectrophoresis using rabbit antiserum to bovine serum (Microbiological Associates, Lot No. 15015), the SA monomer fractions (MA. B1, B2) have been found to contain only albumin; traces of α-globulins were observed in Fractions C, D and E.

Fractionation under elution protocol (b) (Table II) achieves separation of MA, NMA-B1 and NMA-B2 fractions in about 24 hours. The isolation of MA (small part is overlapped with NMA-B1) can be accomplished utilizing elution protocol (c) (Table II) in 10 to 12 hours (conveniently overnight), being eluted only with 0.06 M phosphate (whole run, including re-equilibration, takes

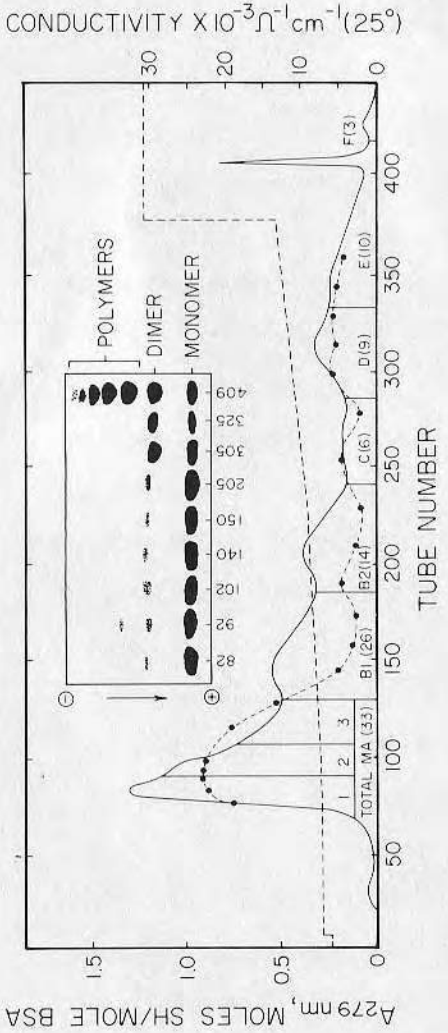

FIGURE 1

The elution profile of commercial BSA Fraction V after fractionation on DEAE-Sepharose CL-6B at pH 7.0 (gel bed 2.5 x 58 cm, Vt of 290 ml, ≥ 100 ml/h, 10 ml/tube, 4 g of BSA Fraction V Miles Lot No. 280, elution protocol [a] in Table II). ——, absorbance of eluate in 0.5 cm cell at 270 nm; ·····, -SH content of eluted albumin; ----, conductivity of buffer delivered to the column at the time given by the eluted fraction. The percentage of the relative amount of BSA fractions is given in parenthesis. Inset, polyacrylamide gel electrophoresis performed on representative tubes of each BSA fraction. MA, mercaptalbumin; fractions B1 through F contain mainly nonmercaptalbumin; fractions D and E contain more dimer(s) than monomer. The heterogeneity of the BSA fractions is discussed in the text.

not more than 30 hours). The SA sample does not have to be dialyzed prior to the fractionation; the only requirements are pH 7.0 and ionic strength equivalent to ≤ 0.05 M sodium phosphate.

Fractionation of Commercial BSA - Fraction V on DEAE-Sepharose Cl-6B at Low pH

Chromatography on DEAE-Sepharose CL-6B at low pH, as described by Berglöf for HSA,[10] has been chosen for the isolation of BSA from fresh serum. Preliminary experiments were carried out on commercial BSA-Fraction V. The results are shown in Figure 2. Some protein impurities have been removed at pH 5.0. SA has been eluted as expected at pH 4.65. As the peak at pH 4.0 also contained SA, it was hoped that fractionation of commercial BSA under conditions in Figure 2 would result in quick separation of protein impurities and also in separation of monomer fraction from dimer and higher oligomers. However, the latter was not the case.

Some of the SA fractions isolated at pH 7.0 (see Figure 1) were rechromatographed on DEAE-Sepharose CL-6B at low pH. While practically all protein from the MA fraction eluted at pH 4.65 and yielded a relatively symmetrical maximum, proteins from fractions B2, D and E were found heterogeneous by chromatography at low pH. The pH 4.65 elution profiles suggested heterogeneity. The rest of the material from fractions B2, D and E was eluted at pH 4.0. Dimer(s) and also trimer from fractions D and E were eluted at pH 4.65 together with the main monomeric fraction. The pH 4.0 fraction contained mainly monomer and only a small amount of dimer(s).

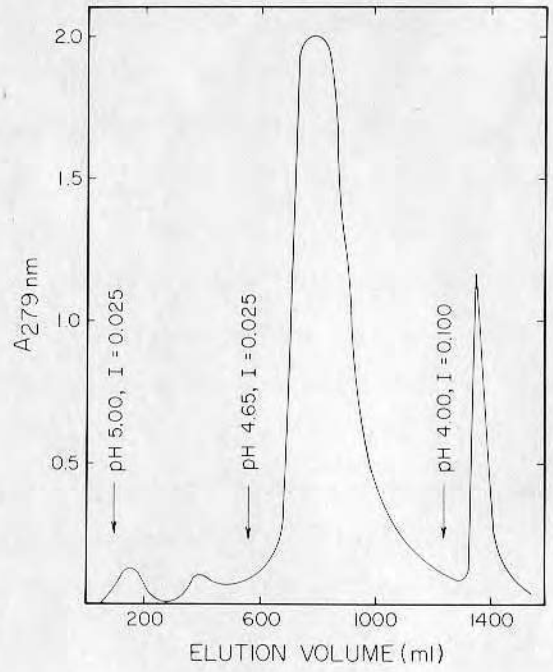

FIGURE 2

Fractionation of commercial BSA Fraction V on DEAE-Sepharose CL-6B at low pH (gel bed 4.5 x 7 cm, V_t of 110 ml, flow up to 1000 ml/h, 20 ml/tube, 3.5 g of BSA - same starting material as in Figure 1, stepwise elution with acetate buffer: pH 5.0 (500 ml), pH 4.65 (800 ml), pH 4.00 (500 ml); re-equilibration with pH 5.0 buffer (500 ml). The elution profile has been obtained by continuous monitoring in a 0.5 cm flow cell.

Isolation of SA from Fresh Serum

Our overall procedure for the isolation of whole BSA as well as for the isolation of various SA fractions from fresh serum is summarized in Figure 6. The heterogeneity of fresh BSA is also apparent from the diagram. In our study we have tried to apply such conditions which, we believe, would provide "native"

SA samples of composition which is very similar to the composition of SA *in vivo*. First of all, we have tried to minimize the possibility of sulfhydryl-disulfide exchange by lowering pH to 5.0 as soon as possible.

We have isolated BSA from fresh serum using ion exchange chromatography on DEAE-Sepharose CL-6B in a two-step purification scheme (see Figure 6). At the first step, the fresh serum was transferred over the column of Sephadex G25 into acetate buffer pH 5.0 and then applied on a short column of DEAE-Sepharose CL-6B pre-equilibrated with the same buffer. Under these conditions all BSA was bound to DEAE-Sepharose CL-6B. Most of the other plasma proteins were gradually eluted at pH 5.0 in two peaks. Practically all "native" BSA (more than 85%) was eluted from DEAE-Sepharose CL-6B with acetate buffer pH 4.65. The rest of the proteins (also containing up to 15% of total SA) were eluted at pH 4.0. A typical run is shown in Figure 3.

BSA monomer, pH 4.65 fraction, was concentrated by ultrafiltration over a PM10 membrane. The ultrafiltration step was followed either by ultradialysis with 0.05 M phosphate buffer, pH 7.0 or by dilution with phosphate buffer to obtain an ionic strength close to 0.04 or 0.05 M phosphate. There was only a trace of α-globulins present in this BSA fraction.

In the second step, BSA samples were fractionated on DEAE-Sepharose CL-6B at pH 7.0. With the aim to study the heterogeneity of "native" BSA, three BSA samples from individual animals were fractionated with elution protocol (a) (Table II); the

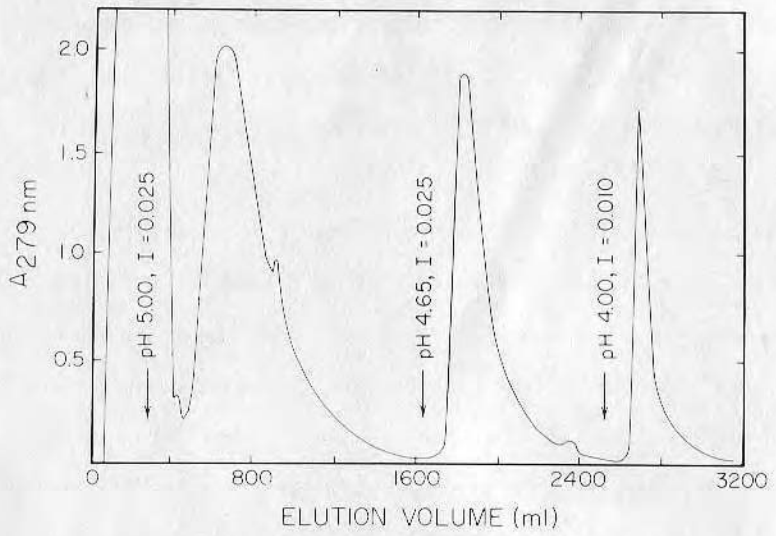

FIGURE 3

Fractionation of fresh bovine serum on DEAE-Sepharose CL-6B at low pH (gel bed 4.5 x 7 cm, V_t of 110 ml, flow up to 1000 ml/h, 20 ml/tubes; 100 ml of fresh bovine serum "desalted" over a 4.8 x 25 cm (V_t of 450 ml) coarse Sephadex G25 column, yielding 335 ml of starting material in acetate buffer pH 5.0; stepwise elution with acetate buffer pH 5.0, 4.65, and 4.00 as shown by arrows on the graph. The elution profile has been obtained by continuous monitoring in a 0.5 cm flow cell. pH 4.65 fraction contains ~ 85% of total "native" BSA monomer and its heterogeneity is shown in Figure 4 (② through ④); the rest of "native" monomer is eluted in pH 4.0 fraction; its subfractionation is shown in Figure 5.

results are shown in Figure 4. The evaluation of the eluted material has been carried out in the same way as in the case of commercial BSA shown in Figure 1. The column and the elution conditions were also the same for fresh BSA samples as for commercial BSA. PAGE of aliquots from individual tubes representing the MA, NMA-B1 and B2 fractions and a pool from fraction C showed only the presence of protein corresponding to SA monomer.

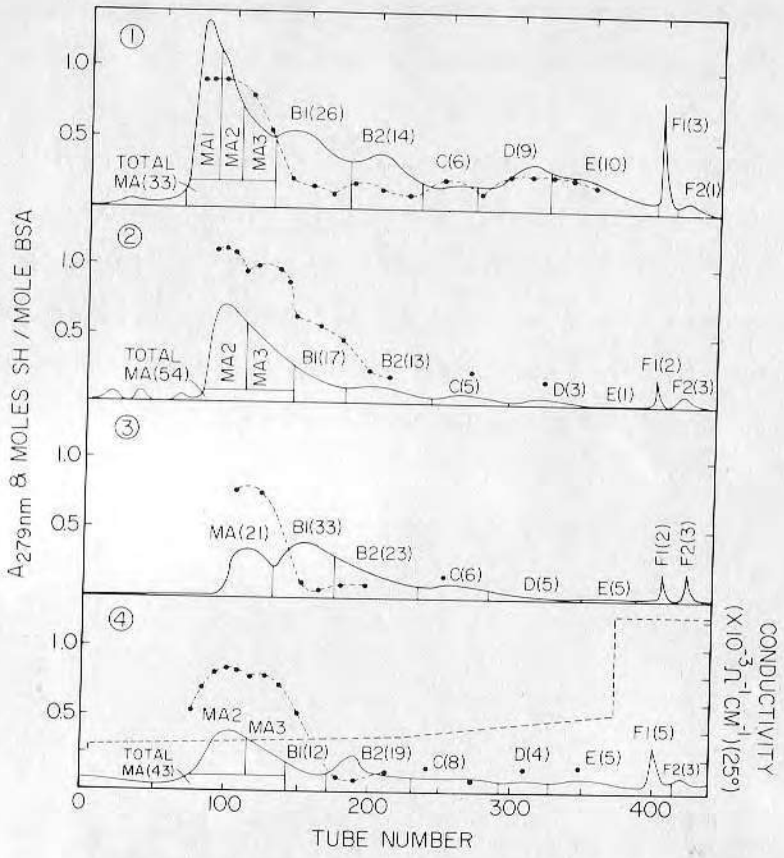

FIGURE 4

The elution profiles of various BSA samples after fractionation on DEAE-Sepharose CL-6B at pH 7.0. ① commercial BSA Fraction V as in Figure 1; ② , ③ , and ④ fresh BSA samples (pH 4.65 fractions, containing BSA monomer and traces of α-globulins) prepared from fresh serum of individual animals by method shown in Figure 3. Preparation of samples is described in Materials and Methods. Conditions of fractionations are the same as in Figure 1 except the amount of sample. The percentages of the relative amounts of BSA fractions are given in parenthesis. ———, absorbance of eluate in 0.5 cm cell at 279 nm; -------, -SH content of eluted albumin; the conductivity of buffer delivered to the column at the time given by the eluted fraction is shown in Ⓓ by ------.

This observation has been confirmed by immunoelectrophoresis (IE). Fraction D contained monomer and a trace of dimer. BSA has been absent in F1 and F2 fractions from fresh samples.

Protein material from the pH 4.0 fraction (see Figure 3) has also been ultrafiltered, ultradialyzed with 0.05 M phosphate and fractionated on DEAE-Sepharose CL-6B at pH 7.0. The results are presented in Figure 5. PAGE and IE have shown BSA monomer to be present almost exclusively in fractions D and E from fresh SA. No BSA has been eluted in the MA position.

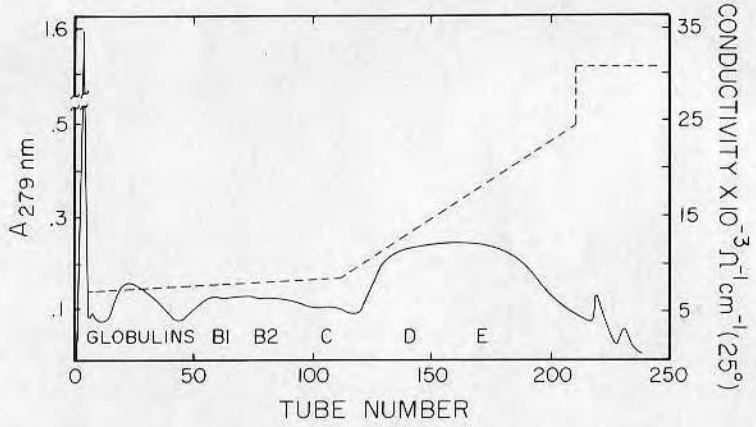

FIGURE 5

The elution profile of pH 4.0 fraction (see Figure 3) on DEAE-Sepharose CL-6B at pH 7.0. 125 ml pH 4.0 fraction ultradialyzed and ultrafiltered to 10 ml in 0.05 M phosphate buffer and fractionated on a 0.9 x 28 cm (V_t of 19 ml) gel bed at 25° by gradient elution at an approximate flow rate of 72 ml/h, 3 ml per tube collected. Immunoelectrophoresis demonstrates only α-globulins with absorption coefficients higher than BSA in the pre-MA and MA positions. Moderate amounts of α-globulins are found in the B1 and B2 positions. PAGE and IE have shown BSA monomer to be present almost exclusively in fractions D and E. ———, absorbance of eluate in 1.0 cm cell at 279 nm; ----, conductivity of buffer delivered to the column at the time given by the eluted fraction.

pH 4.65, suggested by Berglöf[10] for the specific elution of HSA, is just outside the "N-F" transformation range; all SA molecules at pH 4.65 should be in the N (native) form. Ultrafiltration has been carried out at this pH under N_2 at +4°C, as well as ultradialysis with 0.05 M phosphate, pH 7.0. After that the SA sample was applied immediately to the DEAE-Sepharose CL-6B at pH 7.0. This pH is at the lower limit of the pH 7 to 9 range where evidence of the neutral transition has been suggested[4] and yet still outside the range of maximum reactivity of the sulfhydryl group.[16]

As in the case of fractionation of commercial sample, use of elution protocol (b) (Table II) enables overnight separation of MA and NMA-B1 and NMA-B2 fractions from fresh serum/plasma. However, fraction B1 overlaps part of MA3 and vice versa.

If necessary, complete separation of -SH containing molecules from NMA-B1 fraction (and this applies also to NMA-B2 and NMA-C fractions) could be achieved by covalent chromatography using, e.g., Thiol-Sepharose by Pharmacia or the recently described Sepharose - (glutathione-2-pyridyl-disulfide) conjugate.[17] Homogeneity/heterogeneity of NMA fractions should not be affected by this procedure as NMA molecules do not bind to the column and therefore they do not have to be eluted with cysteine-containing buffer.

Unless various precautions are taken,[3] the content of free-SH group in MA fraction drops quickly from 0.95-0.98 to about 0.85-0.80 moles SH per mole SA.

Heterogeneity of BSA from Individuals as Compared to Commercial BSA

Our fractionation procedure, when used repeatedly on the same batch of commercial BSA, has been found (Figure 1) to give highly reproducible results, yielding practically identical elution patterns. The chromatographic heterogeneity of BSA is not due to the presence or absence of FFA,[18] our treatment of fresh SA samples for FFA removal[19] did not result in noticeable changes of the elution profile. Various SA fractions from fresh SA samples were denoted according to their elution positions with conductivities corresponding to the ones observed for SA fractions from commercial BSA (Figure 4).

Fractions F1 and F2 have been present in all fresh SA samples and also in commercial BSA. PAGE and IE did not reveal any SA molecules to be present in F1 and F2 from fresh SA samples. However, fraction F from commercial BSA contained various amounts of SA molecules from monomer to pentamer.

There has been a considerable decrease in the amount of fraction D in fresh BSA samples, pH 4.65 fraction, and also fraction E was present in extremely small amounts or non-existent in the material from pH 4.65 fraction (see Figure 4). However, up to 15% of total BSA monomer from fresh serum has been eluted at pH 4.0, yielding mainly fractions D and E after rechromatography on DEAE-Sepharose CL-6B pH 7.0 (Figure 5). The complex heterogeneity of D and E fractions is discussed in more detail in the next section.

Fraction C has been found to be present in all fresh SA samples as well as in commercial BSA; its content of about 5.5% of the total was about the same in all the samples investigated. The relatively high -SH group content (∿ 0.15 to 0.20 mole SH/mole SA) in fraction C in both commercial BSA and fresh samples was unexpected.

The relative amounts of B2 fraction from fresh SA samples were equal or even higher than the amount of B2 from commercial BSA. The relatively small -SH content was similar in all B2 fractions - from both commercial and fresh SA samples. There is a high probability that most of the SA molecules in fraction B2, as isolated from commercial BSA, are already present *in vivo*, and only a small part of the B2 fraction is due to artifacts.

While the amounts of B2 and C fractions seem to be fairly similar in various fresh SA samples, large variability has been observed in the amounts of B1 and MA fractions (Figure 4).

Heterogeneity of BSA Fractions

In the previous sections we have been referring to various SA fractions rather than to SA components because none of the SA fractions is completely homogeneous.

MA fraction: the elution profile of SA with high content of free SH suggests heterogeneity within the MA fraction. We notice the presence of at least three "subfractions" (Figures 1 and 4). Thus, the MA elution curve was divided into three sections: MA1, MA2, and MA3. It was found that MA "subfractions" differed in stability of the -SH group, the MA2 being the most

labile. The MA1 subfraction is the most homogeneous as verified by its rechromatography. The MA1 fraction was missing in all three fresh BSA samples. In the sample with the large amount of B1, only the MA3 "subfraction" was observed. The other two fresh samples seemed to contain both MA2 and MA3 "subfractions," MA2 being present in the larger amount.

The question whether the MA1 "subfraction" exists in vivo only in some individuals or whether MA1 is an artifact of isolation and storage procedures cannot be answered yet. There is the possibility that MA1 could represent the "aged" MA, which has been observed and isolated as component A by Foster, et al.[4] It should also be noted that inside every MA "subfraction" there are at least 15-25 percent of molecules in which their free SH group is lost easily (and/or is not detectable by the DTNB method). However, in this case the "loss" of free SH is not accompanied by dimer formation nor by an immediate change in chromatographic behavior.

Fraction B1: it is difficult or practically impossible under the described conditions to obtain fraction B1 free of MA molecules. There is always some overlap between the MA3 and B1 fractions. There is a possibility of removing the -SH containing molecules from the NMA-B1 monomer by covalent chromatography.[17] Fraction B1 is believed to be NMA, a mixed disulfide between cysteine and "normal" MA.[5] Which MA "subfractions" or subpopulations should be considered as "normal" is difficult to envisage. There is some weak evidence that perhaps the MA2 "subfraction" could form NMA-B1 under given circumstances in vivo.

Fraction B2 and fraction C: according to Anderson's hypothesis[5] there should be a difference between NMA-B2 and NMA-B1 fractions in terms of disulfide pairing. The same would apply to the C fraction. The suggested presence of Cys in NMA-B2 and of GSH in NMA-C has not yet been tested. The presence of -SH containing molecules (from 8 to 18%) has been observed even in these fractions from both commercial and fresh BSA samples.

Both fraction D and fraction E, when isolated from commercial BSA-Fraction V, seem to be quite heterogeneous by PAGE, -SH determination (presence of about 0.25 moles SH per mole of SA) and by rechromatography on DEAE-Sepharose CL-6B at low pH. Rather surprisingly, dimers and higher oligomers are eluted at pH 4.65, while the monomeric BSA from fractions D and E from commercial samples is further resolved into pH 4.65 and pH 4.0 fractions.

Unlike the case of commercial BSA Fraction V, the fractionation of fresh BSA (pH 4.65 fraction, $\geq$ 85% of total BSA monomer) on DEAE-Sepharose CL-6B at pH 7.0 yields only about 3.5 to 5% of pH 4.65 material in fraction D, and none or a very small amount of BSA monomer in fraction E. However, up to 15% of total fresh BSA monomer is eluted at pH 4.0 (see Figure 6). Rechromatography of this material on DEAE-Sepharose CL-6B at pH 7.0 yields BSA monomer almost exclusively in elution positions of fractions D and E (Figure 5).

Thus, dimers and higher oligomers, as well as BSA monomer(s), present in D and E fractions of commercial BSA samples which elute with pH 4.65 buffer from DEAE-Sepharose CL-6B are artifi-

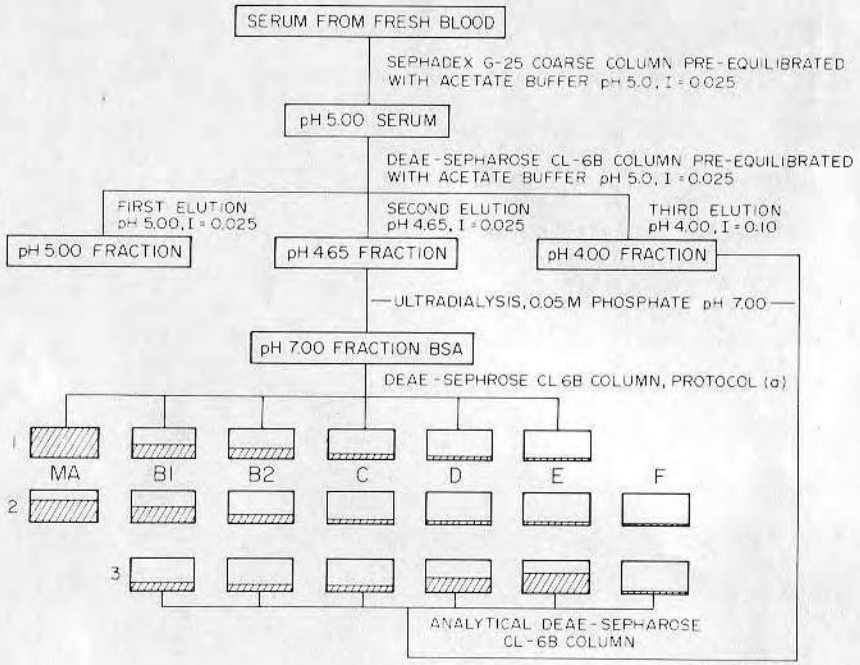

FIGURE 6

Elution sequence and conditions for the isolation of whole BSA and its various fractions from fresh serum. The relative quantities of each fraction are indicated by the amount of cross-hatching. The total area cross-hatched for each fractionation represents 100 percent of the protein for that fractionation. 1) BSA fractions from fresh serum pH 4.65 fraction (see Figure 4 ②); 2) BSA fractions from commercial Fraction V (see Figure 4, ①); 3) BSA fractions from fresh serum pH 4.00 fraction (see Figure 5). MA denotes a SA monomer having one free SH group per molecule of SA; B1 through E represent nonmercaptalbumins, a SA monomer devoid of free SH group. The extent of the heterogeneity of SA even in fresh SA samples is obvious from the diagram. The heterogeneity of various chromatographic fractions is discussed in the text.

cial BSA components. Moreover, the experiments with fresh serum suggest that the part of SA monomer from D and E fractions which elutes from DEAE-Sepharose CL-6B at pH 4.0 corresponds to BSA molecules present in vivo.

CONCLUSIONS

Significant differences exist between commercial BSA-Fraction V and BSA isolated from animals by chromatographic methods. There are more distinctive differences among the individual fresh BSA samples (Figure 4).

Large amounts of fractions D and E, which are present in commercial SA samples, are "artifacts" due to various effects on "native" SA monomer. The presence of these artificial fractions contributes significantly to the heterogeneity of some SA samples. Therefore, we propose that SA fractions D, E, and F should be separated from the rest of SA material before any serious biochemical, biophysical, or biological studies are carried out.

NMA fraction C ($\sim$ 5.5% of total BSA) and NMA-fraction B2 ($\geq$ 13% of total BSA) seem to be fairly constant components in both fresh and commercial BSA samples.

The amounts and ratio of NMA-B1 and MA fractions vary in individual SA samples, however, the sum of these two fractions seem to be fairly constant, or at least similar in various SA samples.

How BSA monomer or BMA from fresh serum compare to commercial samples in terms of the amount of bound metals, bilirubin, FFA, traces of various proteases and other ligands being carried by SA in blood stream was not studied.

The reported isolation and fractionation scheme (Figure 6) can be scaled either up or down and makes it possible and con-

venient to work with albumin preparations from individuals. In the case of human samples, our first step of isolation could be replaced by Blue Sepharose chromatography.[14,21] Hydrophobic chromatography must also be considered.[22]

The procedure of Curling, et al.,[20] using SP-Sephadex C-50 at pH 5.2 in the final step of purification of whole HSA monomer, would probably be more convenient for the commercial preparation of HSA for clinical purposes, while fractionation on DEAE-Sepharose CL-6B at pH 7.0, as described in this paper, would enable isolation of "individual" SA fractions for various studies, not only from fresh pooled serum/plasma, but also from serum/plasma of individuals.

ACKNOWLEDGEMENTS

We thank Mr. Dennis Coleman for his helpful discussions and technical assistance, Ms. Kathryn Irons for performing the polyacrylamide gel electrophoresis, Mr. Ronald Ruff for buffer preparation and osmolarity measurements, and Mr. Gary Bates for performing the immunoelectrophoresis. This work was supported by NIH Grant HL 18519.

REFERENCES AND NOTES

1. The abbreviation SA, as used in this paper, denotes both serum and plasma albumin. Other abbreviations commonly used are: BSA bovine serum albumin, HSA, human serum albumin; MA, mercaptalbumin (a SA monomer having one free SH group per molecule of SA); NMA, non-mercaptalbumin or non-mercaptalbumins (a SA monomer devoid of free SH group); SH, free sulfydryl; FFA, free nonesterified long-chain fatty acids; DTNB, 5,5'-dithiobis (2-nitrobenzoic acid); PAGE, polyacrylamide gel electrophoresis; IE, immunoelectrophoresis.

2. W.L. Hughes, Jr., J. Amer. Chem. Soc., 69, 1836-1837 (1947).

3. J. Janatova, J. Med., 5, 149-216 (1974).

4. J.F. Foster, in "Albumin Structure, Function, and Uses," V.M. Rosenoer, M. Oratz, M.A. Rothschild, eds., Pergamon Press, 1977, pp. 53-84.

5. L.-O. Andersson, Biochem. Biophys. Acta., 117, 115-133 (1966).

6. J. Janatova, O. Mikes, and J. Sponar, Collect. Czech. Chem. Commun., 33, 788-800 (1968).

7. J. Janatova, J.K. Fuller, and M.J. Hunter, J. Biol. Chem., 243, 3612-3622 (1968).

8. G. Ellman, Arch. Biochem. Biophys., 82, 70-78 (1959).

9. N. Cefka, P. Pihl, L. Holmqvist, F. Grossmuller, J. Chromatogr., 57, 145-147 (1971).

10. J. Berglof, in "DEAE-Sepharose CL-6B and CM-Sepharose CL-6B for Ion Exchange Chromatography," Pharmacia Fine Chemicals, 1976, pg. 8-10.

11. F. Rothstein, V.M. Rosenoer, and W.L. Hughes, "Albumin Structure, Function, and Uses," V.M. Rosenoer, M. Oratz, and M.A. Rothschild, eds., Pergamon Press, 1977, pg. 7-25.

12. A. Wichman and L.-O. Andersson, Biochem. Biophys. Acta, 372, 218-224 (1974).

13. S. Aslam, D.P. Jones, and T.R. Brown, Anal. Biochem., 75, 329-335 (1976).

14. J. Travis, J. Bowen, D. Tewksbury, D. Johnson, and R. Pannell, Biochem. J., 157, 301-306 (1976).

15. S. Angal and P.D. Dean, Biochem. J., 167, 301-303 (1977).

16. A. Svenson and J. Carlsson, Biochem. Biophys. Acta., 400, 433-438 (1975).

17. J. Carlsson and A. Svenson, FEBS Letters, 42, 183 (1974).

18. J.K. Noel Fuller and M.J. Hunter, J. Biol. Chem., 247, 7391-7406 (1972).

19. R.F. Chen, J. Biol. Chem., 242, 173-181 (1967).

Reprinted from **ANALYTICAL CHEMISTRY,** Vol. 50, Page 2078, December 1978

Low-Temperature Positive Secondary Ion Mass Spectrometry of Neat and Argon-Diluted Organic Solids

Harry T. Jonkman and Josef Michl*

Department of Chemistry, University of Utah, Salt Lake City, Utah 84112

Robert N. King and Joseph D. Andrade

Department of Materials Science and Engineering, University of Utah, Salt Lake City, Utah 84112

Secondary ion mass spectrometry of neat solid propane, *n*-pentane, benzene, toluene, and of propane imbedded in an argon matrix were observed at temperatures varying from 10 to 110 K and show fragmentation patterns similar to those known from ordinary electron impact mass spectrometry. The effects of the nature and energy of the primary probe ion and of the sample temperature were investigated. The analytical potential of the method, e.g., for reactive species trapped in inert matrices, is noted.

In the course of work with heat-sensitive involatile organic and biological materials and with highly reactive species isolated in inert matrices, it frequently appears desirable to complement other spectroscopic methods by mass spectral data. Since in these instances the species of interest cannot be easily transferred to the gas phase without change, standard mass spectrometry is of little direct use and methods such as field desorption (*1*) have been investigated. In recent years, a limited amount of exploratory work on organic solids using plasma desorption mass spectrometry (PDMS) (*2*, *3*) and secondary ion mass spectrometry (SIMS) (*4–18*) has been performed in several laboratories and appears to show considerable promise.

In SIMS, a beam of primary ions or neutral atoms bombards a solid sample and etches its surface. The sputtered material is ejected as positive ions, negative ions, and neutrals. The secondary ions are collected and analyzed in a mass spectrometer. The method is well established as a tool for investigation of the surface of metals and semiconductors (*4–7*) and has also been used to study the absorption of hydrocarbons on such surfaces (*19*). We now report an investigation of the suitability of the SIMS technique for the characterization of organic samples held at cryogenic temperatures and the first SIMS measurement on an argon-matrix isolated species (*20*).

EXPERIMENTAL

The spectra were measured on a 3M Model 525 Ion Scattering and Secondary Ion Mass Spectrometer equipped with a 4096 channel Nicolet 1170 signal averager. The ion gun used in this instrument requires a stationary backfill of the sample chamber with the ion beam gas of about 6×10^{-5} Torr, and this limited our experiments to the use of helium and neon which do not condense on the cold sample plate at the temperatures we used (≥10 K for He, ≥35 K for Ne). The sample plate was made of oxygen-free high conductivity copper and was attached to the cold head of an Air Products Displex closed-cycle cryostat, whose temperature could be adjusted between ambient and 10 K. It was positioned in such a way that secondary ion mass spectrometry (SIMS) and ion scattering spectroscopy (ISS) could be performed simultaneously. In the 3M instrument, the secondary ions are not accelerated and those which reach the UTI Model 100C quadrupole mass analyzer attached at a 90° angle with respect to the ion gun give rise to the observed SIMS spectrum (a pre-filter removes neutrals and ions with kinetic energy higher than 20 eV). The rare gas ions scattered at 138° are analyzed by a cylindrical mirror analyzer and yield the ISS spectrum.

The vacuum system consisted of two sorption pumps and a Varian Vacion diode ion pump (500L/s). The liquid nitrogen cryopanel provided in the instrument was not used in the low-temperature experiments since the large cold surface of the closed-cycle cryostat already provided efficient cryopumping. After bakeout and before cryopumping and sample deposition, a background pressure on the order of 1×10^{-9} Torr was established. The remaining gas mixture contained primarily nitrogen and water, as established by remnant gas mass spectrometry.

The ion probe gases were (99.95% pure) ^{3}He and (99.98% pure) ^{20}Ne (Monsanto Research Corporation). The ion beam was defocused to about 2-mm diameter for the SIMS experiments (the largest of the three available beam sizes). The maximum available beam raster was used. The ion beam current was approximately 10 $\mu A/cm^2$ but could not be measured exactly in these experiments, since the sample plate was grounded.

The organic samples used were of spectrograde quality except for propane, which was 99% pure (Union Carbide). Their vapors, pure or diluted with high purity (99.9995%) argon (Matheson Co.), were prepared in a separately pumped vacuum manifold, oil diffusion pumped to 1×10^{-6} Torr. About 1×10^{-4} mol were bled in over about 30 min through a calibrated leak valve which had an outlet about 0.5 cm above the cold sample plate, keeping the total pressure in the main chamber below 2×10^{-7} Torr whenever the vapor pressure of the sample at the temperature of the cold plate permitted. At low deposition temperatures (up to 35 K), where most of our work was performed, the sample formed an elongated spot near the center of the copper plate, but at the highest temperatures used, it covered most of the plate. At the lower temperatures, the pressure in the sample chamber was below 1×10^{-8} Torr after sample deposition and before admission of the ion beam gas, except in the experiments with argon. In the experiments performed at the highest temperatures used, the total pressure after sample deposition was of the order of 1×10^{-6} Torr. There is no doubt that in the experiments at 35 K and below, the measured signal originated in the surface of the organic solid and not in the small amount present in the gas phase, since the organic fragment ions gradually disappeared and were replaced by the ions of copper and its contaminants (Na, K) when the ion beam was deflected off the sample spot to a clean area of the plate. Even at the higher temperatures, there is no evidence that any of the observed SIMS signal originated in the gas phase (see Discussion).

To obtain reliable SIMS data, the use of a low-energy electron floodgun was essential to overcome surface charging by continuous ion bombardment. The adjustment of the flooding current was done by trial and error until a stable maximum SIMS intensity was obtained. At lower floodgun currents and resulting positive charging of the sample surface, intensities of all peaks were lower, but their relative proportions remained nearly unchanged. However, higher than optimum floodgun currents were carefully avoided after it was found that they caused distortions in relative peak intensities, generally favoring fragments with lower m/e ratios (cf. Figure 1).

RESULTS

In the present study, ISS was used only to confirm the presence of carbon and argon on the appropriate section of the cold plate and to map out their spatial distribution by the rastering technique. ISS also gave useful information during depth profiling of the argon matrix isolated samples. However, our primary focus was on SIMS.

It was established rapidly that the spectra are well reproducible and that the fragmentation pattern is basically similar as in ordinary electron impact mass spectrometry. Noticeable differences occur in relative fragment ion intensities and are described further below for the four compounds investigated.

Effect of Experimental Variables on SIMS. The following observations were made for the four hydrocarbons.

(i) The spectra were independent of the sample temperature, and also the overall intensity did not vary significantly (the actual temperature range explored was a function of sample volatility, e.g., 10 to 110 K for *n*-pentane in 10° increments). At higher temperatures less electron floodgun current was required.

(ii) The spectra of the hydrocarbons were independent of the nature of the primary ions ($^{3}He^{+}$ or $^{20}Ne^{+}$). Only the relative abundances of the CH_2^{+} and CH_3^{+} fragments increased by a few percent when $^{3}He^{+}$ was used as probe ion in the spectra of propane and *n*-pentane.

(iii) The spectra were independent of the kinetic energy of the primary ions within the range 100 eV to 3 keV.

(iv) The spectra obtained at low probe ion energies (below 1 keV) were independent of time for several hours. At higher ion energies, especially above 2 keV and after prolonged ion bombardment at lower energies, gradual appearance of fragment ions of higher m/e ratios than the molecular ion was observed in the case of the two alkanes. In particular, we observed C_6 and C_7 fragments from *n*-pentane, and C_4 and C_5 fragments from propane. The abundance of these higher mass peaks remained low even after several hours (cf. Figure 2) and the intensity distribution of the other fragments was not affected. No signs of sample decay were observed for the two aromatics within our detection limits.

(v) The spectra of propane were of lower intensity but otherwise identical when it was diluted with argon up to the ratio 1:150 (Figure 3). In the diluted samples of propane, C_4 and C_5 fragments were not observed even after prolonged ion bombardment.

SIMS Fragmentation Patterns. The SIMS data for the solid samples were compared with those obtained for the same compounds in the gas phase using electron impact (50 eV) and the same UTI quadrupole mass analyzer. These latter spectra are similar to the electron impact spectra reported in the literature (*21*) but are not identical because of possible distortions due to the pre-filter and since the quadrupole mass analyzer favors the relative intensities of the lower mass fragments (the relative sensitivity curve for our analyzer is shown in Ref. 13). The comparison between the fragmentation

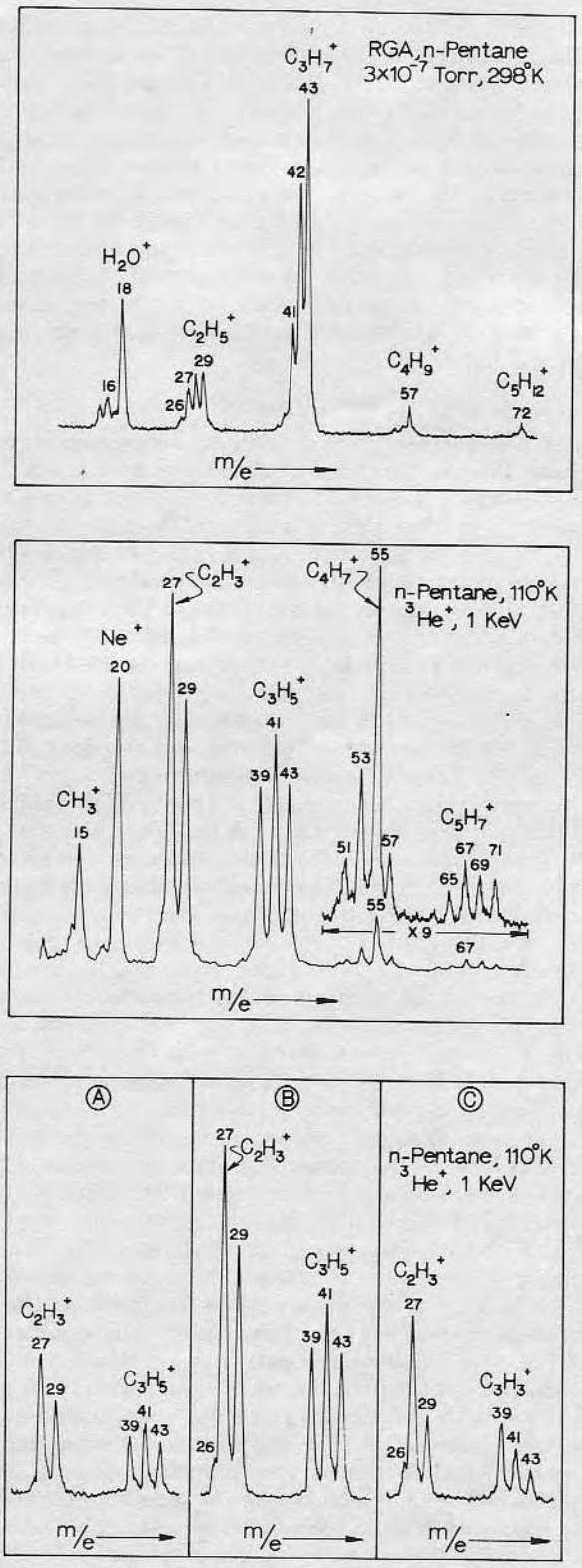

Figure 1. Neat *n*-pentane. Top: Electron impact mass spectrum obtained in the remnant gas analysis mode of the quadrupole mass spectrometer. Center: Positive SIMS (8 scans, 2-min scan time). The ^{20}Ne peak is due to traces of neon implanted in the matrix during a previous experiment with a $^{20}Ne^+$ beam. Bottom: Positive SIMS with electron floodgun current too low (A), optimum (B), and too high (C)

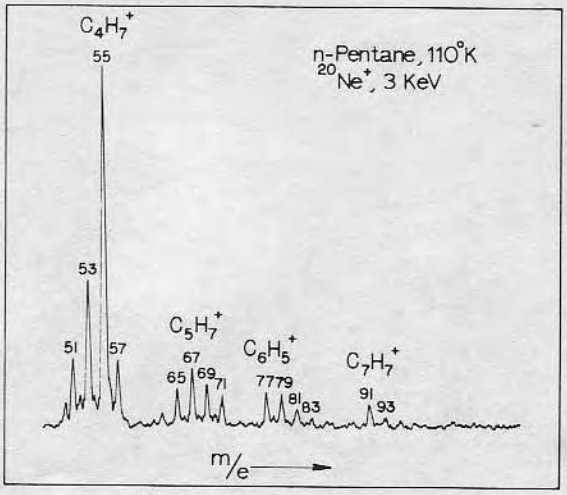

Figure 2. Positive SIMS of neat *n*-pentane after several hours of bombardment with 3-keV $^{20}Ne^+$ ions (higher mass region only, 32 2-min scans averaged)

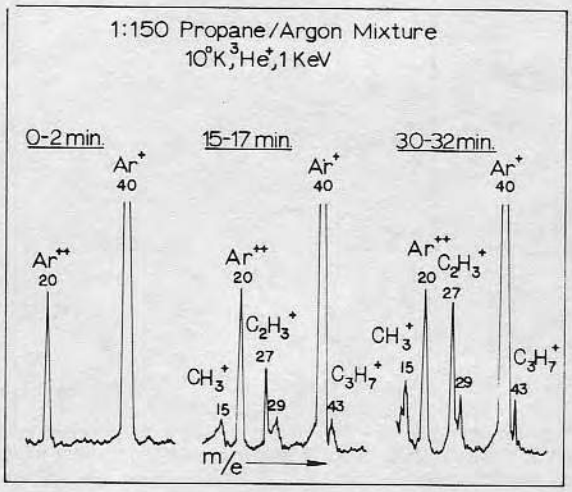

Figure 3. Positive SIMS depth-profiling of a propane–argon matrix. Single 2-min scans. The A_2^+ peak has about 10% of the intensity of A^{2+}, all impurity peaks are even weaker

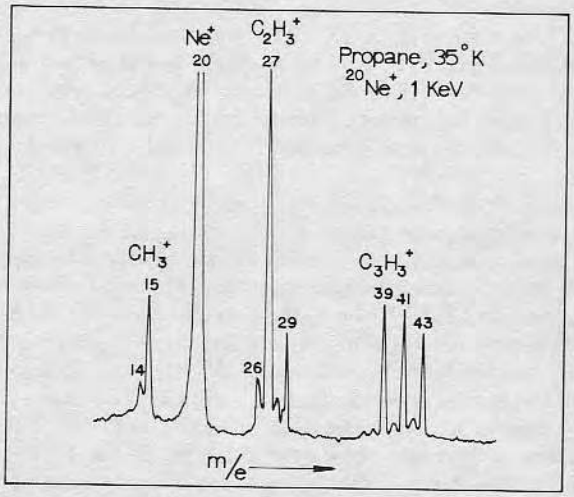

Figure 4. Positive SIMS of neat propane. A single 10-min scan. No peaks above noise level were observed at *m/e* values higher than those shown

patterns obtained by SIMS and electron impact mass spectrometry revealed interesting differences in relative abundances of fragments.

(i) *n-Pentane* (Figure 1). Within each C_n group, the $C_nH_{2n+1}^+$ and $C_nH_{2n-1}^+$ fragments are in general the most abundant. The former is the more abundant in electron impact mass spectrometry, but as could be expected (22), the latter is the more abundant in SIMS. Among the various C_n groups, the C_3 is most abundant in electron impact spectra (especially m/e = 43, $C_3H_7^+$), while the C_2 group is more intense in SIMS (especially m/e = 27, $C_2H_3^+$). The parent molecular ion peak, although weak, is easily observable in the

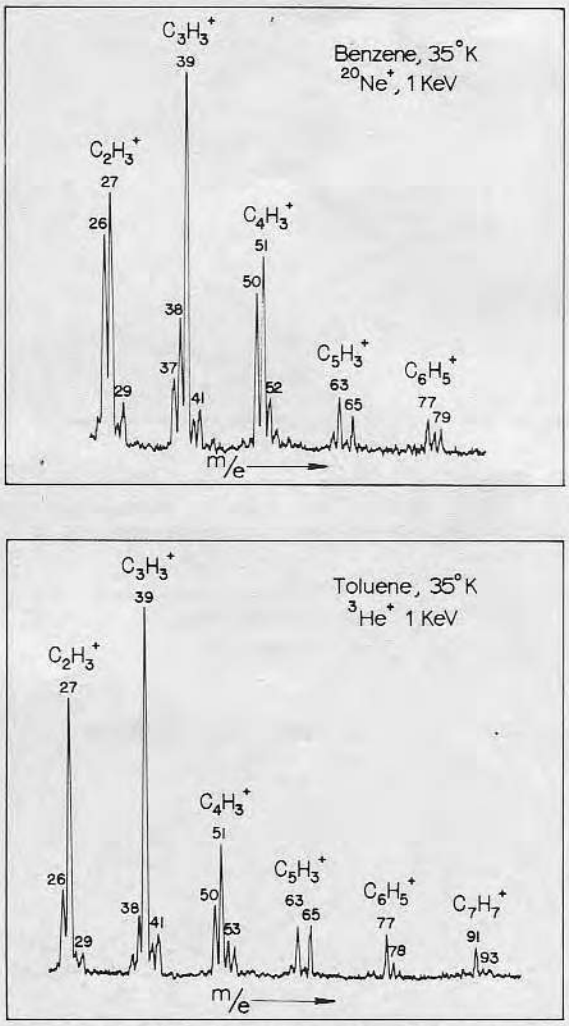

Figure 5. Positive SIMS. Top: neat benzene, bottom: neat toluene. Single 10-min scans

electron impact mass spectra, but is absent in SIMS. In SIMS, the highest m/e peak observed corresponds to the $(M - 1)^+$ ion at $m/e = 71$.

(ii) *Propane* (Figure 4). The great similarity to the *n*-pentane spectrum is apparent. Again the strongest peak, $C_2H_3^+$, is of the $C_nH_{2n-1}^+$ type. The C_2 fragments are the most abundant and no parent molecular ion fragment is observable. The highest m/e peak corresponds to the $(M - 1)^+$ ion at $m/e = 43$.

(iii) *Benzene and Toluene* (Figure 5). Unlike the spectra of the alkanes, the spectra of both aromatics show the molecular ion peak, albeit in much weaker relative abundance than in the electron impact spectra. The most abundant fragment in SIMS is the $C_3H_3^+$ ion at $m/e = 39$ for both benzene and toluene, while in electron impact spectra it is the molecular ion for benzene and the $(M - 1)^+$ ion for toluene. In both types of spectra, the CH_2^+ and CH_3^+ fragments are very weak or absent. The SIMS cracking patterns of both benzene and toluene show weak peaks of the $(M + 1)^+$ ions in intensities far in excess of those expected for natural ^{13}C abundance.

(iv) *SIMS of Argon Matrix Isolated Propane* (Figure 3). Except for the presence of a strong A^+ ($m/e = 40$) peak, weaker A^{2+} ($m/e = 20$) and A_2^+ ($m/e = 80$) peaks, and for an overall decrease in intensity, SIMS of propane is the same for a neat solid and for molecules imbedded in a solid argon matrix. The highest dilution tried was 1:150 and the signal-to-noise ratio was still quite good even for a single scan, indicating strongly that even more dilute mixtures will be amenable to SIMS investigations. The relative abundance of the argon ions and the organic ions shows an interesting time dependence at the beginning of ISS and SIMS experiments on a fresh argon matrix. At first, the relative abundance of the organic ions is very low compared with A^+. As spectral scans are repeated, the abundance of the organic ions relative to A^+ ions gradually grows until it finally attains a plateau and shows no further change (Figure 3). This effect appears both in SIMS and in ISS. We assign these changes to a gradual removal of the topmost layers of the matrix by sputtering. It is reasonable that the layers which condensed last during the deposition should be enriched in the more volatile component.

DISCUSSION

Our main goal is to develop SIMS as a supplementary tool for identification of molecules isolated in inert matrices. To accomplish this, we need to show that such matrices are not destroyed by overheating, that the signal-to-noise ratios are adequate, and that the fragmentation patterns are insensitive to experimental conditions and are interpretable. Our secondary aim is to assess the usefulness of low-temperature SIMS for analysis of neat organic samples. Room-temperature measurements of this latter type have been reported both for selected low-molecular weight organic solids (*13–18*) and for several polymers (*8–12*), but little attention has been paid to the possible overheating and ion–molecule reactions in the neat solids. These dangers are minimized when very low primary ion current densities are used (static SIMS) (*15, 16*) but this then does not permit depth profiling which may be of considerable interest in analytical applications. The present results show that neither inadequate sensitivity nor sample destruction by overheating and secondary reactions are a problem with cooled samples under conditions of dynamic SIMS. Also, the cooled probe is advantageous for fundamental investigations of the fragmentation reactions since very simple hydrocarbon substrates can be used.

Our remaining concern has to do with the extent of ion fragmentation. If the fragmentation were excessive or strongly dependent on the experimental conditions, the value of the method as an analytical tool would be sharply decreased. Previous room-temperature SIMS data on organic solids coated on metals reported either relatively little fragmentation initially, but quite rapid decay of the sample with time (*15, 16*), or an extent of fragmentation which was higher than in ordinary electron impact mass spectra, but not prohibitive (*13, 14, 17, 18*). Our experience with the four molecules chosen for this study parallels the latter results: fragmentation is stronger than in electron impact mass spectra but is not prohibitive, and the fragment ion m/e values which emerge are those which have already proved to be useful in organic structure determination. The lack of sensitivity of the spectra to experimental conditions is encouraging. Since the instrument had no ion collection optics, its sensitivity was rather low, and, moreover, we cannot be sure that the relative abundances of the secondary ion detected are in any simple relation to the relative abundances of the secondary ions formed, and little can be said about mechanisms at this stage. Charge-transfer clearly is a strong candidate, particularly in view of the similarity of our relative fragment ion intensities to those reported in charge–transfer mass spectra (*23*), but it is interesting to note that we observe essentially no differences in spectra obtained with $^3He^+$ and with $^{20}Ne^+$, and that our spectrum of *n*-pentane is almost identical with the reported spectrum of polyethylene obtained using a neutral atom primary beam (*12*). Whether the ionization occurs on the surface or near the surface after ejection of the organic species into the vapor phase is presently not known. There is no doubt, however, that the observed fragments originate

from molecules which reside in the surface of the solid. This is particularly clear in the experiments at 35 K and below in view of the measured low pressure of the organic material in the gas phase ($<1 \times 10^{-8}$ Torr), of the parallel SIMS and ISS depth-profiling results, and of the experiments with an ion beam deflected to an uncoated area of the sample plate. The occurrence of higher mass fragments from the alkanes after extensive bombardment, in abundances independent of sample temperature (for pentane, up to 110 K), proves that even at the highest temperatures used little if any of the observed SIMS spectrum originates in the gas phase ($<1 \times 10^{-6}$ Torr). This conclusion is also in accordance with the lack of dependence on the nature of the primary ion, with the temperature-independence of the relative fragment ion abundances, and with the absence of any pronounced temperature dependence of the overall intensity.

It is clear that our experimental setup can be improved considerably, not only by extracting the secondary ions into the mass spectrometer, but also by insulating the cold sample plate electrically, permitting a measurement of the primary ion current and improving the floodgun control, and by using a differentially pumped ion gun which will allow the use of additional types of primary ions. With such improvements, it appears quite realistic to expect that even very dilute solid samples of organic materials will be amenable to SIMS investigations.

Important conclusions from this work for analytical use of SIMS on cooled organic solids are (i) while some bombardment damage to the sample undoubtedly occurs, it has negligible effect on the spectra observed under our conditions; (ii) the fragmentation pattern is insensitive to the type and kinetic energy of the probe ion and to the temperature of the sample; (iii) the extent of fragmentation is not prohibitive and the nature, but not relative abundances, of the fragment ions are identical to those known from electron impact mass spectrometry. Further work on various types of organic substrates is needed to establish the generality of these conclusions.

Possible applications of low-temperature SIMS are many, from analysis and depth-profiling of polymers and biological materials to investigation of the course of metal atom aggregation or photochemical fragmentations in argon matrices and to investigation of fundamental aspects of ion–molecule reactions.

LITERATURE CITED

(1) A. L. Burlingame, B. J. Kimble, and P. J. Derrick, *Anal. Chem.*, **48**, 368R–403R (1976).
(2) D. F. Torgerson, R. P. Skowronski, and R. D. Macfarlane, *Biochem. Biophys. Res. Commun.*, **60**, 616–621 (1974).
(3) R. D. Macfarlane and D. F. Torgerson, *Science*, **191**, 920–925 (1976).
(4) A. Benninghoven, *Surf. Sci.*, **35**, 427–457 (1973).
(5) H. W. Werner, *Vacuum*, **24**, 493–504 (1974).
(6) H. W. Werner, *Surf. Sci.*, **47**, 301–323 (1975).
(7) A. Benninghoven, *Crit. Rev. Solid State Sci.*, 291–316 (1976).
(8) G. D. Tantsyrev and N. A. Kleimenov, *Dokl. Akad. Nauk SSSR*, **213**, 649–652 (1973).
(9) G. D. Tantsyrev and M. I. Povolotskaya, *Khim. Vys. Energ.*, **9**, 380–383 (1975).
(10) G. D. Tantsyrev, N. A. Kleimenov, M. I. Povolotskaya, and N. M. Bravaya, *Vysokomol. Soedin., Ser. A*, **18**, 2218–2222 (1976).
(11) G. D. Tantsyrev, M. I. Povolotskaya, and N. A. Kleimenov, *Vysokomol. Soedin., Ser. A*, **19**, 2057–2065 (1977).
(12) G. D. Tantsyrev and M. I. Povolotskaya, *Vzaimodeistvie At. Chastits Tverd. Telom*, **1974**, 219–222; *Ref. Zh., Khim.*, **1975**, Abstr. No. 9S15.
(13) F. W. Karasek, *Res./Dev.*, **25** (11), 42–44, 46 (1974).
(14) F. M. Devienne and J. Giroud, Fifth C. R. Symp. Int. Jets Mol. 1975, paper no. B7; *Chem. Abstr.*, **87**, 126687u, 1977.
(15) A. Benninghoven, D. Jaspers, and W. Sichtermann, *Appl. Phys.*, **11**, 35–39 (1976).
(16) A. Benninghoven and W. Sichtermann, *Org. Mass Spectrom.*, **12**, 595–597 (1977).
(17) H. Grade, N. Winograd, and R. G. Cooks, *J. Am. Chem. Soc.*, **99**, 7725–7726 (1977).
(18) H. Grade, R. J. Day, and R. G. Cooks, Abstracts, 29th Pittsburgh Conference on Analytical Chemistry and Applied Spectroscopy, Cleveland, Ohio, Feb. 27–Mar. 3, 1978, p 383.
(19) M. Barber, J. C. Vickerman, and J. Wolstenholme, *J. Catal.*, **42**, 48–53 (1976).
(20) For a short communication of the argon matrix results, see H. T. Jonkman and J. Michl, *Chem. Commun.*, 751–752 (1978).
(21) "Atlas of Mass Spectral Data", E. Stenhagen, S. Abrahamsson, and F. W. McLafferty, Ed., Vol. 1, Interscience, New York, 1969.
(22) A. Benninghoven, *Surf. Sci.*, **28**, 541–562 (1971).
(23) J. H. Futrell and T. O. Tiernan, *J. Chem. Phys.*, **39**, 2539–2545 (1963).

RECEIVED for review May 30, 1978. Accepted September 12, 1978. Work supported by National Science Foundation grant CHE-76-02446. The 3M Company Analytical Systems Division provided partial support for instrumentation.

METHODS TO CONSTRUCT ARTIFICIAL ORGANS

Thomas R. Kessler, J. L. Foote, J. D. Andrade, and W. J. Kolff

No doubt countless investigators have labored many hours over the design of a prosthetic implant which looks promising on paper, only to see it go the way of many a "good idea" which could not be constructed in the laboratory due to the lack of the proper technical skill. However, to consider the alternative of farming out a design to industry all too often results in becoming trapped in the continuous cycle of testing, return to the factory for modifications, and then retesting. Consequently, in the interests of avoiding high retooling costs, and bound by the need to gain financial support for an idea which shows promise, the investigator turns again to the laboratory for a workable model, only to find that he must still cope with the frustrating job of developing the time consuming and further costly technology to construct such a device. Once committed, decisions concerning the interrelationships between design concepts, materials to be used, the systems to drive them, reliability, and costs are often bogged down in endless compromises in order to make them adaptable for laboratory fabrication. Given a certain design, can we construct it from the chosen material and will it function properly on our driving system with any kind of reliability? With these odds, it is no surprise then that it is difficult to attract new talent into the artificial organs field. While this is certainly not the most important factor, it is a contributing one, the elimination of which would go a long way toward facilitating greater and more meaningful contributions. It is, therefore, the intent of this paper to delineate a system which has been found to give predictable and reproducible results and which is adaptable for use in the laboratory for the construction of artificial organs.

BASIC MOLD CONSTRUCTION

Objectives. Of the very few materials suitable for laboratory fabrication, those which exclude the use of cumbersome and costly injection molding equipment stand as the most utilized. Some examples are silicone rubber, latex, and the urethanes. Basic to the construction and development of prosthetic devices involving the use of these materials is the need for a method to allow the repeated production of molds which can be layered or dip coated. Ideally, such a process should well suit itself for adaptation to all materials used. The following techniques have been found most effective.

Study models. As a preliminary step prior to the construction of a particular organ it is often necessary, both for design considerations, and as a study aid, to make a cast of the natural counterpart (Figure 1). Such an impression is useful to record representative spacial and anatomical relationships, to determine the size of the prosthesis, and, in particular, the disposition of the various connecting vessels. For this, silastic brand RTV A Mold Making Rubber* is injected with the aid of a standard refillable type caulking gun and a Tycos manometer to monitor pressures. The selected organ is first isolated by excision, or dissection in situ, and by clamping those vessels necessary to contain the RTV but allowing still others to remain open for the passage of air ahead of the rubber. From this point, the organ selected will govern the setting time used. For example, the lungs should be injected with a very slow setting time to permit good penetration; whereas, the heart involves the injection of each chamber separately under carefully monitored natural pressures in order to obtain an accurate impression. It, therefore, requires a much faster setting time. The RTV is prepared by mixing it with 10% by weight of RTV thinner. This results in a viscosity approximately 35 poises or 1/4 the original, and a consistency quite well suited for passage through vessels as small as 1 mm in diameter. The proper amount of catalyst for the prescribed setting time is added, mixed, then transferred to the caulking gun for injection. Once injected, the material is allowed to equilibrate to the desired pressure and held until set. The final cast can then be removed by dissecting most of the gross tissues and dissolving the remainder with a solution of sodium hydroxide. The resulting impression will be accurate in every detail from coronary arteries and heart valves to the bronchioles of the lungs. The information thus compiled can then be applied to a preliminary clay model of the proposed prosthesis.

Clay models. The use of modeling clay provides an intermediary, very forgiving of a changed mind (Figure 2). It can be worked and reworked to a very smooth surface with olive oil and chamois, or water. The volume of material involved can be approximated by simple water displacement techniques without disturbing the surface, and its size increased without the difficulties encountered with other materials, such as plaster.

Agar impression. The next consideration is the problem of converting the clay sculpture into a workable model. Were it possible to make a direct impression in RTV, it would be a simple process indeed. However, the RTV Mold Making Rubber will not cure in contact with the oils present in modeling clay and, therefore, must be duplicated in a second step through the use of agar hydrocolloid duplicating compound. This material, available from dental supply houses, is a reusable gel which when melted down can be used to form a negative impression for further duplication in plaster. For this purpose a double boiler is needed to liquefy the compound.

*Engineering Products Division, Dow Corning Corporation, Midland, Michigan.

From the Division of Artificial Organs, Department of Surgery, College of Medicine, University of Utah, Salt Lake City, Utah.

This work supported by Public Health Service via National Heart and Lung Institute Grants HE-12725, HE-12727 and Contract NIH-69-2181; The Christina Foundation and The Lad L. and Mary Hercik Fund.

Contrary to the directions supplied with the material, accurate impressions can be obtained of the clay with temperatures as high as 140°F; however, since large amounts of compound are usually necessary it may require 2 full hours for cooling. It is also helpful to pour the agar directly over the clay rather than down the side of the container. This insures the elimination of bubble formation on the cooler clay. Once set, the agar is cut in half, the clay model removed, and the 2 halves reassembled in its original container for casting. Until the plaster is cast, the agar impression should be filled with water. This will prevent shrinkage and prohibit the material from leeching water from the plaster cast which will follow.

Plaster cast. The model can now be reconverted to its original state with the notable exception that it will exist in a much more permanent form. After the water is poured from the agar, the plaster can be cast in the usual manner. While orthopedic plaster is adequate for this purpose, the denser, more regular crystalline formation of dental stone provides a cast which is harder and smoother and is therefore recommended. Further shaping and sanding to remove flashing, rough edges, and irregularities will render the surface an almost ceramic-like appearance. The cast should then be allowed to dry for 24 hr and covered with as many coats of Krylon* brand clear acrylic spray as is necessary to impart a gloss to the surface. It is important to note here that the dental stone cast is unsuitable as it stands for use as a mold for layering or dip coating. The mold material of choice must be one which is non-porous, for the final cast must have the smoothest surface possible and should not cause bubbles in the rubber. These bubbles are usually produced when expanding air escapes from porous materials during the heat cure.

RTV molds. While the use of RTV Rubber as a mold material is familiar to most, its advantages are never more fully realized than when applied to this type of developmental work. When used as directed, it provides a permanent yet alterable record, capable of servicible temperatures up to 600°F and into which can be repeatedly cast the material used as a form for the final construction. Of the many viscosities available, silastic D RTV Mold Making Rubber has sufficient tear strength to withstand release from all but the most extremely undercut areas, and has, therefore, been used almost exclusively. The accuracy achieved in the impressions made with this rubber is almost disturbing at times as it will faithfully reproduce every flaw. This further emphasizes the importance of beginning with the smoothest possible original. The dental stone cast should be suspended from the top of a container in preparation for pouring the RTV. For this, discarded milk cartons provide a convenient disposable container which releases well from the rubber. In the interests of avoiding an excess of material and the unpleasant situation of not having mixed enough, an effort should be made to approximate the correct volume needed for the mold. This can be done with the aid of lead shot, polyethylene pellets, or using the epolene granules to be described in the next section. The pellets can be poured into the carton and around the dental stone cast until it is completely covered. They are then transferred to the container which will be used to mix the RTV, and the level marked. If then replaced by fresh RTV to this mark and the thinner and catalyst added, the resulting volume will afford a safe margin of coverage. The completed mixture is then evacuated until all air bubbles are removed. To make certain that no air bubbles will be trapped on the more intricate configurations, the RTV can be brushed on, and the assembly evacuated a second time. In most instances neither of these is necessary. Finally, it is important to record the position of the dental stone cast before it is concealed by the RTV. This mark would indicate where to cut the cured RTV so as to later facilitate the removal of the stone (Figure 3).

The completed mold is now ready for casting. Materials such as Devcon C+ epoxy, Paraplast# hot-melt, Cerrotru& alloy metal, or Epolene C-10° wax are all compatible with RTV and cast very well. Other advantages of employing RTV become evident with use. If, for example, it is found necessary to change the mold, only those sections which are to be altered must be cut out and new RTV added as before. When modifications progress to a point where the mold is out-moded, it can be shredded in a food grinder and used with new RTV as a filler, to save on material. Most important however, the mold can now faithfully reproduce parts identical to the original clay for a virtually unlimited number of cycles.

Epolene cast. Cast materials used for designs constructed of any of the rubbers previously suggested for laboratory use must meet certain requirements. Ultimately, the cast should have a smooth surface, be non-porous, capable of forming the selected materials, of withstanding the curing temperature, of being removed without damage to its overlay, and should be consistently reproducible. Such a material, Epolene C-10, was suggested by Dr. V. Mirkovitch and further developed by Dr. T. Akutzu, now of the University of Mississippi Medical Center. Epolene is a low molecular weight polyethylene available in granular form which can be melted on a hot plate for pouring. Its softening point is 220°F and its viscosity at 300°F is 9400 cps, allowing it to flow into most intricate configurations. It can be ground, sanded, or carved and at 35¢/lb provides a very inexpensive disposable medium for layering or dipping. Preparation is simple, convenient, and very flexible. However,

*Krylon, Incorporated, Norristown, Pennsylvania.
+Devcon Corporation, Donvers, Massachusetts.
#Rezolin Incorporated, Santa Monica, California.
&Cerro Corporation, New York, New York.
°Eastman Chemical Products, Incorporated, Kingsport, Tennessee.

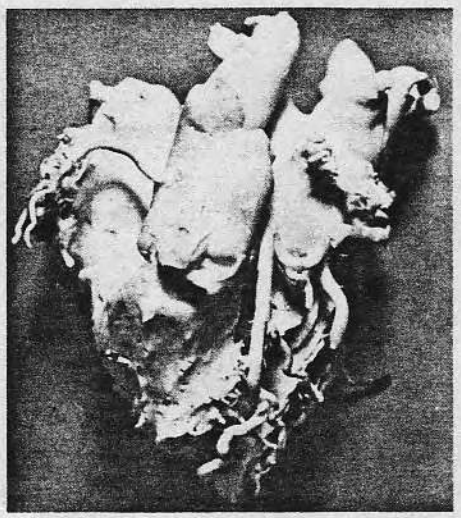

Figure 1. RTV mold of the natural heart.

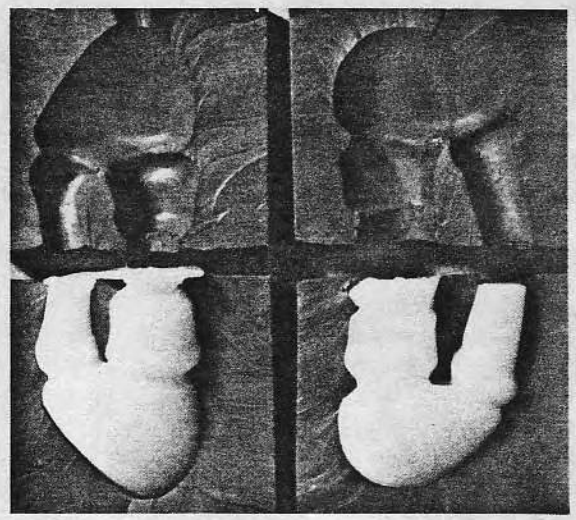

Figure 4. Epolene cast in RTV mold.

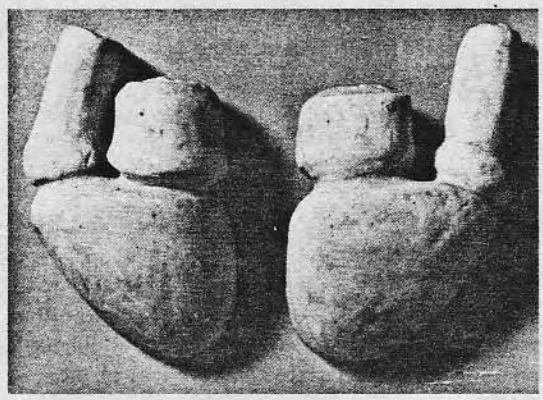

Figure 2. Clay model original.

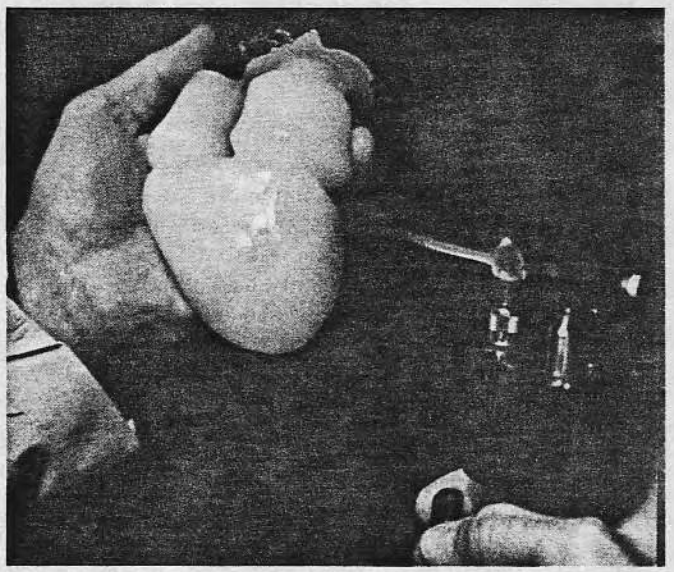

Figure 5. Flaming the Epolene.

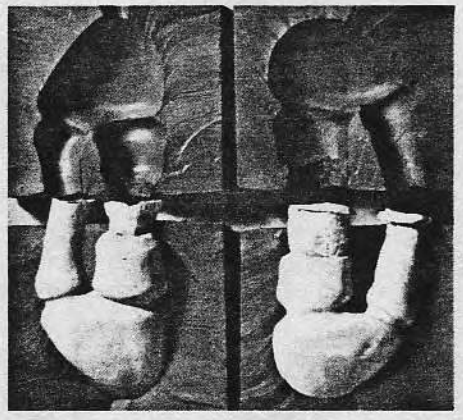

Figure 3. RTV molds of dental stone casts.

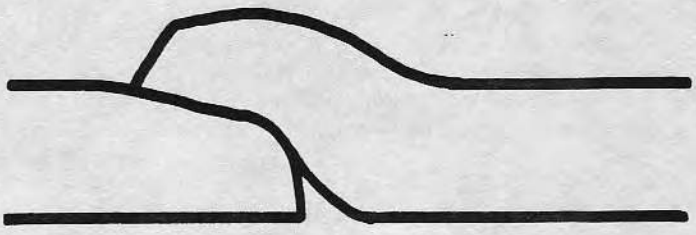

Figure 6. Compressed silastic edges without feathering.

certain precautions must be taken to ensure a good cast. The material is best melted in a pan which makes the most use of the available heating surface, and is preferably stainless steel. This ensures that the heat is evenly distributed to the granules and will not permit too much dissipation out through the side walls. Care must also be taken not to allow the temperature to remain above the melting point too long so as to prevent boiling and subsequent oxidation of the Epolene. This renders the material gummy and unpourable. While the melting of the granules proceeds, the RTV mold should be refrigerated at freezing for 30-45 min so that when the cast is made, the Epolene will set immediately in contact with the cold RTV, thus prohibiting bubble formation. Moisture condensation on the mold walls has been a problem at times, but can be reduced to negligible if the cast is made immediately upon removal from the refrigerator. Setting time varies with the thickness of the part, but can be hastened by immersing the mold in cold water. The RTV mold can now be opened to remove the Epolene cast, and it can now be worked down to the final finish (Figure 4). Flashing may need to be ground off or further sanding done before glazing the finished surface. Accomplishing this last treatment is best done by controlled flaming with a Hanau* alcohol torch (Figure 5). By forcing air through the alcohol flame with a trigger operated bellows, a continual regulation is possible for controlled flaming of delicate parts of the Epolene cast. The initial flaming is treated by wiping the cast with methyl ethyl ketone to remove any scorch marks and to help smooth the surface further. Follow with one more final light flaming and the cast is complete, having a smooth continuous surface onto which latex or urethane may be dipped, or silicone rubber sheeting layered. The resulting cast is a lightweight, easy-to-handle mold, which after the material overlay is cured, can be melted out without incurring damage.

MATERIALS APPLICATIONS

Silicone rubber. While mold shape may be common to all types of materials used for prostheses construction, mold preparation is peculiar to each. When silastic uncured calendered sheeting is applied, it is necessary to coat the Epolene mold with a thin layer of polyvinyl alcohol. A solution using DuPont Elvanol grade 50-42+ granules applied to the mold will provide a water soluble separator which will prevent the Epolene from adhering to the wall of the silastic when melted out. Application of the PVA is best achieved by smearing it on with a finger, as brushes tend to produce bubbles which will dry in place. Once dried the mold is ready for layering.

Application of uncured silastic sheeting is similar for most prostheses. The electrostatic nature of the non-wettable surface requires a dust-free atmosphere, the use of surgeon's gloves to facilitate handling of the sheeting without contamination, and some sort of corrosion resistant instruments for adaptation of the silastic. Manipulation of the molds presents handling problems which vary according to the complexities of their configuration - a situation often remedied by imbedding long wood screws in uncovered areas of the Epolene. In all cases, a concerted effort should be maintained to minimize contact with that surface which will provide the final blood-materials interface. Sheeting is handled only by surplus at the edges, and when intricate forms warrant it, stainless steel dental plastic instruments can be used to conform the silastic to the mold.

One area of real concern with layering is the seams formed by the junction of the free edges of the silastic sheeting. A successful edge-free seam cannot be made by direct overlap. Failure of the rubber to join completely when compressed leaves a groove and consequently a rough edge on that surface in contact with the blood (Figures 6 and 7). A more acceptable technique is to oppositely feather each edge of the rubber so that their fit compliments each other without increasing the thickness of the sheet. The very thin edge placed next to the mold makes for easier and more complete fusion (Figures 8 and 9). Feathering is done in either of 2 ways. The silastic sheet can be placed on a glass slab and the edges feathered with a surgical blade or directly on the mold by smearing with dental instruments. Silastic layered in this manner will present a surface virtually free of seam lines.

During adaptation of the silastic, precautions should also be taken to avoid entrapping air next to the mold. This could result in the formation of aneurysms in the silastic from heat expansion during the cure. However, small bubbles can be controlled by first volcanizing the rubber under the pressure of an autoclave for a minimum of 15 min at 240°F. By this time the silastic will have been set in its layered form and much of the Epolene melted out. Once the remainder of the Epolene is removed, the prosthesis should be boiled in water to remove any PVA residue which may still be present. The process is completed with a 4 hr oven cure at 300-325°F.

Latex. Similar procedures are followed by dipping Epolene molds into latex rubber. However since coagulants are used, it is not necessary to use a separating medium between mold and latex. The prepared mold is dipped into a coagulant, then into the latex, and again into a second coagulant. The process can be repeated until the desired thickness of latex is built up on the mold. The latex is then washed for 30 min in warm water and subjected to an 87°C heat cure for 90 min. During this time, the Epolene melts out as before and the latex

*Hanau Engineering Company, Incorporated, Buffalo, New York.

+E. I. DuPont De Nemours and Company, Incorporated, Wilmington, Delaware.

is recovered. This material is available from the Duracraft Corporation and is especially formulated to maintain strength when cured between 2 mold surfaces.

Urethanes. Prepolymers of urethane operating on a base-catalyst system and block copolymers which are solvent cast are also compatible with Epolene molds. Since the softening point of Epolene is 104°C it can well withstand the copolymer drying temperature of 90°C. The Epolene, however, must be cast in such a way that a hollow shell mold is formed. This is done to allow the mold to be broken out rather than melted, as most urethanes cannot withstand higher temperatures. Casting procedures are accomplished in the same manner except that from 3-5 min after the molten Epolene is cast, it is poured back out and the mold allowed to stand inverted until cool. The hollow cast is then removed and flamed as before.

SUMMARY AND CONCLUSIONS

From early 1968 until the present, over 100 artificial ventricles and many more related prostheses were constructed including left and right heart bypasses, coronary perfusion circuits, special endotracheal tubes, cannulas for the closed-chest left ventricular bypass, balloons for the intra-aortic balloon pumping system, inlet-outlet parts for artificial kidneys, and special one-piece bladders with valves. These were done using variations of the process outlined above and have resulted in only 4 structural failures in the almost 3 yr of its use. Artificial ventricles have been continually pumped for a period exceeding 8 mo for in vitro testing and have now reached 7 days in vivo with no materials breakdown. It is felt, therefore, that a method has been found which is reliable and adaptable for use with materials for the construction of artificial organs on a laboratory basis.

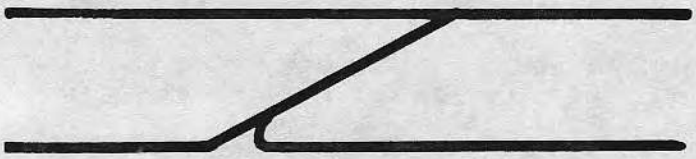

Figure 7. Wrong technique. A rough edge is still exposed to the blood.

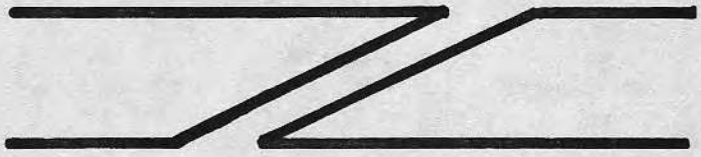

Figure 8. Ideal junction.

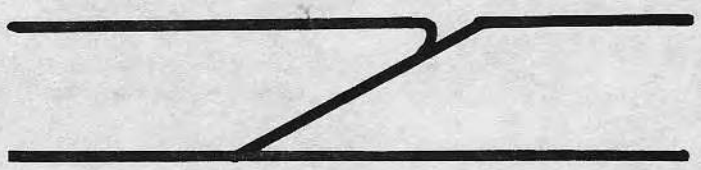

Figure 9. Acceptable. The edge is on the outside.

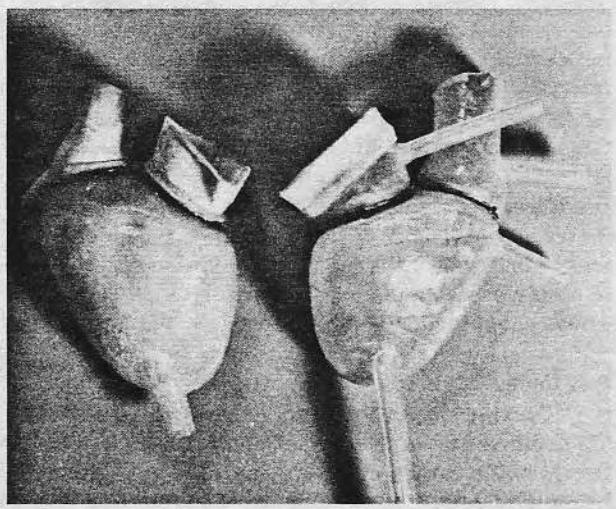

Figure 10. Two ventricles. The left ventricle is latex rubber with a urethane housing. The right is silastic with a urethane housing.

Literature Cited

1. Boretos, J.W., Pierce, W.S., Baier, R.E., Leroy, A.F., Donachy, H.J., J. Biomed. Mater. Res., 1975, 9, 327.
2. Stupp, S.I., Kauffman, J.W., Carr, S.H., J. Biomed. Mater. Res., 1977, 11, 237.
3. Paik Sung, C.S., Hu, C.B., Merrill, E.W., ACS Polym. Preprints., 1978, 19(1), 20.
4. Paik Sung, C.S., Hu, C.B., J. Biomed. Mater. Res., 1979, 13, 45.
5. Paik Sung, C.S., Hu, C.B., J. Biomed. Mater. Res., 1979, 13, 161.
6. Andrade, J.D., Iwamoto, G.K., McNeill, B., Shibatani, K., ACS Organ. Coatings Plastics Chem. Preprints, 1976, 36(1), 161.
7. Lyman, D.J., Knutson, K., McNeill, B., Shibatani, K., Trans. Am. Soc. Int. Org., 1975, 21, 49.
8. Lyman, D.J., Albro, D., Jr., Jackson, R., Knutson, K., Trans. Am. Soc. Artif. Int. Org., 1977, 23, 253.
9. Hanson, S.R., Harker, L.A., Ratner, B.D., Hoffman, A.S., J. Lab. Clin. Med., 1980, 95, 289.
10. Gott, S.R., Baier, R.E., "Evaluation of Materials by Vena Cava Rings in Dogs," NHLI Report PH 43-68-84-3-1, National Institutes of Health, Bethesda, MD, 1972.
11. Clark, D.T., Thomas, H.R., J. Polym. Sci., Polym. Chem. Ed., 1976, 14, 1671.
12. Knutson, K., and Lyman, D.J., ACS Organic Coatings and Plastics Chemistry Preprints, 1980, 42, 621.
13. Hu, C.B., Paik Sung, C.S., ACS Polymer Preprints, 1980, 21(1), 156.
14. DaCosta, V.S., Brier-Russell, D., Trudel, G., Waugh, D.F., Salzman, E.W., and Merrill, E.W., J. Coll. Interf. Sci., 1980, 76, 594.

RECEIVED March 10, 1981.

D. W. Dwight, et al., eds, Photon, Electron, Ion Probes of Polymer Structure and Properties
ACS Symp. Series #162, 1981.

Surface Analysis of Silicon: Alloyed and Unalloyed LTI Pyrolytic Carbon

R. N. KING and J. D. ANDRADE

Department of Materials Science and Engineering, Department of Bioengineering and Surface Analysis Laboratory, University of Utah, Salt Lake City, UT 84112

A. D. HAUBOLD and H. S. SHIM

Carbo-Medics, Inc., 11388 Surrento Valley Road, San Diego, CA 92121

LTI pyrolytic carbon is one of the very few synthetic materials generally accepted as suitable for long-term blood contact applications (1). Although a number of hypotheses have been formulated with respect to the blood tolerability of materials, a general theory or mechanism is not yet available. Nyilas, et al., (2) have shown that in certain situations the local hemodynamics can play a predominant role, while in most cases the solid-blood interfacial properties have been shown to be equally important (2, 3). It is assumed that understanding the plasma protein adsorption processes on solids used for blood-contact applications will lead to a better understanding of solid-blood interactions (1, 2, 3).

In terms of LTI carbon surfaces, a number of preliminary studies of plasma protein adsorption are available (4, 5, 6, 7). Kim, et al., (4) have utilized radioiodinated (I^{125}) proteins to measure adsorption of individual proteins and protein mixtures on LTI carbon surfaces. Their results indicate a very rapid adsorption of albumin onto the LTI carbon surface, consistent with Kim's model of blood interactions via a platelet-adhesion mechanism (8). Microcalorimetric and electrophoretic mobility studies of protein adsorption on LTI carbon surfaces have been done by Chiu, et al., (5). The extension of the adsorbed protein layers have been directly measured by Fenstermaker, et al., (6) and Stromberg et al., (7) at NBS using ellipsometric methods.

Most of these studies have been performed on relatively uncharacterized LTI carbon surfaces. Since we assume that a large part of blood compatibility depends on the nature of the solid-plasma interface, particularly with respect to protein adsorption, we have elected to characterize some of the surface properties of LTI carbon in hopes of further understanding the solid-blood interaction mechanisms.

In this paper we concentrate on the nature of the LTI carbon surface as determined by X-ray photoelectron spectroscopy (XPS),

and energy-dispersive X-ray analysis (EDAX). These data are discussed with reference to additional literature data on LTI carbon surfaces obtained by infrared spectroscopy, chemical reaction analysis, and electrochemical methods.

Background

The lattice structure of most pyrolytic carbon crystallites is characterized by carbon atoms arranged in planar hexagonal arrays, with varying degrees of lattice perfection. X-ray diffraction results suggest that the planar arrays are either slightly "wrinkled," or contain single or multiple lattice vacancies (9), and that the layer spacings are found to be somewhat greater than those found in graphite. This slightly distorted lattice, in which the layers are arranged roughly parallel and equidistant but not otherwise mutually oriented, has been termed "turbostratic" by Biscoe and Warren (10). Hosemann (1), in more recent X-ray studies on the crystal lattices of polymers, has introduced the term "paracrystalline" in describing similar lattice distortions. The former terminology, however, has been generally adopted in the carbon literature.

On the microstructural level, several types of pyrolytic carbons may be deposited each with one of four distinctly different structures, ranging from layered, highly anisotropic forms to structures with very small, randomly-oriented crystallites with no preferred orientation. All of these structural variations are a result of modifications in processing conditions. In this particular study, only the isotropic forms of both pure LTI carbon and co-deposited LTI carbon-silicon alloyed carbon (Pyrolite® - registered trademark of Carbo-Medics, Inc., San Diego, California) were investigated.

In addition, it is important to note that the isotropic forms of pyrolytic carbon produce at least a two-phase microstructure during formation, consisting of the previously-described turbostratic microcrystalline phase along with an amorphous carbon phase presumably interspersed between the crystalline regions (12).

In activated carbons a high internal porosity is formed by removal of much of the amorphous carbon by elevated temperature treatment, leading to a carbon material with a very high surface area (13).

In the case of the alloyed carbon, microcrystalline silicon carbide particles are randomly interspersed in the carbon matrix. The presence of this SiC phase greatly contributes to the hardness and wear resistance of these alloys compared to pure pyrolytic carbon.

The surface chemistry of carbon has been extensively studied and reviewed (14-18). It is generally believed that a variety of carbon-oxygen functional groups are present on carbon surfaces. Their nature and concentration are dependent on the sample history and depend, for example, on processing variables.

Carbon-oxygen combinations appear to be crystallographically specific. Mattson and Mark (15) report that molecular oxygen preferentially attacks graphite crystals at the edges of the layer planes at a rate nearly 20 times that of the atoms within the basal planes. From these data it is reasonable to assume that the surface oxide concentrations on carbons which have been mechanically polished would contain more oxygen than samples which have not been surface finished. It will subsequently be shown that the surface oxidation of LTI pyrolytic carbon is significantly increased by surface finishing.

While a large number of oxygen-containing functional groups have been reported on carbon surfaces, the most generally accepted are carboxyls, hydroxyls, and quinone-like carbonyls. These are illustrated in Figure 1 as they might appear on the plane edges of a turbostratic crystallite.

A variety of other carbon-oxygen groups have been suggested, including lactones, anhydrides, peroxides, ethers, and esters (14-18). These surfaces oxides have been studied by functional group reactions (18), titration, and infrared spectroscopy (15, 17).

The quinone-like carbonyl groups have received considerable attention in several electrochemical studies (15, 19, 21). Such studies clearly show anodic and cathodic peaks which can be interpreted as arising from the formation and reduction of quinone-like groups on the surface. Our laboratory has also verified these results using cyclic sweep voltammetry. Similar quinones or quinone-like groups have been identified by infrared studies (17) and by specific wet chemical reactions (20).

The most characteristic feature of quinones is their ease of reduction and reoxidation; they play a part in the redox processes of many living systems (22). Furthermore, they can interact with amino and sulfhydryl groups. One might therefore expect quinone-like groups to participate in protein adsorption and perhaps cell adhesion although no direct evidence is available to support this hypothesis. Studies of quinone-like groups on activated carbon surfaces (23) indicate such groups can participate as electron donors in donor-acceptor complexes with adsorbed molecules (17, 24).

Much of the above data on activated carbon surfaces can be correlated with the results on isotropic pyrolytic carbon surfaces due to the similarities in microstructure. The advantage of the pyrolytic carbon is in the reproducibility of the carbon surface (15) utilizing carefully controlled processing conditions.

Materials and Methods

Unalloyed and silicon alloyed LTI carbon samples were prepared at Carbo-Medics using the "steady-state" fluidized bed process developed by Akins and Bokros (25).

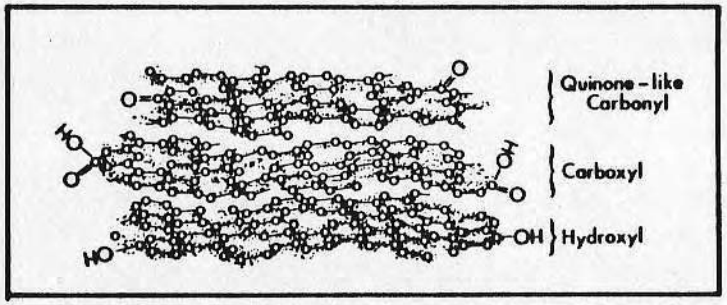

Figure 1. Oxygen-containing groups on turbostratic carbon plane edges (modified from Ref. 9))

The unalloyed LTI pyrolytic carbon was prepared by introducing small graphite plates into a fluidized bed consisting of spherical ZrO_2 particles. Carbon deposition on the plates was accomplished by pyrolyzing a gas mixture of about 25 vol. % propane - 75 vol. % He (diluent gas) in a temperature range of 1300° to 1400°C. The resulting plate coatings consisted of completely isotropic, turbostratic crystallites (approximately 24 Å to 40 Å crystals) (12). Densities range from ~1.5 to 1.8 gm/cm^3, with an anisotropy ratio of less than 1.1 (9).

Pyrolytic carbon for some biomedical applications often requires a harder, more wear-resistant surface than is attainable with pure carbon. By alloying the pyrolytic carbon with a silicon carbide phase, the microhardness of the carbon surface can be roughly doubled (25). Preparation of the alloyed pyrolytic carbon is generally equivalent to that of the unalloyed carbon. The main processing difference is the addition of methyltrichlorosilane to the propane-He gas mixture. This pyrolyzing mixture produces an additional SiC phase in the final pyrolytic carbon. The alloyed microstructure is generally similar to pure LTI carbon in that a completely isotropic turbostratic structure results, with the added benefit of a silicon carbide phase for improved wear resistance. Densities are slightly higher (~2.0 to 2.2 gm/cm^3) due to the additional SiC phase, with an anisotropy ratio again less than 1.1. Coating thickness for both types of carbon were on the order of 0.3 to 0.5 mm. For our studies, three lots of both the unalloyed and silicon-alloyed LTI pyrolytic carbons, all from the same runs, were prepared. Lots for the unalloyed LTI pyrolytic carbon (designated as LTI-A, LTI-B, and LTI-C) and silicon-alloyed LTI pyrolytic carbon (LTI/SI-A, LTI/Si-B, and LTI/SI-C) differed only by finishing operations. Cleaning and polishing procedures for both the unalloyed and silicon-alloyed lots were identical.

Lots LTI-A and LTI/SI-A were placed in clean glass vials immediately after coating and examined without any subsequent handling or treatment. Lots LTI-B and LTI/SI-B were ultrasonically cleaned in isopropyl alcohol, air dried, and stored in glass vials prior to study. Lots LTI-C and LTI/SI-C were ground and polished in several steps, and contacted various metal oxides, silicon carbide, diamond, water, detergent, isopropyl alcohol, and ethyl alcohol. Final cleaning was done in ethyl alcohol, air dried, and stored in clean glass vials. Several additional samples of LTI-C were packaged in a soft blue foam, representative of the surface which is normally delivered to medical device manufacturers for further processing and application in medical devices.

X-ray photoelectron spectra were obtained with a Hewlett-Packard 5950 B instrument utilizing monochromatic Al $K_{\alpha 1,2}$ radiation at 1487 eV. The samples were mounted in air, inserted into the spectrometer, and analyzed at ambient temperatures in a 10^{-9}

torr vacuum. Power at the X-ray source was 800 watts. Instrument resolution in our spectrometer during this analysis series was measured as 0.76 eV for the full width at half maximum of the C-1s peak from spectroscopic grade graphite. An electron flood gun operating at 0.3 mA and 5.0 eV supplied a flux of low energy electrons to the carbon surface to minimize heterogeneous charging artifacts in the resulting spectra.

Wide scans (0 to 600 eV) were performed for surface elemental analyses as well as detailed 20 eV scans of the C-1s (275 to 295 eV) region. Several standards were also analyzed under the same scan conditions in order to obtain accurate chemical shift data for various carbon-oxygen functional groups. These included poly(ethylene terephthalate), poly(ethylene oxide), and anthraquinone. The latter was run at $-50^{\circ}C$ in order to minimize volatility under our high vacuum conditions. Additional spectra were obtained on spectroscopic grade graphite for comparison purposes. All spectra were charge referenced to a C-1s line for an alkyl-like carbon at 284.0 eV.

Scanning electron micrographs were produced on a Cambridge Mark II Stereoscan SEM equipped with an EDAX 707B/NOVA accessory for elemental microanalysis of bulk regions. An edge of each sample was coated with silver paint in order to assure conductive contact between the samples and specimen holders. The analyzing vacuum was about 10^{-4} torr.

Results and Discussion

SEM/EDAX. Figures 2a, b and 3a, b are representative of the surface morphologies and bulk elemental analyses of the "as formed" lots of LTI-A, B and LTI/SI-A, B pyrolytic carbons. As shown in Figures 2a and 3a, the surface of both the unalloyed and silicon-alloyed carbons is composed of disorganized particulates resulting in a rough and highly porous topography. The ultrasonic isopropyl alcohol cleaning process (LTI-B and LTI/SI-B) seems to remove many of the more loosely adherent carbon granules resulting in much finer surface debris for those materials compared to lots LTI-A and LTI/SI-A.

EDAX analysis of these materials, as illustrated in Figures 2b and 3b, show little difference between the samples with the exception of the silicon peak found in the carbon-silicon alloy. It should be noted that EDAX is inherently insensitive to the lower atomic number elements due to the low fluorescent yields of the lighter elements, internal absorption, and low transmission factors for these elements through the beryllium detector window of the instrument. Thus, carbon and oxygen are notably absent from the conventional EDAX spectra.

Figures 4a, b and 5a, b show the results of the surface finishing process on lots LTI-C and LTI/SI-C. The surface roughness and porosity are shown to be significantly decreased, with a corresponding disappearance of the granular structures

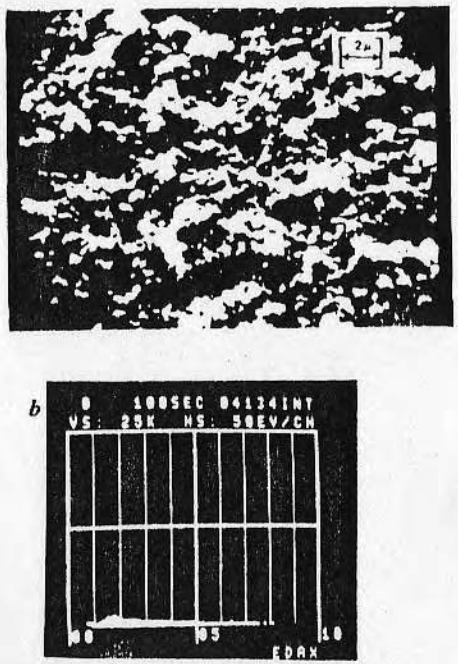

Figure 2. (a) Surface topography of "as formed" unalloyed pyrolytic carbon (LTI-A), 2600×. (b) EDAX analysis of "as formed" unalloyed carbon (LTI-A). Note absence of identifiable spectral lines. Vertical scale — 25,000 counts, data accumulation time — 100 s.

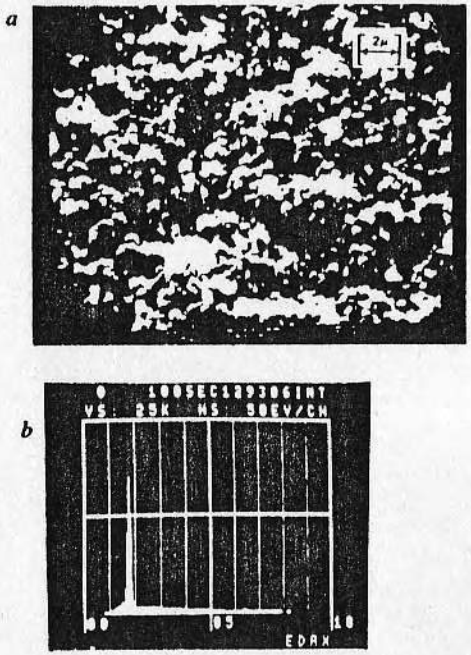

Figure 3. (a) Surface topography of "as formed" silicon-alloyed pyrolytic carbon (LTI/SI-A), 2600×. (b) EDAX analysis of "as formed" silicon-alloyed pyrolytic carbon (LTI/SI-A). Major spectral line is silicon. Vertical scale — 25,000 counts, data accumulation time — 100 s.

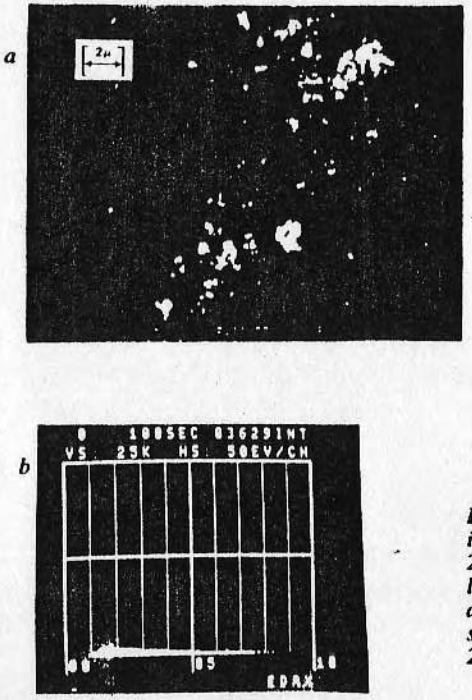

Figure 4. (a) Surface topography of polished unalloyed pyrolytic carbon (LTI-C), 2600×. (b) EDAX analysis of particulate-free region of above polished unalloyed pyrolytic carbon. Identifiable spectral lines are absent. Vertical scale — 25,000 counts, data accumulation time — 100 s.

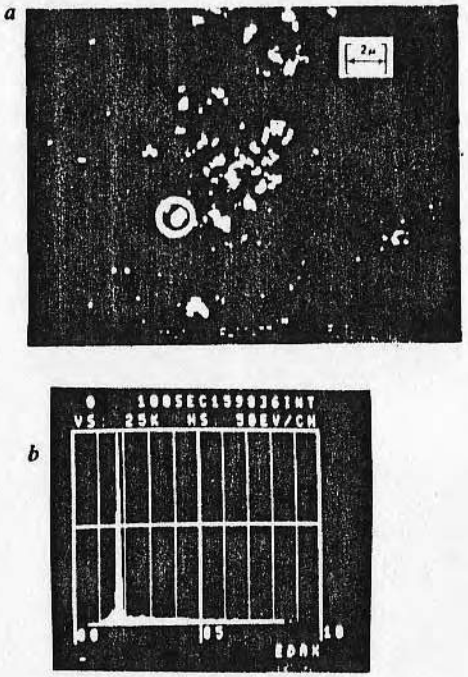

Figure 5. (a) Surface topography of polished alloyed pyrolytic carbon (LTI/SI-C), 2600×. (b) EDAX analysis of particulate-free region of above polished silicon-alloyed pyrolytic carbon. Major spectral line is silicon. Vertical scale — 25,000 counts, data accumulation time — 100 s.

noted in lots A and B. Particulate matter is still evident on both surface, however. These surfaces were examined "as received," and may represent either insufficient cleaning of the polished surface, or the presence of embedded particles from the grinding process. Evidence to support the latter conclusion is shown in Figure 6, which is the EDAX analysis of the particulate area circled in Figure 5a. The additional peaks in the spectrum are aluminum (indicating the particle may be Al_2O_3 which may be embedded during the finishing operation), and iron (which is the result of back-scattered electrons exciting Fe X-rays from the final lens assembly of the Stereoscan).

ESCA. The surface elements determined from wide-scan ESCA analysis for the various lots of unalloyed pyrolytic carbon (LTI-A, B, C) are given in Table I. We have adopted Scofield's theoretical cross-sections (26) for semi-quantitatively normalizing our ESCA spectra with respect to carbon.

Table I

ESCA Elemental Concentration for Unalloyed LTI Carbon Samples. Atomic Ratios Normalized to 100 Carbon Atoms

LTI Lot Code	C	O	Si	Trace (< 1.0)
A	100	1.8	--	--
A	100	1.2	--	--
B	100	1.4	--	--
C-"as Received" in glass	100	10.8	--	--
C-packaged in Form	100	8.5	1.9	S, P, Cl, Al
C-packaged in Foam and Methanol Cleaned	100	8.2	--	Cl
Foam Packing	100	39.9	12.3	N(∿ 2.8)

As noted in the table, Lots A and B of the unalloyed LTI carbon were identical, with a carbon/oxygen ratio slightly less than 50:1. No other elements were detected on the surface. Detailed analysis of the C-1s region of these samples shows a small chemically-shifted peak in the major C-1s region indicating what appears to be an ether- or hydroxyl-like carbon-oxygen bond.

The "as received" LTI-C sample stored in glass shows a substantial increase in the oxygen concentration of the surface region. In contrast, the LTI-C sample packaged in blue foam again

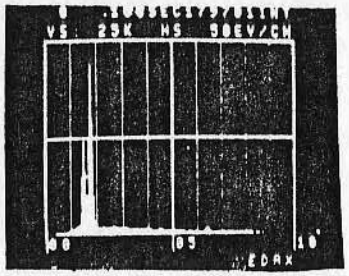

Figure 6. EDAX analysis of particulate area circled in Figure 5a. Note additional aluminum and iron lines in spectrum, assumed to result from the polishing process. Vertical scale — 25,000 counts, data accumulation time — 100 s.

shows a much higher oxygen concentration and also a substantial quantity of silicon. Other elements present on this surface include traces of sulphur, phosphorous, chlorine, and aluminum.

The foam packed lot LTI-C was then ultrasonically cleaned in absolute methanol for five minutes and rescanned under identical conditions. As shown in Table I no silicon was evident in this spectrum. The fact that the silicon spectral lines were readily removed by this washing process suggested a surface contaminant as the source of silicon, possibly a silicone release agent. The only likely source of such a contaminant is the blue foam in which these specific samples were packaged. ESCA examination of this foam packing material revealed relatively high concentrations of silicon on the surface as well as nitrogen and chlorine. This suggests a polyurethane foam with a silicone-type release agent, and traces of possible NaCl from handling. Studies of the methanol-cleaned LTI-C material (silicon-free) contacted with the foam confirmed that the silicon (silicone) on the foam can readily be transferred to the carbon surface.

The carbon/oxygen ratio on the surface of both the "as received" in glass and methanol-cleaned LTI-C is about 10:1, suggesting that the finishing operation on unalloyed pyrolytic carbon increases the oxygen concentration on the surface by a factor of 5 compared to the "as formed" Lots LTI-A and B. It is assumed that the trace elements detected on the surface are also a result of the polishing operation.

Table II summarizes the ESCA elemental analyses for the three lots of silicon-alloyed pyrolytic carbon (LTI/SI-A, B, C). Again lots A and B are roughly similar, with a carbon/oxygen ratio of about 40:1, or a slightly higher oxygen content than that found for the unalloyed material. The C-1s spectrum likewise shows an ether-like carbon-oxygen bond, similar to that observed in the unalloyed material.

Table II

Elemental Concentrations for Silicon-Alloyed LTI/SI Carbon Samples. Atomic Ratios Normalized to 100 Carbon Atoms

LTI/SI Lot Code	C	O	Si	Al	Cl
A	100	3.4	3.0	--	--
A	100	2.9	1.6	--	--
B	100	2.7	1.2	--	--
B	100	2.2	1.2	--	--
C	100	9.6	0.9	1.2	1.0
C-Methanol Cleaned	100	12.2	0.7	1.6	0.7

The LTI/SI-C carbon results again illustrate that the carbon/oxygen ratio is significantly increased by the polishing process. While the relative increase compared to the "as formed" LTI/SI lots is slightly less than that found for the unalloyed material (a factor of 3 to 4 compared to the five-fold increase for the unalloyed), the final carbon/oxygen ratio is approximately 10:1 for the polished silicon-alloyed carbon.

A careful examination of the C-1s and O-1s regions of the oxygen-containing compounds listed in Table III allow us to deduce the nature of the carbon-oxygen functional groups on the surface of the polished lots LTI-C and LTI/SI-C.

The C-1s spectra of poly(ethylene terephthalate), poly(ethylene oxide), and anthraquinone are shown in Figure 7. All spectra were internally charge-referenced to an alkyl-like C-1s line at 284.0 eV. As shown in the figure, the oxygen-containing functional groups in these model compounds result in pronounced chemical shifts in the C-1s spectra.

Note also that the area ratios of the various carbon peaks shown in Figure 7 can be used to predict the stoichiometry of these compounds. For example, from Table III the mer structure of poly(ethylene terephthalate) shows two ether-like groups, two ester-like groups, and six alkyl- or aromatic-like groups for a ratio of 1:1:3, respectively. In Figure 7, the C-1s spectrum of this polymer shows the predicted 1:1:3 ratio, the O-1s region (not shown) gives a 1:1 ratio of the singly and doubly bonded oxygen.

Table III thus summarizes the chemical shift data of Figure 7, which was subsequently used to estimate the nature of the oxygen-containing functional groups found on the LTI-C and LTI/SI-C carbon surfaces.

The 1:1 silicon/aluminum ratio in Lot C persists even after methanol cleaning. This would support the earlier observation that a portion of the grinding media, in particular Al_2O_3, may be firmly embedded in the surface during polishing.

The chlorine present on the surface may be a result of surface contamination or possibly a chemically bound form in the surface structure. Note that the SiC phase in these materials is a pyrolysis product of methyltrichlorosilane, which conceivably could introduce some chlorine in the final structure. Our previous experience with a variety of surfaces has shown that ultrasonically cleaning the surface in absolute methanol usually eliminates most surface contaminants caused by handling. Unfortunately, no means were available for depth-profiling the alloyed carbons to determine the presence of chlorine below the surface.

Figure 8 shows the C-1s spectra for "as received" LTI-C unalloyed carbon stored in glass, LTI/SI-C silicon-alloyed carbon and a spectroscopic grade graphite. The scale factors for the spectra have been increased by a factor for five compared to those in Figure 7 in order to enlarge the carbon-oxygen functional group regions. While distinct peak separations cannot be observed in the spectra due to the high intensity of the major C-1s line, the

Table III

Organic Models for Determination of Carbon-Oxygen Functional Groups by XPS; Oxygen-Containing Functional Group Data from the C-1s Line of Poly(ethylene) terephthalate), Poly(ethylene oxide), and Anthraquinone

Compound and Mer Structure	Observed Binding Energy (eV)*	:BE**	Fraction of Total Oxygen	Functional Group	
Poly(ethylene terephthalate)	284.0	0.0	--	-C-C-or 	alkyl and/or aromatic
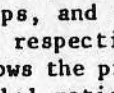	285.6	+1.6	.5	-R-O-R-	ether-like
	288.0	+4.0	.5		ester-like
Poly(ethylene oxide)					
$(CH_2CH_2O)_n$	285.8	+1.8	1.0	-R-O-R-	ether-like
Anthraquinone	284.0	0.0	--	-C-C-or 	alkyl or aromatic
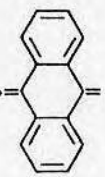	286.5	+2.5	1.0	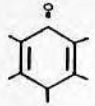	quinone-like

* Charge-referenced to C-1s at 284.0 eV.

** Binding Energy -284.0 eV = :BE

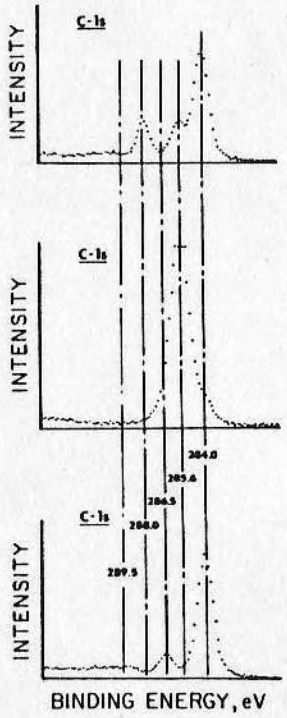

Figure 7. The C-1s ESCA spectra of poly(ethylene terephthalate) (top), poly-(ethylene oxide) (center), and antraquinone (bottom). All spectra charge-referenced to alkyl-like C-1s at 284.0 eV.

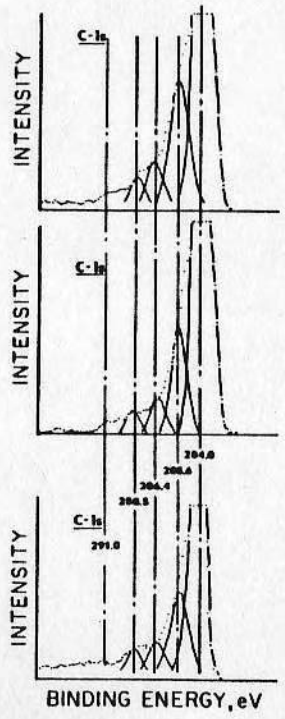

Figure 8. The C-1s ESCA spectra of polished unalloyed (top) and alloyed (center) LTI carbon, compared to graphite (bottom). All spectra charge-referenced to alkyl-like C-1s at 284.0 eV.

asymmetry evident on the high binding energy side of the peak is indicative to several additional carbon species, presumably chemically bound to oxygen. Using the chemical shift data of Figure 7 and Table III, the carbon and oxygen regions were roughly resolved (by maintaining the same full-width at half-maximum peak intensity) to form the peaks superimposed on the spectra in Figure 8.

These peaks are shown to reasonably account for the asymmetry in the C-1s spectra of the carbon surfaces. These data lead us to believe that the assigned peaks are reasonable to a first approximation, and correspond to the carbon-oxygen functional groups indicated in Table III. Figure 8 also illustrates that the graphite spectrum shows similar carbon-oxygen functionality.

In addition, a higher energy feature is noted in the C-1s spectra which comprises less than 3% of the total carbon. If this is assigned to a carbon-oxygen group, it roughly corresponds to a carbonate-like carbon, as reported by Clark (29). However, Clark (30) has also demonstrated that low kinetic energy $\pi \rightarrow \pi^*$ shake-up transitions for aromatic polymers invariably lead to satellite peaks located from 6 to 7 eV above the alkyl-like C-1s. One would, therefore, expect to see such satellites in the C-1s spectra of poly(ethylene terephthalate), anthraquinone, graphite, and the pyrolytic carbons, since all exhibit varying degrees of aromaticity. Such peaks are suggested in Figures 7 and 8 and are shown to fall roughly within the same region for all of the C-1s spectra. Of these two possible explanations, in our opinion, the higher binding energy peak seen in these spectra is likely due to the $\pi \rightarrow \pi^*$ shake up satellite, which is expected to be present.

Table IV summarized the ESCA data obtained on the polished carbon surfaces along with estimates of percentages of the carbon-oxygen groups on the surface. Roughly 85-90% of both the unalloyed and Si-alloyed carbon surfaces are shown to be oxygen-free, with the remainder consisting of three major types of oxygen-containing functional groups; approximately 60% are of the ether-like variety, 25% are quinone-like, and the remaining 15% are ester-like.

These data partially correlate with the XPS data of several investigators. Marsh, et al., (27), using a non-monochromatized X-ray source, have reported a 50% maximum oxygen coverage on the surface of a variety of pyrolytic carbons reacted with oxygen. It is important to note, however, that the carbons used in the present study were prepared quite differently, and not specifically reacted with oxygen. They further reported deconvoluting the O-1s spectra into five distinct peaks. They were unable, however, to assign them to particular oxygen-containing functional groups. We cannot justify this large number, even though our spectra appear to be better resolved. Recently Evans and Thomas (28) studied single crystals of graphite and diamond surfaces and suggested that >C-O-C< or >C-OH surface groups were probably present in roughly equal concentrations on oxygenated carbon surfaces.

Table IV

Estimations of Oxygen-Containing Functional Groups on Polished LTI Pyrolytic Carbon and Graphite Surfaces

Material	Estimated Binding Energy (eV)*	BE**	Approximate % of Higher Energy Forms of Carbon	Functional Group
LTI-C unalloyed carbon	284.0	0.0	--	alkyl or aromatic
	285.76	+1.76	63	ether-like
	286.34	+2.34	23	quinone-like
	288.48	+4.48	9	ester-like
	291.00	+7.00	6	$\pi \rightarrow \pi^*$ satellite or carbonate-like
LTI/Si-C silicon-alloyed carbon	284.0	0.0	--	alkyl or aromatic
	285.60	+1.60	65	ether-like
	286.40	+2.40	23	quinone-like
	288.54	+4.64	8	ester-like
	291.00	+7.00	4	$\pi \rightarrow \pi^*$ satellite or carbonate-like
Graphite	284.0	0.0	--	alkyl or aromatic
	285.60	+1.60	67	ether-like
	286.56	+2.56	21	quinone-like
	288.16	+4.16	7	ester-like
	291.00	+7.00	5	$\pi \rightarrow \pi^*$ satellite or Carbonate-like

The data also correlate with the electrochemical investigations of Epstein, et al., (21), i.e., that quinone-hydroquinone groups are most likely present on LTI carbon surfaces. They further concluded that such groups can be readily converted electrochemically from one to the other. As previously noted, our data indicates that approximately 25% of the surface oxygen is quinone-like in nature.

Conclusions

At least three major types of carbon-oxygen functional groups are present on polished LTI and LTI/SI carbon surfaces. The origin of these oxygen-containing species is predominately the polishing process, during which the oxygen content increases nearly five-fold compared to the unpolished materials.

Both the XPS and EDAX results indicate that surface contaminants composed of aluminum compounds are also introduced during polishing. SEM analysis of the surfaces was unable to determine whether or not these contaminants are firmly embedded in the carbon surface. From our XPS data, we have found that approximately 85-90% of the carbons do not appear to be chemically-bonded to oxygen. The remaining 10 to 15% contain three major types of oxygen functionality. From the chemical shift data, we estimate that 60% of the carbon-oxygen functional groups are either-like in nature, 25% are quinone-like, and the remaining 15% are ester-like or carboxylic in nature. These results were very consistent, regardless of the type of carbon surface investigated.

Though the materials examined are expected to be representative of the materials delivered to medical device manufacturers it is possible that other changes could occur. Thus these results should not be extrapolated to carbon-containing medical devices until the actual carbon components have been surface analyzed.

Acknowledgement

The authors wish to thank Mr. Gary Iwamoto for his assistance. This work was supported in part by NIH Grants HL16921 and 18519.

Abstract

Low temperature isotropic (LTI) pyrolytic carbon has been studied by X-ray photoelectron spectroscopy, scanning electron microscopy, and energy dispersive X-ray analysis. Both silicon-alloyed and unalloyed carbons were studied, in both as-deposited and polished (finished) forms. The polished materials contain significant amounts of surface oxygen. Approximately 1 in 10 of the carbon atoms in the surface volume analyzed by XPS are

oxidized. About 60% of the oxygen-containing functional groups are ether-like, 25% are quinone-like, and the remaining 15% are ester- or carboxyl-like. Polishing also resulted in small amounts of aluminum on the surface as well as several other impurities. The surface properties of LTI pyrolytic carbon are important in view of its success as a material for medical implant purposes. The literature on the surface properties of carbon is reviewed.

Literature Cited

1. Bruck, S.D., Rabin, S. and Ferguson, R.J., Biomat., Med. Dev. Art. Org., 1973, 1, 191.

2. Nyilas, E., Morton, W.A., Federman, D.M., Chiu, T.H. and Cumming, R.D., Trans. Amer. Soc. Artif. Int. Organs., 1975, 21, 55.

3. Andrade, J.D., Med. Inst., 1973, 7, 110.

4. Kim, S.W., personal communication.

5. Chiu, T.H., Nyilas, E. and Federman, D.M., Trans. Amer. Soc., Artif. Int. Organs., 1976, 22, 498.

6. Fenstermaker, C.A., Grant, W.H., Morrissey, B.W., Smith, L.E. and Stromberg, R.R., Nat. Bur. Stds. Int. Report, NBSIR 74-470 (3/22/74).

7. Stromberg, R.R., Morrissey, B.W., Smith, L.E., Grant, W.H. and Fenstermaker, C.A., Nat. Bur. Stds., Int. Report, NBSIR 75-667 (1/15/75).

8. Kim, S.W., Lee, R.G., Oster, H., Coleman, D., Andrade, J.D., Lentz, D.J. and Olsen, D., Trans. Amer. Soc. Artif. Int. Organs., 1974, 29, 449.

9. Bokros, J.C. in "Chemistry and Physics of Carbon," Ed. P.L. Walker, Jr., 1969, 5, 9.

10. Biscoe, J. and Warren, B.E., J. Appl. Phys., 1942, 13, 364.

11. Hoseman, R., Polymer, 1962, 3, 349.

12. Kaae, J.L., Carbon, 1975, 13, 55.

13. Smisek, M. in "Active Carbon, M. Smisek and S. Cerny, Eds. (Elsevier Publishing Company, Amsterdam, 1970).

14. Puri, B.R., in "Chemistry and Physics of Carbon," Ed. P.L. Walker, Jr., 1970, 6, 191.

15. Mattson, J.S. and Mark, H.B., Jr., "Activated Carbon-Surface Chemistry and Adsorption from Solution," (Marcel Dekker, New York, 1971).

16. Snoeyink, V.L. and Weber, W.J., Jr., Prog. Surf. Memb. Sci., 1972, 5, 63.

17. Mattson, J.S., Lee, L., Mark, H.B., Jr., Weber, W., Jr., J. Colloid Interface Sci., 1970, 33, 284.

18. Donnet, J.B., Carbon, 1968, 6, 161.

19. Blurton, K.T., Electrochimica Acta., 1973, 18, 869.

20. Elliott, C.M. and Murray, R.W., Anal. Chem., 1976, 48, 1247.

21. Epstein, B.D., Dalle-Molle, E., and Mattson, J.S., Carbon, 1971, 9, 609.

2. Thomson, R.H., "Naturally Occurring Quinones," (Butterworths, London, 1957).

3. Garten, V.A. and Weiss, D.E., Aust. Chem. Soc. J., 1955, 8, 68.

4. Mattson, J.S., Mark, H.B., Jr., Malbin, M.D., Weber, W.J., Jr., and Crittenden, J.C., J. Colloid Interface Sci., 1969, 31, 116.

5. Akins, R.J. and Bokros, J.C., Carbon, 1974, 12, 439.

5. Scofield, J.H., J. Elec. Spec. and Related Phen., 1976, 8, 129.

. Marsh, H., Foord, A.D., Mattson, J.S., Thomas, J.M., and Evans, E.J., J. Colloid Interface Sci., 1974, 49, 368.

. Evans, S. and Thomas, J.M., Proc. Royal Soc. London A., 1977, 353, 103.

. Clark, D.T., "Molecular Spectroscopy," A.R. West, Ed., Heydon and Sons, New York, 1977.

. Clark, D.T., "Polymer Surfaces," D.T. Clark and W.J. Feast, Eds., John Wiley and Sons, New York, 1978.

ECEIVED March 25, 1981.

Interfacial Tensions at Acrylic Hydrogel–Water Interfaces

R. N. KING, J. D. ANDRADE,[1] S. M. MA, D. E. GREGONIS, AND L. R. BROSTROM

Department of Materials Science and Engineering, Department of Bioengineering and Surface Analysis Laboratory, University of Utah, Salt Lake City, Utah 84112

Received August 18, 1981; accepted January 26, 1982

The hydrogel–water interface is a highly mobile transition region, perhaps on the order of 100 Å in depth, which interfaces the bulk gel network with the surrounding aqueous solution. Consideration of the adsorption characteristics at such an interface requires information on the interfacial free energy or interfacial tension. Such information is generally difficult to obtain by most conventional methods. In this paper, we have applied underwater contact angle techniques (sessile bubbles) as probes of fully hydrated interfaces. Utilizing work of adhesion and contact angle assumptions, and contact angle data using captive air, octane, and dodecane at the gel–water interface, we have obtained the hydrated gel surface free energy and the gel–water interfacial free energy. The interfacial free energy drops rapidly to near zero as the equilibrium water content of the gel network approaches 30 wt%. Apparently, the surface, even with relatively low water contents, has sufficient mobility to achieve a molecular orientation which minimizes the interfacial tension. Data are presented on copolymers of methyl methacrylate-hydroxyethyl methacrylate, ethyl methacrylate-hydroxyethyl methacrylate, methoxyethyl methacrylate-hydroxyethyl methacrylate, methacrylic acid-hydroxyethyl methacrylate, and dimethylaminoethyl methacrylate-hydroxyethyl methacrylate, all prepared in our laboratories, and a commercially prepared polyacrylamide gel with varying crosslink density. These systems cover the equilibrium water content range from roughly zero to in excess of 90% wt%. Brief discussions of the possible effects of surface and interfacial tension-induced deformation of the gel substrate and the effects of charge density at the interface are also included.

INTRODUCTION

The goal of our research on hydrogel–water interfaces is to attempt to establish a correlation between the measurable surface properties of a material and its eventual biological behavior, both in terms of protein adsorption and cell adhesion interactions.

We have attempted here to probe a number of the variables expected to be involved in protein adsorption and cell adhesion by preparing solid surfaces with a series of controlled properties and characterizing these polymers in equilibrium with water. The general polymer system chosen for this study consists primarily of the methacrylate esters shown in Table I. The methacrylate family offers a variety of monomer types, polymerization chemistry, and copolymerization characteristics which are relatively well documented, at least with respect to other similar systems. Methacrylate monomers generally lead to largely amorphous polymers. Because of their transparency, there is considerable practical interest in the methacrylates. Polymethyl methacrylate is the basis of the hard contact lens industry while polyhydroxyethyl methacrylate is the major polymer for soft contact lenses.

The versatility in the methacrylate system allows one to examine a number of hypotheses regarding interfacial interactions. These are listed in Table II. The minimum interfacial free energy hypothesis, for example, argues that as the interfacial free energy at the polymer–water interface approaches zero, irreversible protein adsorption processes should be minimized (1). This is not to say that adsorption does not occur, but rather that it will probably result in a highly reversible adsorption process at least from a general surface chemistry point of view. Using comonomers of methyl (MMA) or ethyl methacrylate (EMA) and hydroxyethyl methacrylate (HEMA), one can produce a series of copolymers of varying equilibrium water content from roughly 0 to 40 wt%. As the water content increases, the interfacial free energy should decrease, thus permitting a rigorous test of the hypothesis. Even higher water contents are available in the polyacrylamide system (>90 wt%), allowing the full range of water content to be examined.

The charge or polar properties of a surface can certainly lead to specific interactions at an interface which in some cases may dominate the interfacial region. In an aqueous environment, for example, the polar regions of a polymer will be fully interacting with the aqueous phase and thereby contribute to a lowering of the interfacial free energy even though the surface itself may possess a high surface free energy. As seen in Table II, positive and/or negative charge can be incorporated in small extents on either hydrophilic or hydrophobic polymer surfaces by copolymerizing either methyl or ethyl methacrylate (hydrophobic) or hydroxyethyl methacrylate (hydrophilic) with the comonomers methacrylic acid (MAA) or dimethylaminoethyl methacrylate (DMAEMA) for negative or positive charge, respectively (2).

In addition to these adsorption variables, there is evidence from the hydrophobic interactions of proteins with chromatographic supports suggesting that the size of the hydrophobic side chains present at the interface is very important (3). One can probe this effect by simply varying the size of methacrylate side chain from methyl to octadecyl and perhaps beyond, and possibly relate the glass transition temperature to surface mobility.

Even with the versatility and relative ease in preparing methacrylate polymers and copolymers with expected or predictable interfacial properties, it is an altogether different matter to characterize directly the resulting

[1] To whom correspondence should be addressed.

0021-9797/85 $3.00

TABLE I

Base Polymers for Copolymers Used in Characterizing Interfacial Properties

General System: $(CH_2-C(CH_3))_n$: Methacrylate Esters, with $C(=O)-O-R$

-R	Name	Abbreviation	Property
$-CH_3$	Methyl Methacrylate	MMA	Hydrophobic
$-CH_2-CH_3$	Ethyl Methacrylate	EMA	Hydrophobic
$-CH_2-CH_2-OH$	Hydroxyethyl Methacrylate	HEMA	Hydrophilic
$-CH_2-CH_2-O-CH_3$	Methoxyethyl Methacrylate	MEMA	Hydrophobic
$-H$	Methacrylic Acid	MAA	Negative Charge
$-CH_2-CH_2-N(CH_3)_2$	Dimethylaminoethyl Methacrylate, HCl Salt	DMAEMA	Positive Charge

TABLE II

Model Polymer/Copolymer Systems for Investigating Protein Adsorption and Interfacial Interaction Hypotheses

Hypothesis	Model System
Effect of decreasing interfacial free energy (by varying equilibrium water content)	MMA–HEMA copolymers EMA–HEMA copolymers Polyacrylamides (~0 to 90 wt% H_2O)
Effect of positive and negative charge on rigid, hydrophobic surfaces	MMA–MAA copolymers (negative charge) MMA–DMAEMA copolymers (positive charge)
Effect of positive and negative charge on flexible, hydrophilic surfaces	HEMA–MAA copolymers (negative charge) HEMA–DMAEMA copolymers (positive charge)
Effect of mobility of polymer molecules and chain segments (by varying length and Tg)	Methacrylate esters Methyl → octyl → lauryl → octadecyl → · · ·

interfacial properties. We have chosen to use underwater contact angle methods because of our interest in investigating the fully hydrated polymer–water interface. This method differs from the more classical advancing angle contact angle method in that it more directly measures the polar contributions at the interface since, as mentioned earlier, these regions are fully interacting in an aqueous environment. The classical measurement of advancing angles in air or water vapor primarily probes the apolar regions, thereby giving in essence a low estimate of the polar properties of the solid surface. The fully hydrated, water-equilibrated solid is thus a much more representative surface for probing interfacial tension properties.

The basic captive sessile drop geometry and method of measurement is given in Fig. 1. Considering Fig. 1 with air as the probing fluid, we have (4)

$$\gamma_{SV} = \gamma_S - \pi_e = \gamma_{SW} + \gamma_{WV} \cos \theta_{air}. \quad [1a]$$

With octane or another water-immiscible liquid (L) as the probe we have:

$$\gamma_{SL} = \gamma_S - \pi_e = \gamma_{SW} + \gamma_{WL} \cos \theta_L. \quad [1b]$$

Here the supscript L refers to the water-immiscible liquid (octane or dodecane for this work), subscript V refers to water vapor, and π_e is the water vapor equilibrium spreading pressure. We chose to use water vapor in Eq. [1b] since the surface is fully equilibrated with water at the instant the octane drop is applied. The θ measurement is made as quickly as possible after the instant of contact. The quantities to be obtained from the experiment are γ_{SV}, the fully water-equilibrated solid surface tension and γ_{SW}, the solid–water interfacial tension.

In Eqs. [1a, 1b], the quantities $\gamma_{WV} \cos \theta_{air}$ and $\gamma_{WL} \cos \theta_L$ are directly measurable, i.e., the water–air (γ_{WV}) and water–octane (γ_{WL}) interfacial tensions and the angles between the solid and either air (θ_{air}) or octane (θ_L) as measured through the water phase. The quantities γ_{SV} or γ_{SL} and γ_{SW} are unknowns which we approximate through use of the harmonic mean equation (5–7):

$$\gamma_{SL} \approx \gamma_{SV} + \gamma_{LV} - 4\left(\frac{\gamma^d_{SV}\gamma^d_{LV}}{\gamma^d_{SV} + \gamma^d_{LV}}\right) - 4\left(\frac{\gamma^p_{SV}\gamma^p_{LV}}{\gamma^p_{SV} + \gamma^p_{LV}}\right) \quad [2]$$

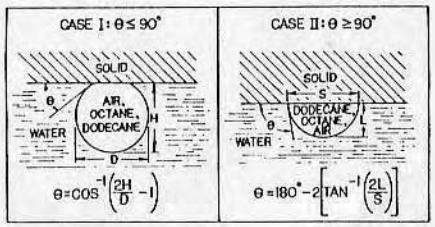

FIG. 1. Schematic representation of the contact angle geometry and bubble dimension measurement using underwater captive air, *n*-octane, and dodecane bubbles.

and

$$\gamma_{SW} \approx \gamma_{SV} + \gamma_{WV} - 4\left(\frac{\gamma^d_{SV}\gamma^d_{WV}}{\gamma^d_{SV} + \gamma^d_{WV}}\right) - 4\left(\frac{\gamma^p_{SV}\gamma^p_{WV}}{\gamma^p_{SV} + \gamma^p_{WV}}\right), \quad [3]$$

where the superscripts d and p refer, respectively, to the dispersion and polar components of the interfacial free energy.

By substituting Eqs. [2] and [3] into [1b] one obtains

$$\gamma^d_{SV}\left(\frac{\gamma^d_{WV}}{\gamma^d_{SV} + \gamma^d_{WV}} - \frac{\gamma^d_{LV}}{\gamma^d_{SV} + \gamma^d_{LV}}\right) + \gamma^p_{SV}\left(\frac{\gamma^p_{WV}}{\gamma^p_{SV} + \gamma^p_{WV}} - \frac{\gamma^p_{LV}}{\gamma^p_{SV} + \gamma^p_{LV}}\right) = \frac{\gamma_{LW} \cos \theta + \gamma_{WV} - \gamma_{LV}}{4} = K. \quad [4]$$

There are two unknowns, γ^d_{SV} and γ^p_{SV}, in this equation. Since the value of K depends on the liquid used, by selecting two or more immiscible liquids of known polar (γ^p_{LV}) and apolar (γ^d_{LV}) character, one can set up a series of equations which can be simultaneously solved by an iterative method (within a given error tolerance) to determine the γ^d_{SV} and γ^p_{SV} components of the fully hydrated solid surface. The solutions for this method are available (4).

Here we shall discuss the solutions for the special case which considers the octane–water–solid and air–water–solid systems. For the octane–water–solid system:

$$\gamma_{LV} = \gamma^d_{LV} = 21.6 \text{ dyne/cm at } 25°C$$

$$\gamma^p_{LV} = 0 \text{ dyne/cm}$$

and the *n*-octane–water interfacial tension is 50.5 dyne/cm at 25°C. Octane is chosen because its dispersion component equals that of water:

$$\gamma^d_{LV} = \gamma^d_{WV} = 21.6 \text{ dyne/cm}.$$

Here we assume that the spreading pressure for water vapor on liquid octane is zero. In addition, these conditions require that the polar component of water and the *n*-octane–water interfacial tension be equal:

$$\gamma_{LW} = \gamma^p_{WV} = 50.5 \text{ dyne/cm}.$$

Substituting these values in Eq. [4] and rearranging in terms of γ^p_{SV} yields the simplified form:

$$\gamma^p_{SV} = \frac{50.5K_{octane}}{(50.5 - K_{octane})}, \quad [5]$$

where

$$K_{octane} = \frac{\gamma_{LW} \cos \theta_L + \gamma_{WV} - \gamma_{LV}}{4}$$

as determined via K in Eq. [4]. Thus, measuring an octane underwater contact angle basically yields an estimate of the polar component, γ^p_{SV}, of the fully hydrated solid surface.

For the air–water–solid system:

$$\gamma_{LV} = \gamma^d_{LV} = \gamma^p_{LV} = 0 \text{ dyne/cm},$$

and the water–water-saturated air interface (γ_{WV}) is 72.1 dyne/cm at 25°C. In this case, Eq. [4] can be reduced and rearranged in terms of γ^d_{SV} to yield

$$\gamma^d_{SV} = \frac{\gamma^d_{WV}K_{air} - \gamma^p_{SV}\{\gamma^d_{WV}\gamma^p_{WV}/(\gamma^p_{SV} + \gamma^p_{WV})\}}{\gamma^d_{WV} - K_{air} + \gamma^p_{SV}\{\gamma^p_{WV}/(\gamma^p_{SV} + \gamma^p_{WV})\}}. \quad [6]$$

Again as determined from Eq. [4]:

$$K_{air} = \frac{\gamma_{WV}(1 + \cos \theta_{air})}{4}.$$

Using the results of Eq. [5] and the measurement of an air underwater contact angle, the dispersion component (γ^d_{SV}) of the solid surface can be obtained via Eq. [6]. The sum of γ^d_{SV} and γ^p_{SV} is, of course, γ_{SV}, the hydrated solid surface tension which can be substituted into the harmonic mean equation in order

to estimate γ_{SW}, the solid–water interfacial tension.

The harmonic mean approximation involves a number of assumptions with respect to the polar or nondispersive interactions. One must realize that the assumptions can be questioned and constitute a serious limitation in the treatment. The reason we have chosen to use the harmonic mean approach in the estimate rather than a geometric mean is based on the work of Wu (5–7), which compared the geometric mean, harmonic mean, and combination approximations with experimentally determined values of the surface tension of molten polymers. In his estimation, the harmonic mean gave the best agreement with his experimental values. In general, Wu found that the harmonic mean more accurately predicted the interfacial tension between polymers, between a polymer and an ordinary liquid, and for general systems in which the polarizabilities of the interacting elements of each phase were not too different.

Experimental data for the *n*-alkane/water series and a discussion of interfacial properties is available (8, 9).

Figure 2 gives the general set of solutions for various γ^p_{SV} values at 25°C as a function of the underwater octane contact angle, generated via Eq. [4]. Values of γ^p_{SV} can thus vary from zero to of the order of 50.5 dyne/cm. Values greater than 50.5 dyne/cm at 25°C are outside the range of the technique since this is the maximum value of the octane–water interfacial tension. Once γ^p_{SV} has been established for a given octane contact angle, Eq. [5] can be used to derive γ^d_{SV} as a function of the air contact angle for any given octane contact angle. This is shown in Fig. 3 which plots γ^d_{SV} for a given set of octane and air contact angles. Clearly portions of the range of available solutions are not relevant. Values of γ^d_{SV} less than the order of 10 dyne/cm do not have physical significance for solid systems. In addition, for practically all polymer systems of interest here, γ^d_{SV}

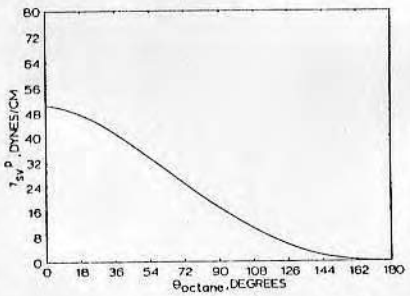

FIG. 2. The harmonic mean estimate of γ^p_{SV} as a function of the underwater octane contact angle.

values greater than 50–60 dyne/cm are unreasonable as well. Solutions for γ^d_{SV} above the surface tension for water (~72–73 dyne/cm at 25°C) are also clearly unrealistic even though they mathematically exist. We have, thus, arbitrarily truncated the data above a γ^d_{SV} value of 80 dyne/cm. Similarly, although the mathematical treatment allows for negative γ^d_{SV} values, we have chosen to display only the positive and physically realistic regions.

The constraints in the γ^p_{SV}, γ^d_{SV} data illustrated in Figs. 2 and 3 are reflected in the data of Fig. 4, which plots the solid–water interfacial tension as a function of both the air and octane contact angles. As expected, γ_{SW} is shown to vary in this treatment from 0 to 72–73 dyne/cm. Note, however, that the constraints on γ^p_{SV} and γ^d_{SV} do not generally allow both the air and octane angles to take on all possible values in all possible combinations and still produce physically meaningful interfacial tensions. Sets of experimental octane and air angles which fall outside these solutions may suggest several possibilities. γ^p_{SV} values greater than 50.5 dyne/cm exist, a good example being glass. A γ^p_{SV} value of 50.5 dyne/cm corresponds to an octane contact angle of zero, i.e., totally nonwetting. Higher values of γ^p_{SV}, however, will also lead to zero octane contact angles. When the octane contact angle reaches zero, the maxi-

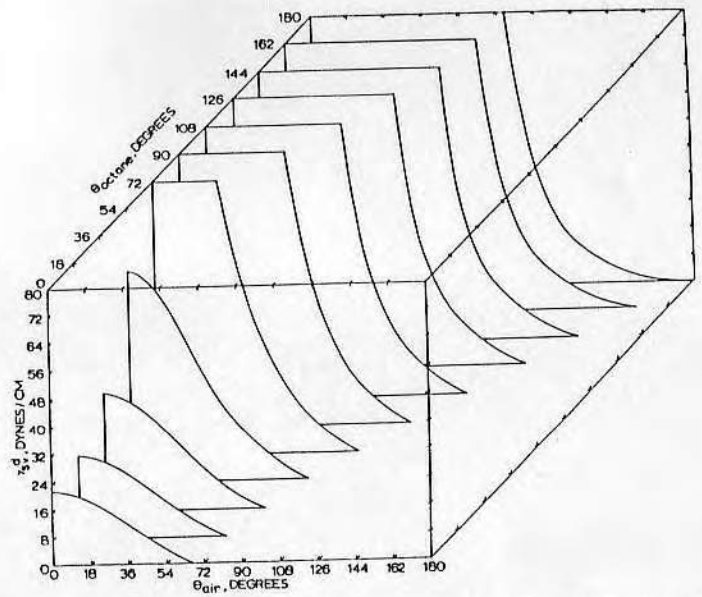

FIG. 3. The harmonic mean estimate of γ^d_{SV} as a function of the underwater air contact angle for a given octane contact angle.

mum value of γ^p_{SV} predicted by the treatment cannot mathematically exceed 50.5 dyne/cm, even though higher γ^p_{SV} values clearly physically can and do exist. Another system, possibly a mercury–water–solid system, would be necessary to probe higher values.

In addition, the presence of impurities in the polymer or in the water, the fact that the octane may be a solvent for a particular polymer or show preferential absorption, or general polymer heterogeneity and/or surface roughness can all be factors which lead to incorrect results. If the problem does not appear to be experimental, it may suggest that for that particular polymer system the assumptions and approximations involved in this theoretical treatment are simply invalid.

To test the applicability of these solutions, the air and octane underwater contact angles were measured on a methacrylate copolymer series, and the corresponding components of the fully hydrated solid surface tension as well as the solid–water interfacial tension were determined.

MATERIALS AND METHODS

Bulk polymer preparation. The origins of the monomers used for this study are as follows. HEMA (see Table 1 for abbreviations) is a gift from Hydro Med Sciences, Inc., New Brunswick, N. J.; it contains 0.04% methacrylic acid, 0.15% diethylene glycol methacrylate, less than 0.02% ethylene dimethacrylate, and 23 ppm of hydroquinone monomethyl ether. The MEMA and EMA monomers were obtained from Polysciences, Inc., Warrington, Pa., and used as received. Gas chromatographic analysis indicated a purity of over 99% for MEMA. The DMAEMA, also from Polysciences, was converted to the HCl salt by bubbling HCl vapor

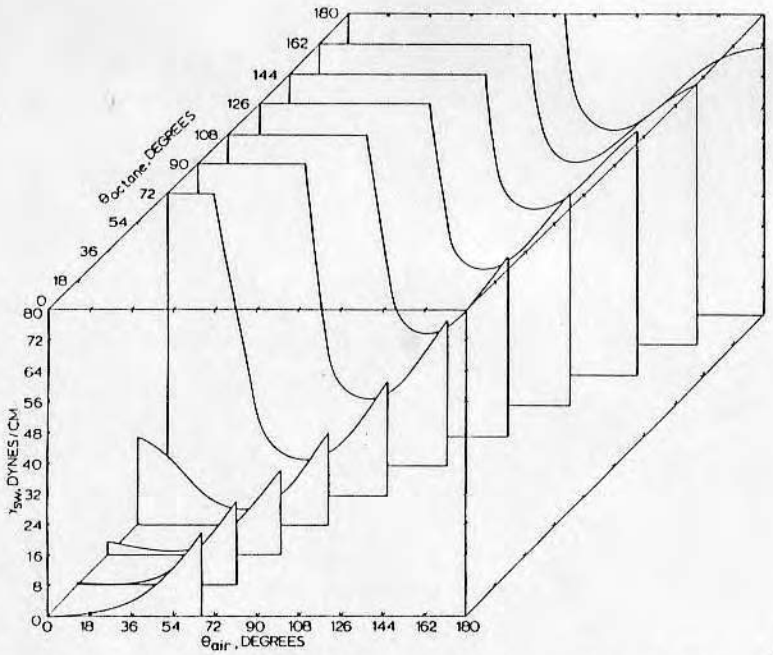

FIG. 4. Interfacial tension as a function of both air and octane underwater contact angles using the harmonic mean estimate.

through the monomer and collecting the precipitate. The MMA and MAA monomers were obtained from the Aldrich Chemical Co., Milwaukee, Wisc., and used as received. The MMA purity is 99% and is inhibited with 65 ppm hydroquinone monomethyl ether. The MAA is 98.5% pure and inhibited with 1000 ppm hydroquinone and 250 ppm monomethyl ether. The polyacrylamide series was obtained as a differentially crosslinked polymer from Ortec, Inc., Oak Ridge, Tenn. The Ortec Gradipore gel was supplied in a storage solution containing 50 ppm of sodium azide. It was subsequently extensively extracted in doubly distilled water for several days with frequent water changes before contact angle characterizations were performed.

Portions of the methacrylate polymerization have been described previously (2, 10, 11), as well as copolymerizations of the HEMA-ionic methacrylate series (2), and will only be briefly discussed here. Since the final fabrication step involves solvent spin casting of polymer films, soluble uncrosslinked polymers are required. Soluble polymers in this series are obtained only above 60% solvent dilutions, and the entire series for this study was obtained by polymerizing either the monomer or comonomer at 9:1 v/v solvent to monomer concentration at 60°C using azobis (methyl isobutyrate) as the initiator (2). The resultant polymers are precipitated in either reagent grade diethyl ether, water, or 60–90 petroleum ether and dried under vacuum to constant weight. These polymerization conditions are listed in Table III. The theoretical weight based on the initial comonomer composition and moles of monomer added was compared to the final dry weight of the precipitated polymer to establish the degree of conversion shown in the table.

TABLE III

Polymerization Data for the Methacrylate Copolymer Series Used in This Study

Copolymers (mole ratio)	Polymerization solvent	Precipitation solvent	Degree of conversion (%)
100 MMA	Toluene	60–90 pet ether	34
99 MMA/1 HEMA	Toluene	60–90 pet ether	44
95 MMA/5 HEMA	90 Toluene/10 EtOH	60–90 pet ether	48
75 MMA/25 HEMA	50 THF/50 EtOH	H_2O	46
50 MMA/50 HEMA	50 THF/50 EtOH	H_2O	44
25 MMA/75 HEMA	50 THF/50 EtOH	H_2O	23
5 MMA/95 HEMA	EtOH	Diethylether	83
1 MMA/99 HEMA	EtOH	Diethylether	85
100 HEMA	MeOH	Diethylether	
100 EMA	Toluene	60–90 pet ether	47
99 EMA/1 HEMA	Toluene	60–90 pet ether	47
95 EMA/5 HEMA	90 Toluene/10 EtOH	60–90 pet ether	44
75 EMA/25 HEMA	50 THF/50 EtOH	H_2O	43
50 EMA/50 HEMA	50 THF/50 EtOH	H_2O	25
25 EMA/75 HEMA	50 THF/50 EtOH	H_2O	61
5 EMA/95 HEMA	EtOH	Diethylether	72
1 EMA/99 HEMA	EtOH	Diethylether	77
All MEMA/HEMA	EtOH	Diethylether	62–70
All HEMA/MAA	MeOH	Diethylether	91–94
All HEMA/DMAEMA	MeOH	Diethylether	92–98

The dried polymers can then be stored and redissolved as needed in a suitable solvent for solvent spin-casting. When crosslinking is desired, hexamethylene diisocyanate is added just prior to casting. The desired amount is governed by the number of moles of polymer in solution. In all polymers and copolymers in this series, the casting solvent was spectral grade dimethyl formamide (Burdick and Jackson Laboratories). Depending on their casting properties, the polymer solutions were either 10 wt%/v or 1 wt%/v.

Film preparation. All polymers with the exception of the polyacrylamide were solvent spin-cast on smooth, particulate free borosilicate glass coverslips (Corning #2, 24 × 24 mm, Corning Glass Works, Corning, N. Y.). The coverslips are separated and inspected for gross scratches. Both surfaces of each coverslip are hand-washed in running tap water with Microclean and a cotton ball and then extensively rinsed in running distilled water. Coverslips are then transferred to a Class 100 laminar flow station, vertically positioned in porcelain slide holders (Coors Porcelain Co., Golden, Co.), immersed in hot chromic acid at 80°C for 5 min, rinsed three times in filtered (0.2 μm nominal) distilled water, rinsed three times in filtered (0.2 μm absolute) reagent grade methanol, and dried in Freon TMS vapor (DuPont) for one to 2 min. Coverslips are then stored in polypropylene slide containers which were previously cleaned by the same process until ready for polymer spin-casting.

Prior to casting, the polymer solutions were filtered through a 0.2-μm Fluoropore filter (Millipore Corp.) and stored in particulate-free brown glass bottles under argon until ready for use. The solutions were then transferred to the laminar flow station where

they were spin-cast on clean glass coverslip substrates using a Headway Research Model EC101 spinning apparatus at 4000 rpm for 20 sec to 1 min. Each coverslip required roughly 1 ml of solution to produce a smooth, uniform polymer film which completely covers the substrate. After casting, the films were placed in a nitrogen-purged particulate-free oven at 60°C for 3 hr. At this stage the polymer films are either returned to their polypropylene storage containers for future use, or transferred to bacteriological grade polystyrene petri dishes and extracted in distilled water overnight. The extracted, fully hydrated surfaces are then directly transferred to the contact angle apparatus.

Water contents and contact angle measurements. Water contents for the entire series were based on dry vs wet weights. The equilibrium water content was defined as follows:

$$\%H_2O = \frac{\text{wet weight} - \text{dry weight}}{\text{wet weight}} \times 100 \quad [7]$$

where the wet weight was determined by very lightly blotting the polymer with filter paper to remove excess surface water followed by a quick weight measurement. Realizing the inherent error in such a process, several wet measurements were obtained and averaged.

Contact angles were determined by measuring the dimensions of underwater captive bubbles of air, *n*-octane, and dodecane, as schematically illustrated in Fig. 1. This method has proven consistently more accurate and less ambiguous than conventional direct angle measurements, particularly for very small θ values.

The *n*-octane used was 99.99% pure (Aldrich Gold Label) and routinely monitored for purity by gas chromatography. The *n*-dodecane was also obtained through Aldrich with a stated purity of 99+%. Since the dodecane–water interfacial tension was in the expected range, no attempts were made to purify it further.

The contact angle apparatus consists of a traveling microscope with 15× eyepiece with fine right angle crosshairs and a 20× long working distance objective, a variable intensity light source, and a micrometer-adjustable X-Y stage vertically mounted on an optical bench. The stage contains a thermally jacketed Plexiglas box in which a chrome-plated adjustable iron plate is suspended. The coverslips are held on the underside of the plate with small magnets with the spin-cast polymer surface exposed. The container is then fitted with doubly distilled water and the plate containing the polymer film is carefully lowered into the container until the coverslip is completely immersed. While the polymer surface is re-equilibrating, the plate is leveled and aligned with the eyepiece crosshairs and the microscope focused on the polymer–water interface. A bubble of either air, *n*-octane, or dodecane with a volume of ~0.1 to 0.2 μl is formed on the end of a microliter syringe tip, positioned underneath the polymer surface, "snapped" from the tip by tapping the syringe with a finger, and allowed to rise to the polymer–water interface. This final geometry is shown in Fig. 1. The X-Y stage is adjusted via the micrometers until the microscope crosshairs are horizontally tangent to the contact point of the bubble with the surface and vertically tangent with one side of the maximum bubble width. Micrometer readings are taken and then the stage moved to place the maximum height of the bubble and opposite maximum bubble width at points of tangency with the crosshairs. These micrometer readings are then subtracted from the first set to produce a unitless height and width which is then substituted into the appropriate equation shown in the figure. Five air, five octane, and five dodecane bubbles were measured on each surface. Very small (0.5 μl) bubbles were used in order to minimize buoyancy corrections, and the immersion bath was maintained at 25 ± 1°C.

Liquid surface tensions were measured with a Fisher surface tensiometer using a 6-cm platinum–rhodium du Nuoy ring cleaned

before each use in an oxygen radiofrequency glow discharge (Plasmod, Tegal Corp.) for 5 min at 400 μm Hg.

RESULTS AND DISCUSSION

Since we did not attempt to determine the copolymer reactivity ratio or to control the comonomer feed rates in this study, the question of copolymer heterogeneity vs homogeneity logically arises. However, based on our past experience with these sytems and the work of several investigators on the same, or similar, copolymer series (12–16), it can generally be concluded that under our given set of molar ratios and polymerization conditions, random copolymerization is assumed with a reasonably narrow composition range. This random array has certainly been the case for copolymers of HEMA–MMA (12, 16), MMA–DMAEMA (13, 16), MMA–MEMA (15), and has been suggested for the MMA/MAA series, depending on the respective amounts of MAA and MMA (14). Exceptions likely exist, however, and some of the resultant scatter in the data to be presented may in fact be due to a lack of copolymer randomness.

Figure 5 presents the water content of the apolar–polar or hydrophobic–hydrophilic comonomer series as a function of comonomer composition. The results are generally identical for the hydrophobic comonomers, MEMA, MMA, and EMA copolymerized with the hydrophilic HEMA comonomer.

Table IV presents the experimental data measured for the methacrylate series and the polyacrylamide gels, listing the water contents, contact angle values, and the deduced interfacial parameters. The range given in the interfacial data is based on the standard deviation of the air and octane angles, i.e., combinations of the lowest and highest values for these angles were used in computing the interfacial values listed.

Figure 6 gives the γ^d_{SV} and γ^p_{SV} data as a function of water content for all of the data in Table IV plotted collectively. The line through the data points represents the "best fit" to a second degree polynomial regression. The scatter is not only a result of the experimental error involved in both the contact angle and water content determinations, but also is inherent in the assumptions involved in this treatment. The trends, however, are clear. The polar component of the surface tension, γ^p_{SV}, increases with increasing water content until it reaches its limiting value of 50.5 dyne/cm for pure water. Similarly, γ^d_{SV} decreases with increasing water content until it reaches the γ^d_{SV} of water, 21.6 dyne/cm, as its limiting value.

The related γ_{SV} and γ_{SW} data are plotted in Fig. 7, again fitting the data to a second degree polynomial. Note particularly that γ_{SW} decreases from the order of 20 dyne/cm even for relatively apolar surfaces and very rapidly approaches zero with increasing water content. At about 30 wt% water, the γ_{SW} is essentially zero within the detection limits of this method.

It is interesting to compare the contact angles of the charged comonomer–HEMA series. As seen in Table IV, the HEMA–MAA system shows no change in water uptake or measured contact angles with increasing concentration of the methacrylic acid

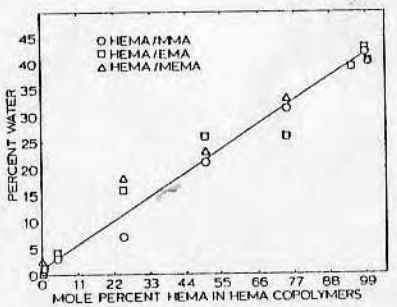

FIG. 5. Equilibrium water contents of the apolar (MEMA, MMA, EMA)–polar (HEMA) comonomer series as a function of comonomer composition.

TABLE IV

Experimental Data for the Methacrylate Ester and Polyacrylamide Polymer/Copolymer Series and Their Deduced Interfacial Properties

Polymer	X-Link (%)	H_2O (%)	Contact angles			Surface and interfacial energies (dyne/cm)			
			θ_{air}	θ_{octane}	$\theta_{dodecane}$	γ_{sv}^{h}	γ_{sv}^{o}	γ_{sv}	γ_{sw}
100 HEMA	1	40	15 ± 1	16 ± 1	18 ± 4	20.3/20.1	49.0/48.6	69.3/68.7	0.06/0.09
100 MMA	0	3	59 ± 2	89 ± 2		44.2/43.3	17.6/16.8	61.8/60.1	23.6/24.1
100 MEMA	0	2	48 ± 2	78 ± 1	74 ± 1	52.4/47.0	21.8/21.0	74.2/68	24.2/21.6
100 EMA	0	≤1	59 ± 2	81 ± 2	82 ± 1	31.2/29.9	21.0/19.3	52.2/49.2	13.9/15.3
99 HEMA/1 MMA	0	42	19 ± 2	18 ± 1	17 ± 2	21.3/20.3	48.1/47.5	69.4/67.8	0.06/0.13
95 HEMA/5 MMA	0	43	18 ± 2	19 ± 1	20 ± 1	21.3/20.3	48.1/47.5	69.4/67.8	0.06/0.13
75 HEMA/25 MMA	0	31	22 ± 1	32 ± 1	32 ± 1	24.1/24.1	43.4/42.5	68.2/66.6	0.7/0.8
50 HEMA/50 MMA	0	21	32 ± 1	49 ± 1	48 ± 1	30.0/30.1	36.2/35.2	66.2/65.3	3.7/4.1
25 HEMA/75 MMA	0	7	43 ± 2	66 ± 1	65 ± 2	40.4/37.0	27.4/26.4	67.8/63.4	12.5/11.6
5 HEMA/95 MMA	0	3	56 ± 4	79 ± 5	76 ± 4	32.8/33.2	23.6/19.3	56.4/52.5	12.0/16.5
1 HEMA/99 MMA	0	2	59 ± 1	86 ± 1	85 ± 1	40.4/39.6	18.4/17.6	58.8/57.2	20.6/21.1
75 HEMA/25 MEMA	1	33	16 ± 1	24 ± 2	22 ± 3	22.5/23.2	47.0/45.6	69.5/68.8	0.15/0.31
50 HEMA/50 MEMA	1	23	23 ± 1	37 ± 1	36 ± 1	26.5/26.6	41.7/40.8	68.2/67.4	1.34/1.54
25 • HEMA/75 MEMA	1	19	30 ± 1	53 ± 1	51 ± 2	34.2/34.4	34.2/33.2	68.4/67.6	5.97/6.47
99 HEMA/1 EMA	0	43	17 ± 1	16 ± 2	16 ± 1	20.3/20.6	49.0/48.1	69.3/68.7	0.06/0.08
95 HEMA/5 EMA	0	39	16 ± 3	20 ± 1	19 ± 1	22.5/20.9	47.5/47.0	70.0/67.9	0.11/0.14
75 HEMA/25 EMA	0	26	24 ± 1	36 ± 1	37 ± 1	25.3/25.3	41.7/40.8	67.0/66.1	1.13/1.32
50 HEMA/50 EMA	0	26	37 ± 1	55 ± 2	53 ± 1	30.0/32.1	33.2/31.3	63.2/63.4	4.9/6.6
25 HEMA/75 EMA	0	16	52 ± 1	69 ± 1	73 ± 2	25.9/25.4	26.4/25.5	52.3/50.9	7.9/8.5
5 HEMA/95 EMA	0	4	67 ± 1	90 ± 3	91 ± 2	28.5/32.9	17.6/15.3	46.1/48.2	16.8/21.2
1 HEMA/99 EMA	0	1	54 ± 1	75 ± 2	72 ± 3	29.8/31.7	23.6/21.8	53.4/53.5	11.0/13.3
99.9 HEMA/0.1 MAA	1	40	17 ± 2	17 ± 2	21 ± 4	20.8/20.3	48.6/47.5	69.4/67.8	0.05/0.13
99 HEMA/1 MAA	1	40	17 ± 3	16 ± 4	19 ± 1	20.6/20.3	49.4/47.5	70.0/67.8	0.04/0.13
97 HEMA/3 MAA	1	39	20 ± 1	19 ± 2	21 ± 1	19.8/20.1	48.1/47.0	67.9/67.1	0.14/0.18
99.9 HEMA/0.1 MAA	2	41	20 ± 1	22 ± 2	23 ± 2	20.3/20.7	47.5/46.3	67.8/67.0	0.13/0.20
99 HEMA/1 MAA	2	40	20 ± 2	20 ± 1	21 ± 1	21.1/20.1	47.5/47.0	68.6/67.1	0.09/0.18
97 HEMA/3 MAA	2	38	17 ± 2	19 ± 2	20 ± 1	21.3/20.9	48.1/47.0	69.4/67.9	0.06/0.14
99.9 HEMA/0.1 DMAEMA	1	40	19 ± 1	19 ± 1	20 ± 1	20.6/20.3	48.1/47.5	68.7/67.8	0.08/0.13
99 HEMA/1 DMAEMA	1	43	20 ± 2	25 ± 1	27 ± 1	22.5/21.5	46.3/45.6	68.8/67.1	0.20/0.25
97 HEMA/3 DMAEMA	1	59	25 ± 2	32 ± 1	33 ± 3	23.1/21.8	43.4/42.5	66.5/67.3	0.59/0.68
99.9 HEMA/0.1 DMAEMA	2	37	18 ± 2	21 ± 2	20 ± 1	21.9/20.9	47.5/47.0	69.4/67.9	0.09/0.14
99 HEMA/1 DMAEMA	2	40	22 ± 1	27 ± 1	27 ± 1	21.5/21.3	45.6/44.9	67.1/66.2	0.25/0.33
97 HEMA/3 DMAEMA	2	53	25 ± 1	30 ± 1	30 ± 1	22.1/22.0	44.2/43.4	66.3/65.4	0.43/0.55
Polyacrylamides	Most	78	17 ± 3	9 ± 5	9 ± 6	19.7/18.9	50.4/49.0	70.1/67.9	0.09/0.20
		84	16 ± 4	14 ± 2	17 ± 3	21.1/19.3	49.4/48.6	70.5/67.9	0.02/0.16
		90	16 ± 1	11 ± 3	15 ± 3	19.4/19.7	50.0/49.0	69.4/68.7	0.12/0.11
	Least	95	13 ± 5	13 ± 4	6 ± 5	21.7/20.6	49.7/48.1	71.4/68.7	0.01/0.08

comonomer. This indicates that the methacrylic acid is uncharged under the conditions of our contact angle measurement in distilled water. The distilled water in this case is essentially very pure, with a pH of approximately 6 and an ionic strength on the order of 10^{-6} mole/liter. Under such conditions the pK of methacrylic acid groups is on the order of seven or larger suggesting that the majority of methacrylic acid groups were not ionized during our measurement. The HEMA–MAA copolymer system would, thus, be identical to pure HEMA in this case, which is what the data imply.

The situation with the HEMA–DMAEMA copolymers, however, is quite different. As mentioned earlier, we actually used the hydrochloride salt of the DMAEMA comonomer. Under these conditions, the pK of the hydrogen-associated nitrogen in the amine is again on the order of seven or greater. Thus, at a pH of 6 the DMAEMA can be considered to be positively charged. Note from Table IV that clearly the water content increases with increasing DMAEMA content, indicating an increased hydrophilicity, and a corresponding change in the contact angle.

Comparing the contact angle data as a function of water content for one of the uncharged systems, we find as expected that the angles decrease with increasing hydrophilicity. This is shown in Fig. 8. If one examines the HEMA–DMAEMA copolymer system, however, we find that the angles increase with increasing comonomer content as shown in Fig. 9. If we were to correct for the change due to increased hydrophilicity the slope of the line in Fig. 9 would be even steeper. This suggests that the surface charge density of the charged copolymer series may significantly influence the interfacial properties, reflected by corresponding changes in contact angle. This is certainly not a new idea (18, 19) and it has recently been suggested that the contact angle may in fact be a method of probing surface charge density (20). Such behavior certainly merits further modeling and analysis in the future.

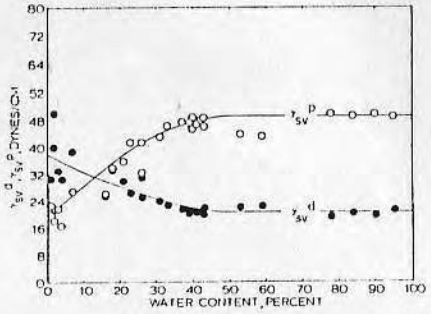

FIG. 6. The harmonic mean estimate of γ_{sv}^{d} and γ_{sv}^{p} via contact angle measurements as a function of copolymer equilibrium water content.

CONCLUSIONS

Using underwater contact angle techniques, water-immiscible liquids, and various assumptions regarding the work of adhesion, one can estimate the total surface tension (γ_{sv}), the dispersion (γ_{sv}^{d}) and polar (γ_{sv}^{p}) components, and the solid–water interfacial tension (γ_{sw}) for fully hydrated gel–water interfaces.

The data obtained appear to be very reasonable and correlate with similar data in the literature, particularly considering that most of the tabulated literature data for such polymers are based on advancing angles which tend to minimize the effects due to

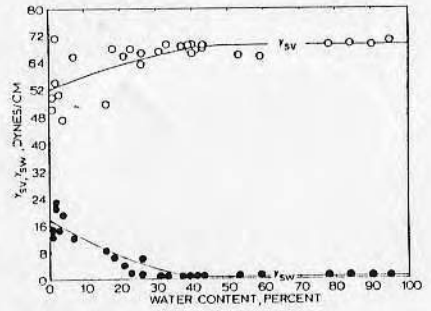

FIG. 7. The harmonic mean estimate of γ_{sv} and γ_{sw} as a function of copolymer equilibrium water content.

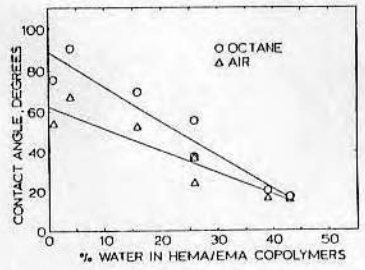

FIG. 8. Air and octane contact angle behavior as a function of water content in an uncharged HEMA–EMA copolymer system.

the hydrophilic character of the surface or interface.

For the polymer series used in this study, variations in the polar/apolar comonomer ratios were shown to produce a series of copolymers with a controllable and wide range of water contents. The solid–water interfacial tension (γ_{sw}) approaches zero with increasing water content and is essentially zero within the limits of this method at an equilibrium water content of approximately 30 wt% and above. Due to the many assumptions involved and the errors inherent in the data measurements, the method is generally insensitive to low values of γ_{sw}, and has considerable error in this region, by perhaps as much as ±5 dyne/cm.

There is some indication from contact angle studies utilizing polymer containing

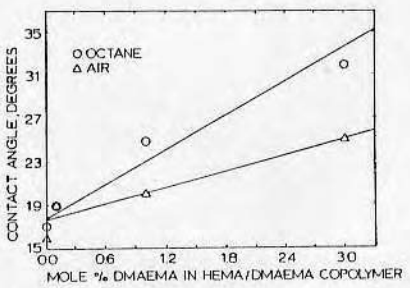

FIG. 9. Air and octane contact angle behavior as a function of water content in the charged HEMA–DMAEMA copolymer system.

surface charge that the surface charge density at the interface may be probed and characterized by contact angle methods.

A number of major research needs and priorities have been identified in this study. As illustrated by the self-consistent surface tensions and interfacial tensions of the *n*-alkane–water series, as required by the harmonic mean estimation of the interfacial free energy, it was shown that a much better approximation or estimate of nondispersive interactions at interfaces is needed.

Another need is a more direct method of accurately determining the surface and interfacial tensions of solids and solid–water interfaces, respectively. The relatively precise methods of measuring low interfacial tensions for liquid–liquid interfaces unfortunately do not apply to solids, and this is certainly a major limitation in the study of solid interfaces.

Finally, one disadvantage of contact angle methods is the inherent question of contact angle-induced deformation on a highly deformable gel system (10). This may lead to data errors and subsequent misinterpretation of the interfacial properties. It is very difficult to model such systems from a linear continuum mechanical approach, and this is another major need area if we must depend on contact angle methods to deduce interfacial information for highly hydrated systems.

ACKNOWLEDGMENTS

Portions of this work were supported by NIH Grant HL 16921-05 and by the Division of International Programs, National Science Foundation, Grant INT-78-24474. Portions of this work were presented at the National Science Foundation Workshop on Interfacial Phenomena, Seattle, Wash., 1979. The authors wish to thank S. Hattori, D. Coleman, and L. Smith for their contributions to this research.

REFERENCES

1. Andrade, J. D., *Med. Instrum.* 7, 110 (1973).
2. Gregonis, D. E., Chen, C. M., and Andrade, J. D., *in* "Hydrogels for Medical and Related Applications" (J. D. Andrade, Ed.), p. 88. ACS Symposium Series 31 American Chemical Society, Washington, D. C., 1976.
3. Hofstee, B. H. J., *J. Macromol. Sci. Chem.* **A10**, 111 (1976).
4. Andrade, J. D., Ma, S. M., King, R. N., and Gregonis, D. E., *J. Colloid Interface Sci.* 72, 488 (1979).
5. Wu, S., *J. Polym. Sci.* **34**, 19 (1971).
6. Wu, S., *J. Macromol. Sci. Revs. Macromol. Chem.* C10, 1 (1974).
7. Wu, S., *ACS Org. Coatings Plastic Chem. Preprints* 40, 19 (1979).
8. Aveyard, R., and Haydon, D. A., *Trans. Faraday Soc.* **61**, 2255 (1965).
9. Fowkes, F. M., *J. Phys. Chem.* **84**, 510 (1980).
10. Andrade, J. D., King, R. N., Gregonis, D. E., and Coleman, D. L., *J. Polym. Sci. Symp. C.* **66**, 313 (1979).
11. Gregonis, D. E., Russell, G. A., Andrade, J. D., and DeVisser, A. C., *Polymer* **19**, 1279 (1978).
12. Varma, I. K., and Patnaik, S., *Eur. Polym. J.* **12**, 259 (1976).
13. Tanabe, H., and Nakano, K., *Yakuzaigaku* **22**, 193 (1962), from *CA* 59, 7656 G (1963).
14. Ryabov, A. V., Kargin, V. A., Emel'yanov, D. N., and Turshatova, N. E., *Vysokomol. Soedin., Ser A* **9**, 319 (1967), from *CA* **66**, 8605r (1967).
15. Yakota, K., Kani, M., and Ishii, Y., *J. Polym. Sci., Ser A1* **6**, 1325 (1968).
16. Askill, I. N., Annis, D., and Gilding, D. K., *Trans Soc. Biomat.* 11 (1978).
17. Tanford, C., "Physical Chemistry of Macromolecules," Chapt. 8. John Wiley, New York, 1967.
18. Adams, N. K., and Jessop, G., *J. Chem. Soc.* 1863 (1925).
19. Bockris, J. O'M., and Reddy, A. K. N., "Modern Electrochemistry," Vol. 2, Chapt. 7. Plenum Press, New York, 1970.
20. Holly, F. J., *J. Colloid Interface Sci.* **61**, 435 (1977).

Proc. European Dialysis & Transplant Assoc.
Vol. 7, 1970

A Comparative Study of Membranes for Dialysis—Membrane Test Procedures

H KLINKMANN, J D ANDRADE, R L KIRKHAM and D J LYMAN
Medical Policlinic, University of Rostock, German Democratic Republic and the University of Utah, Salt Lake City, Utah, USA

During the last eight years, there has been a great increase in research on membranes for haemodialysis. Little of this work, however, has progressed into pre-clinical in vivo testing. Indeed, because of the lack of standardised membrane testing procedures, it is often difficult to even compare membranes from different laboratories.

The membrane is an important part of the artificial kidney device. While the dialyser design parameters such as blood channel height, blood channelling, pressure drop and flow rate relationships in both blood and dialysis compartments etc all contribute to overall dialysis performance, any fundamental change in solute transport or selectivity must reside in the membrane.

The purpose of this paper is to outline suggested membrane test procedures which will measure properties of membranes which are important to their performance in artificial kidney devices. These properties and their values are not to be used as criteria for determining the acceptability levels for membranes nor to guarantee clinical effectiveness of safety. They are, at this current state-of-the-art level, solely to be used to guide future membrane research and development. As a result, the authors envisage a continuing upgrading and modifying of these tests and procedures as our knowledge of chronic uraemia and its treatment grows.

EXPERIMENTAL

Materials

Cuprophane dialysis membrane (Seattle Artificial Kidney Supply Company, ultrafiltration of 0.27 ml/hr/in^2) is a regenerated cellulose membrane made by the cuprammonium process. The material was conditioned for use by soaking it for six days in several changes of distilled water to remove all additives (~13% by weight, consisting primarily of urea, diethylene glycol and glycerol) [Personal communication from W Bandel, J P Bemberg, Aktiengesellschaft].

The copolyether-ester membranes, based on polyoxyethylene glycol, were prepared by a modified solution polymerisation reaction (Lyman & Loo, 1967). The copolyether-hydrocarbon membrane is based on polyacrylonitrile and polyoxyethylene glycol (Lyman et al, 1970a). The polypeptide membrane is based on polysacrosine (Lyman et al, 1970b). The polyethylene/NVP membrane was prepared by radiation grafting N-vinyl pyrrolidone onto polyethylene film (Lyman et al, 1970c).

Two modified cellulose membranes, Cuenophane and Cadophane, were prepared by regenerating cellulose from cupriethylenediamine-hydroxide and cadmiumethylene-hydroxide, respectively (Klinkmann et al, 1970).

Nephrophane is a regenerated cellulose membrane made by the sodium cellulose xanthogenate process. This material has been post-treated by a special stretching technique and uses sorbitol and glycerin as additives to the slurry from which the membrane is case (Klinkmann et al, 1969, 1970).

The Union Carbide membranes (Neflex) are fibre reinforced cellulose membranes (Klinkmann et al, 1970). These are also called DVF membranes.

Apparatus

The dialysis cell used in these studies to obtain relative membrane dialysis characteristics is that developed by Lyman and Loo (1967). [See also Lyman et al, 1964, for detailed procedures.] The dialysis cell is stirred internally by a slow stream of nitrogen entering through a capillary which extends to the bottom of the dialysis cell; a circulating tube pump having a capacity of about 1 l/min is used to circulate the bath fluid. The dialysis cell is placed in a modified 1 l resin kettle which is used as the dialysis bath. The whole dialysis assembly is placed in a constant temperature bath maintained at 30^{o}C (+ 0.1^{o}) (Figure 1).

To obtain more definitive membrane properties, two additional diffusion cells are used.

The modified diffusion cell used to obtain filtration coefficients, Lp, and reflection coefficients, σ, is shown schematically in Figure 2 (Fritzinger et al, 1970).

A Leonard-Bluemle cell (Kaufmann, 1965) is used to obtain solute permeability coefficients, ω (shown schematically in Figures 3 and 4). This cell utilises stirrers on either side of the membrane to minimise any boundary layer effects in solute permeability. The sampling port has been modified from the original syringe-type stopcock to a rubber septum similar to that found in a gas chromatograph injection port. With the modified sampling port, a syringe can be used, and with the proper length needle samples can be withdrawn from the centre of the cell.

Ultrafiltration data were also routinely obtained using the Amicon ultrafiltration cell, model 401 (Table I).

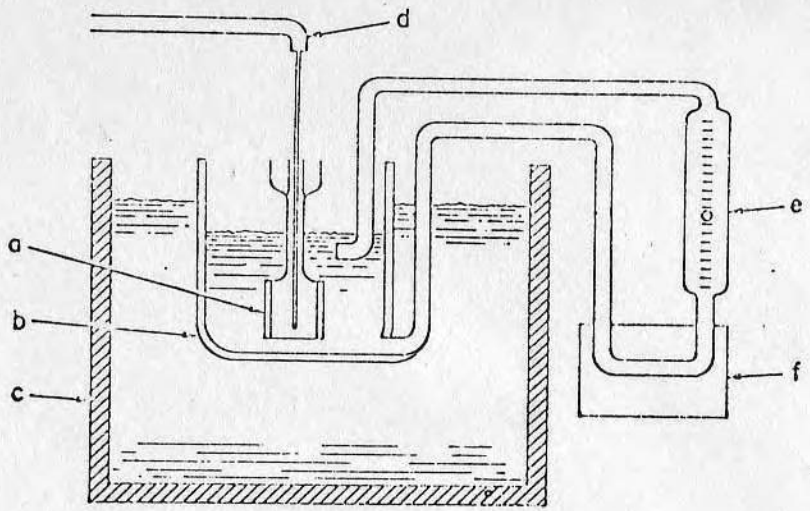

Figure 1. Schematic drawing of Dialysis Assembly.
(a) Dialysis cell; (b) Modified cylindrical flask; (c) Constant temperature bath;
(d) Circulating pump; (e) Nitrogen bubbler

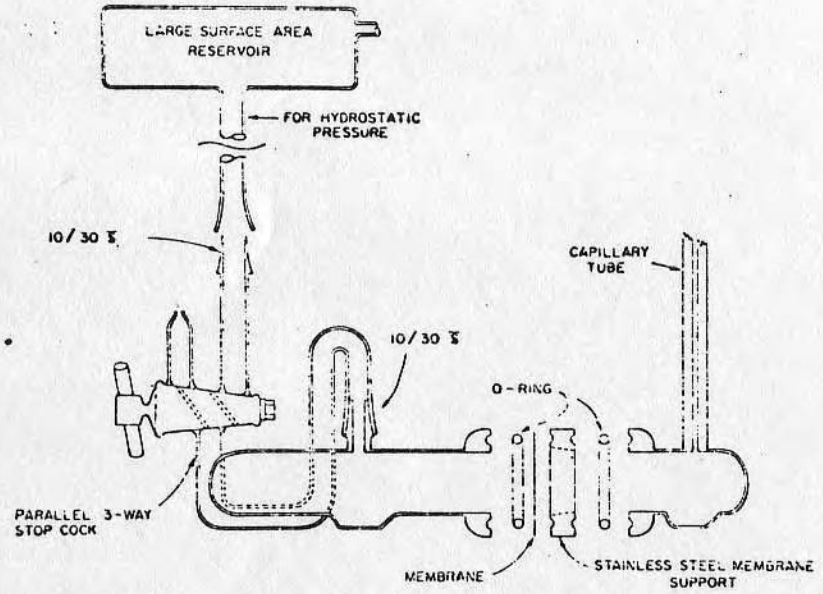

Figure 2. Schematic drawing of cell used to measure volume flow for filtration and reflection coefficients

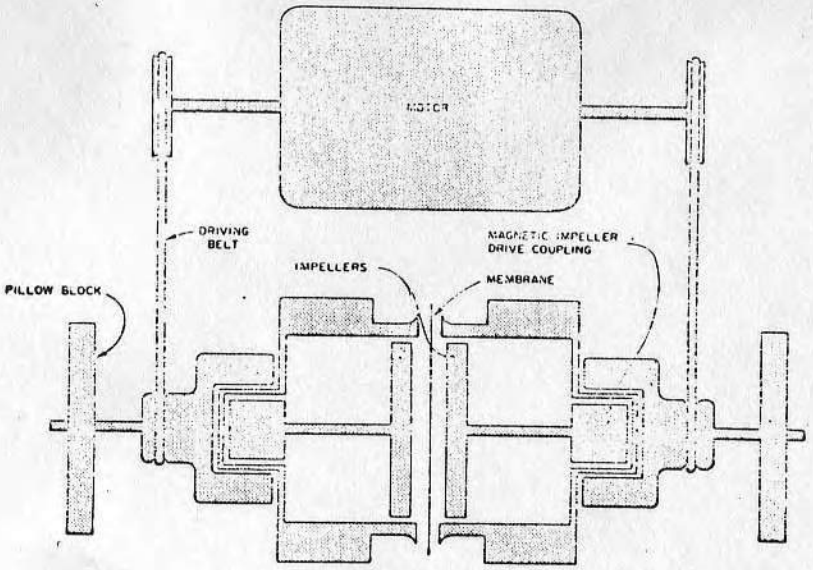

Figure 3. Schematic drawing of Leonard-Bluemle cell

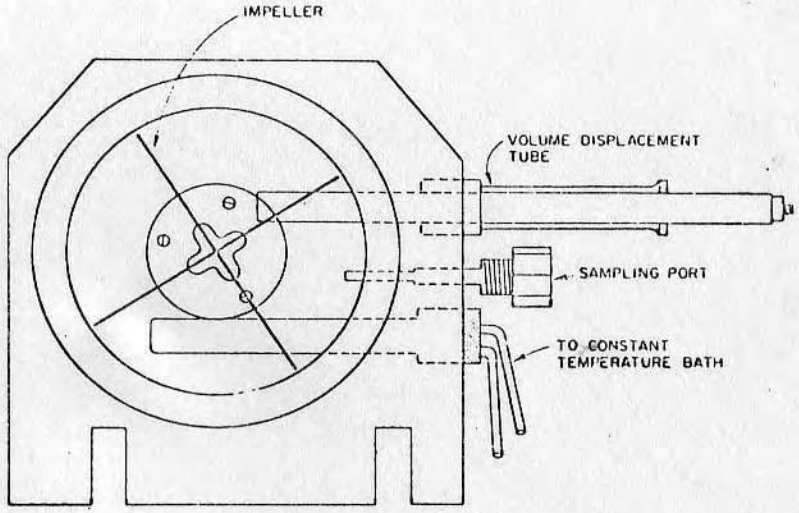

Figure 4. Schematic drawing of the Leonard-Bluemle cell looking inside the right compartment

Table I. Ultrafiltration data for various membranes

Membrane	Wet Membrane Thickness, mils	Ultrafiltration ($ml/min/cm^2 \times 10^{-2}$)
Cadophane I	6.5	1.946
Cadophane II	5.8	0.484
Cadophane III	1.8	0.055
Cuenophane	0.5	0.210
Nephrophane	1.8	0.133
Neflex 22A (DVF)	4.4	0.080
Neflex 24 (DVF)	6.5	0.043
Cuprophane	0.9	0.050

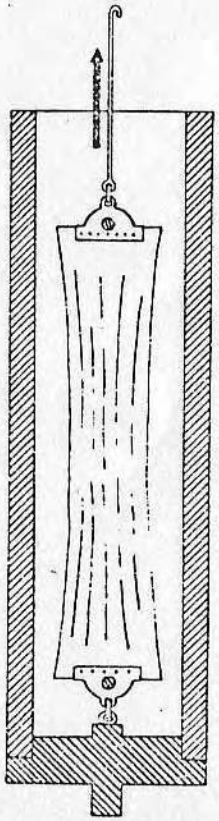

Figure 5. Wet tensile test cell

The mechanical properties of wet membranes were measured using the simple cell shown in Figure 5, which is designed and constructed to permit the tensile testing of membranes in water or in dialysate solution. The wet membrane sample (13 x 150 mm) is first clamped in the grips such that the actual sample test length is 100 mm. One of the grips is attached to the bottom connector of the tensile cell. The other grip is attached to the moveable crosshead. The cell is filled with water, and the test is conducted at a crosshead speed of 5 mm/min.

The wet burst pressure (ASTM, 1969a) of a membrane was determined by measuring the pressure required to rupture a 25 mm diameter circular sample. The membrane sample is clamped between two rubber O-rings in the test cell (Figure 6) then immersed in water and nitrogen pressure applied until rupture occurs.

RESULTS

In relative dialysis measurements, aliquots of solution were removed from the dialysis bath at specific intervals and analysed. Semi-log plots of percent solute remaining versus time allows determination of the half-time

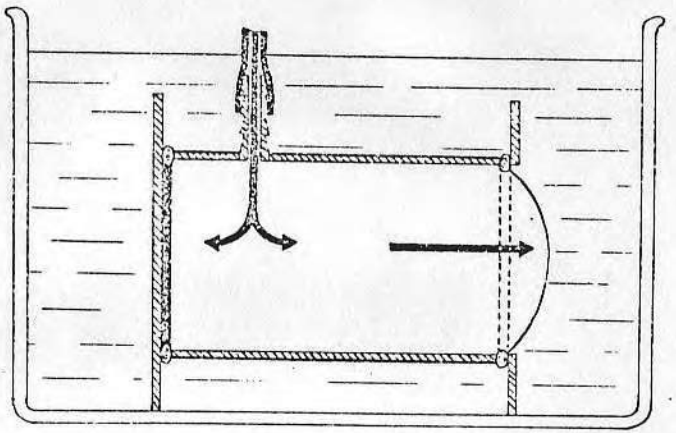

Figure 6. Burst test cell

rate of transport value ($T_{\frac{1}{2}}$). Typical data are reported in Table II. Since the parameters of cell volume, bath volume membrane area, solute concentration, temperature, etc are accurately controlled, diffusion coefficients are easily calculated from the above data.

In the determination of the filtration coefficient, Lp, the volume flow (cc/sec per unit membrane area) was determined by measuring the change in liquid height in the capillary as a function of time. Lp is calculated from: $Lp = (J_v/\Delta P)$, at zero osmotic pressure.

These data are tabulated in Table III.

Using the same cell, the reflection coefficient, σ, can be determined from the ratio of the volume flow, J_v, to the product of the filtration coefficient, Lp, and the osmotic pressure difference, $\Delta\pi$, when the applied press- ΔP, is zero.

$$\sigma = -(J_v/Lp\,\Delta\pi)_{\Delta P} = 0$$

However, experimentally it is often easier to measure the volume flow when a hydrostatic pressure is applied across the membrane. The complete expression for σ is then

$$\sigma = \frac{J_v - Lp\Delta P}{Lp\,\Delta\pi}$$

The reflection coefficient was determined by two procedures making use of both expressions for σ (data tabulated in Table III). In both cases, the right comparment contained 0.1 M solution, while the left contained water; $\bar{c}_s$ = 0.05 M, and $\Delta\pi$ is negative for this configuration.

Determination of permeability coefficients of the membrane is done on the Leonard-Bluemle cell (Kaufmann, 1965; Fritzinger et al, 1970; Lyman

Table II. Relative half-time rates of transport of various compounds

COMPOUND	MOL.WT.	HALF-TIME RATES								
		Cuprophane	Cellophane	Nephrophane	Cuenophane	Cadophane I	Cadophane II	Cadophane III	Neflex[a] 22A	Neflex[a] 24
Urea	60.8	68	73	60	172	21	24	87	193	236
L-alanine	89.1									
B-alanine	89.1									
Creatinine	113.1	123	145	105	358	36	46	166	342	370
Uric Acid	168.1	320								
Ascorbic Acid	176.1	178								
Glucose	180	223								
Thiamine Chloride	337.3	160								
Sucrose	342	270	326	267	660	68	63	396	755	685
Raffinose	5045	450								
Bacitracin	1411	720								
Polysarcosine	6700	15% in 30 hr.								
Insulin[b]	12000	None								

COMPOUND	HALF-TIME RATES (cont.)														
	Copolyester[c] I	II	III	IV	V	Copolyurethane I	II	III	IV	V	VI	Polyether-hydrocarbon	Polypeptide	Polyethylene/NVP I	II
Urea	58	118	125	106	71	122	153	164	195	115	144	349	92	286	106
L-alanine		505				288	782	492	1075	870					
B-alanine		355				264	782	1070	1425		295	374	264		
Creatinine	117					214	364	309	406	360					
Uric Acid	217														
Ascorbic Acid	135	403				244	312	369	437		300	353			
Glucose	268	403	1180	952	304	390	820	665	1340	1080	837	705	241	1104	414
Thiamine Chloride	150														
Sucrose	397	1050													
Raffinose	930														
Bacitracin	568														
Polysarcosine	36% in 30 hr.														
Insulin[b]	26% in 30 hr.														

[a] Not corrected for membrane thickness: Neflex 22A was 4.4 mils; Neflex 24 was 6.5 mils wet thickness.

[b] At this pH and concentration (1 mg/ml) the insulin may be present as the dimer.

[c] Data from refs.; Lyman et al., 1964; Lyman and Loo, 1967; Lyman et al., 1970.

Table III. Filtration, reflection, and permeation coefficients, per unit membrane area, 30°C

Membrane/Solute	Normalized Lp $cm^3 dyne^{-1} sec^{-1}$	σ Unitless	Normalized ω moles $dyne^{-1} sec^{-1}$
Cuprophane:			
Urea	12.02×10^{-14}	0.026	10.68×10^{-17}
Glucose	10.15×10^{-14}	0.088	2.41×10^{-17}
Sucrose	8.58×10^{-14}	0.174	1.67×10^{-17}
Copolyester:			
Glucose	6.56×10^{-14}	0.314	1.72×10^{-17}

& Yum, 1970) at stirrer speeds ranging from 150 to 600 RPM. The initial and final concentrations of solute in the right side of the cell are measured, and the permeability coefficient calculated as follows:

$$U = \frac{\ell n[(1 + \frac{V_1}{V_2})\frac{\sigma}{\sigma_2} - \frac{V_1}{V_2}}{S(\frac{1}{V_1} + \frac{1}{V_2})t}$$

where U = permeability coefficient; t = measurement time; V_1, V_2 are the volumes of the left and right compartments; and s is the membrane area. The data are tabulated in Table III.

The stress-strain characteristics of the membrane are measured in both the parallel and transverse direction (ASTM, 1969a). Typical curves are shown in Figure 7. The thickness of the membrane is measured in its wet state before the test. The data recorded here were obtained with a light wave micrometer.

Stress was determined by calculating the load over the cross sectional area (Table IV). The time axis of the curves were converted to strain. The modulus value recorded is the break modulus or modulus at fracture, i.e. the slope of the dotted lines in Figure 7. Definitions and explanations of the terminology used in the mechanical characterisation of materials are available in the literature (ASTM, 1969b).

The wet burst pressure was determined by measuring the pressure required to rupture a circular sample, using a procedure similar to that described by the ASTM as D774-67 (ASTM, 1969c). The cell is connected to a pressure source and gauge and then immersed in water. Pressure is applied

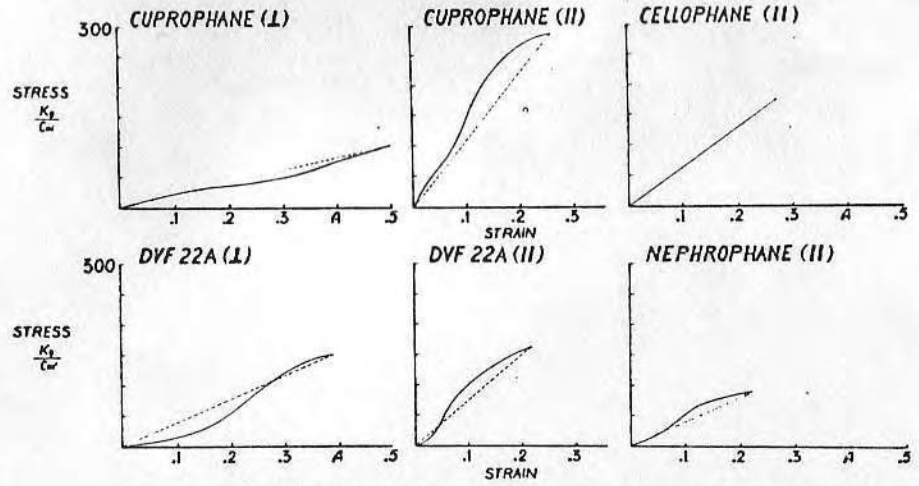

DOTTED LINE DENOTES LINE USED FOR FRACTURE MODULUS DETERMINATION
⊥ : TEST SAMPLE CUT PERPENDICULAR TO ROLL DIRECTION
II : TEST SAMPLE CUT PARALLEL TO ROLL DIRECTION

Figure 7. Stress-strain characteristics of membranes

in 50 mm Hg increments until rupture occurs. The burst pressures are tabulated in Table IV.

As a preliminary report, twelve clinical trials at the University of Utah confirmed some of our in vitro testing results. Self-wound coils with Neflex (Union Carbide) membrane (surface $1m^2$) showed an average clearance for urea of 109.6 ml/min and for creatinine, 75.5 ml/min. The small self-wound nephrophane coils (surface $0.3m^2$) showed the following mean values for clearances: urea, 98.4 ml/min; creatinine, 86 ml/min; uric acid, 87 ml/min; phosphorus, 81.3 ml/min.

DISCUSSION AND CONCLUSION

In the development or selection of new polymer membranes for use in artificial kidney devices, it would be desirable to have property values which are related to their in vivo performance. These would include solute permeability, ultrafiltration, mechanical strength, toxicology, and blood compatibility and thrombogenicity.

Several tests are proposed for determining the bulk properties of membrances which relate to their use in artificial kidney devices. It must be kept in mind, however, that these values are not to be used to determine the aaceptability levels for membranes, but are only guides to help select membranes which might be used in a particular experimental situation.

At the present state-of-the-art, no tests are proposed for the toxicology, and blood compatibility and thrombogenicity properties. It is obvious, of course,

Table IV. Typical mechanical property data for various membranes*

MEMBRANE**	FRACTURE LOAD (Kg)	FRACTURE STRESS Kg/cm^2	FRACTURE ELONGATION %	FRACTURE MODULUS Kg/cm^2	WET THICKNESS (mm)	BURST PRESSURE (mmHg)
Cellophane-11	1.2	210	32	640	0.045	520-570
Cuprophane-11	0.7	290	26	1160	0.020	260-370
Nephrophane-11	0.5	100	22	422	0.046	210-260
Neflex 13-11 (DVF)	2.6	175	24	730	0.117	>760
Neflex 14-11	2.4	160	21	750	0.120	>760
Neflex 16-11	2.5	155	20	775	0.127	>760
Neflex 22A-11	2.4	165	22	750	0.117	>760
Cuprophane-1	0.3	110	51	210	0.020	
Nephrophane-1	0.2	30	45	70	0.046	
Neflex 13-1	1.9	130	43	300	0.117	
Neflex 14-1	2.0	130	39	330	0.120	
Neflex 16-1	1.6	100	35	290	0.127	
Neflex 22A-1	2.2	150	40	380	0.117	

*American Society for Testing and Materials Standards--D882-67

**11 denotes sample cut parallel to roll direction
1 denotes sampel cut perpendicular to roll direction

that toxic extractables should be excluded from any membrane polymer. While preliminary tests have been reported (Lyman et al, 1968 and 1970) for determining the blood compatibility of polymer surfaces, and have been extended to include hydrophilic surfaces, little is known of chronic toxicology effects resulting from blood damage occurring at the polymer surface.

ACKNOWLEDGMENT

Much of the research summarised in this paper was supported by the National Institute of Arthritis and Metabolic Diseases, Artificial Kidney - Chronic Uremia Program, contract numbers PH-43-66-493, PH-43-68-1027, and NIH 70-2017.

REFERENCES

American Society for Testing and Materials (ASTM) (1969a) Book of ASTM Standards, D882-67, Part 27

American Society for Testing and Materials (ASTM) (1969b) Book of ASTM Standards, D638-68

American Society for Testing and Materials (ASTM) (1969c) Book of ASTM Standards, D774-67, Part 15

Fritzinger, B. K., Bauman, S. K. and Lyman, D. J. (1970) Journal of Biomedical Materials Research. In press

Kaufmann, T. G. (1965) Ph.D. Thesis, Columbia University, New York

Klinkmann, H., Holtz, M., Willgerodt, W., Wilke, G. and Schoenfelder, D. (1969) Proceedings of the European Dialysis and Transplant Association. Volume V. Page 78. Excerpta Medica, Amsterdam

Klinkmann, H., Lyman, D. J., Kirkham, R. J., Kulshrestha, V. K. and Kolff, W. J. (1970) Transactions. American Society for Artificial Internal Organs, 16, 121

Lyman, D. J., Loo, G. H. and Crawford, R. W. (1964) Biochemistry, 3, 985

Lyman, D. J. and Loo, B. H. (1967) Journal of Biomedical Materials Research, 1, 17

Lyman, D. J., Brash, J. L., Chalkin, S. U., Klein, K. G. and Carini, M. (1968) Transactions. American Society for Artificial Internal Organs, 14, 250

Lyman, D. J., Klein, K. G., Brash, J. L. and Fritzinger (1970a) Thrombosis et Diathesis Haemorrhagica, 23, 120

Lyman, D. J. and Yum, I. S. (1970b) Manuscripts in preparation

Lyman, D. J., Loo, B. H., Yum, I. S., Stephens, C. C. and Hamilton, R. D. (1970c) Manuscripts in preparation

ASSOCIATION OF GRAFT COPOLYMERS OF ALKYL METHACRYLATES WITH α-METHYL-ω-HYDROXY-POLY(OXYETHYLENE) METHACRYLATES

Čestmír KOŇÁK[a], Zdeněk TUZAR[a], Pavla KOPEČKOVÁ[b], Joseph D. ANDRADE[b] and Jindřich KOPEČEK[b]

[a] *Institute of Macromolecular Chemistry, Academy of Sciences of the Czech Republic, 162 06 Prague 6, Czech Republic*

[b] *Department of Bioengineering and Department of Pharmaceutics and Pharmaceutical Chemistry, University of Utah, Salt Lake City, Utah 84112, U.S.A.*

Received February 21, 1995
Accepted May 28, 1995

Dedicated to Dr Blahoslav Sedláček on the occasion of his 70th birthday.

Solution properties of the statistical copolymers of alkyl methacrylates (AMA) with α-methyl-ω-hydroxy-poly(oxyethylene) methacrylates (MPOEMA) (nonionic polysoaps) were studied using static and dynamic ligh scattering as a function of monomer composition and concentration in aqueous and methyl cellosolve solutions. The solubility of the copolymers in water was found to be dependent on molar contant of AMA. While copolymers with low content of hexyl methacrylate (HMA) (0 and 20 mole %) were directly soluble in water, forming true solutions with a low content of large swollen aggregates, copolymers with a higher content of HMA or lauryl methacrylate (LMA) were not directly dispersable in water. A special procedure, the stepwise dialysis from methyl cellosolve solutions against water, had to be used to prepare them in the pseudomicellar form. The copolymers were directly soluble in methyl cellosolve and its water solution containing up to 60 vol.% of water. Nevertheless, the light scattering experiments were dominated by light scattering of swollen particles of aggregated copolymer molecules. The copolymers were not soluble in the mixtures containing 70–100 vol.% of water. Paramaters of aggregates in the mixture with 60 vol.% of water and in pure water were found to be very similar.

Block copolymers associate and form micelles in selective solvents (i.e., good solvents for one block and precipitants for the other). Micellization of block copolymers has been shown to obey the model of closed association[1,2]. There has been tremendous progress over the past decade in the theory of block copolymer micelle formation[3–8]. Recently, interest in the formation of water-soluble micelles with hydrophobic cores and hydrophilic shells from hydrophobic/hydrophilic diblock and triblock copolymers has rapidly increased[9–15]. The motivation of this activity, besides an effort to understand the structure, thermodynamics of micellar equilibria, and kinetics of micelle formation, as well as other properties, has been the application of micelles in the

40. Tuzar Z., Kratochvíl P.: Collect. Czech. Chem. Commun. *32*, 3358 (1967).
41. Koňák Č., Štěpánek P., Sedláček B.: Czech J. Phys., A *34*, 497 (1984).
42. Štěpánek P. in: *Dynamic Light Scattering: The Methods and Some Applications* (W. Brown, Ed.), p. 177. Clarendon Press, Oxford 1993.
43. Provencher S. W.: Makromol. Chem. *180*, 201 (1979).
44. Gnanou Y., Lutz P.: Makromol. Chem. *190*, 577 (1989).
45. Zhou Z., Chu B.: Macromolecules *21*, 2548 (1988).
46. Lally P., Price C.: Polymer *15*, 325 (1983).
47. Tuzar Z., Bahadur P., Kratochvíl P.: Makromol. Chem. *182*, 1752 (1981).
48. Nyrkova I. A., Khokhlov A. R., Doi M.: Macromolecules *26*, 3601 (1993).
49. Ringsdorf H., Venzmer J., Winik F. M.: Macromolecules *24*, 1678 (1991).
50. Ringsdorf H., Simon J., Winik F. M.: Macromolecules *25*, 5353 (1992).
51. Koňák Č., Kopečková P., Kopeček J.: Macromolecules *25*, 5451 (1992).
52. Koňák Č., Kopečková P., Kopeček J.: J. Colloid Interface Sci. *168*, 235 (1994).

last page

lled release of hydrophobic substances into aqueous media[12,16]. In spite of an preparation of graft copolymers[17], their micellization has received less attention theorists and experimental scientists; these copolymers, however, are believed to remendous commercial significance and engineering interest.

articularly interesting class of water-soluble polymers are the polysoaps[18–29], having ydrophobic and hydrophilic pendant groups (side chains) distributed along the one. They can be visualized as a large number of surfactant moieties attached as hains to the polymer backbone. Both ionic and nonionic polysoaps has been re- d by several authors[18,27–29]. Aqueous solutions of such polymers are characterized w viscosity and high solubilization capacity[20,30]. These properties reflect an aggre- n (association) of the surfactant side chains providing hydrophobic microdomains l "polymeric micelles". The detailed structure of these "polymeric micelles" is ubject to discussion. Two major models have been proposed which have been ed to as "local micelles"[30–32] and "molar micelles"[33–35]. The "local micelle" as- s the intermolecular aggregate of limited number of neighbouring surfactant side s. The model of the "molecular micelle" assumes the formation of at least mon- ecular micelles by aggregation of all side chains of a given macromolecule into ggregate. This model was recently treated theoretically[36,37]. As only few ex- ental data are available, none of the polysoap models can be rejected. Fluores- quenching and neutron scattering studies support the "local micelle" model[38], eas theoretical treatments favour the "molecular micelle" model[36,37].

order to address the issue, statistical copolymers of alkyl methacrylates (AMA) α-methyl-ω-hydroxy-poly(oxyethylene) methacrylates (MPOEMA), which can be ded as graft copolymers AMA-*graft*-MPOE (nonionic polysoaps) were studied static (SLS) and dynamic (DLS) light scattering methods as a function of mer composition and concentration in aqueous and methyl cellosolve solutions. e graft copolymers were originally suggested as compounds which produce (oxyethylene)-rich surfaces on hydrophobic medical materials[25,26] by a simple ng treatment. Such modified surfaces are effective in decreasing protein adsorption cell adhesion. The graft copolymers similar to block copolymer surfactants, such as nic[39], are suitable as drug delivery systems. These AMA-*graft*-MPOE copolymers selected for this study because of the possibility of the tailor-made synthesis of copolymers with various compositions permitting a systematic evaluation of the ionship between their structure and properties. The objective of this study was nd the relation between monomer composition of the graft copolymers and their bility and/or association in water, methyl cellosolve and water/methyl cellosolve ures.

EXPERIMENTAL

Monomers and Chemicals

α-Methyl-ω-hydroxy-poly(oxyethylene) methacrylate with the molar mass of starting POE of 1 900 g/mol (MPOEMA-1900) and 4 000 g/mol (MPOEMA-4000) were prepared by the procedure described in our previous paper[25].

Methyl methacrylate (MMA), hexyl methacrylate (HMA) and lauryl methacrylate (LMA) (Polyscience) were freshly distilled under reduced pressure before use.

2,2′-Azobisisobutyronitrile (AIBN, Aldrich) was purified by recrystallization from methanol and used as an initiator for polymerization.

AMA-MPOEMA Copolymers

The copolymers were prepared by radical polymerization of monomers in toluene at 50 °C for 45 h (Table I).

A polymerization mixture, containing 14.0 wt.% of monomer, 0.6 wt.% of AIBN and 85.4 wt.% toluene, was bubbled with nitrogen for 15 min and then sealed in an ampoule. After the polymerization was finished, polymers were precipitated into cool diethyl ether, washed and dried. To remove non-polymerized macromonomer (about 10–20%, as determined by GCP) the polymers containing POE-1900 were dialyzed for 3 days in a Visking dialysis tubing (molar mass cut-off, 6 000–8 000 g/mol). The polymers containing POE-4000 were purified by using ultrafiltration (Amicon, membrane PM-30) and isolated by lyophilization. The yields of polymers were 60–70%. Monomer composition and molecular characteristics of the copolymers prepared and investigated are summarized in Table I and their structure is shown in Scheme 1.

TABLE I
α-Methyl-ω-hydroxy-poly(oxyethylene) methacrylate–alkyl methacrylate copolymers: monomer composition (mole %)

Copolymer	MPOEMA-1900	MPOEMA-4000	MMA	HMA	LMA
1[a]	80	–	20	–	–
2[b]	80	–	–	20	–
3	40	–	20	40	–
4	25	–	20	55	–
5	20	–	20	60	–
6	25	–	20	–	55
7	–	20	20	60	–
8	–	20	20	–	60
9	–	10	20	–	70

[a] M_{wu} 1 900, M_{wu}/M_{nu} 2.5; [b] M_{wu} 2 000, M_{wu}/M_{nu} 2.4 (M_{wu} and M_{nu}, mass- and number-average molar masses of unimers; M_{wu}/M_{nu} determined by GPC)

As most of the copolymers were not soluble in water (Table I, copolymers 3–9), a special procedure introduced in refs[11,25] was used for preparation of aqueous solutions for light scattering measurements. Copolymer was first dissolved in methyl cellosolve at ≈ 100 °C and the solution was dialyzed against water/methyl cellosolve mixtures. Five mixtures with water contents successively increasing by 20% were used and the last dialysis was against water. Typical concentration of copolymer used for dialysis was 1–2 . 10^{-3} g ml^{-1}. The solutions were diluted to the concentrations needed.

Copolymers 1 and 2 were analyzed on a 1.6 × 80 cm column packed with Sepharose 4B and 6B (1 : 1) and eluted with 0.05 M Tris buffer pH 8.0, which was 0.5 M in NaCl. Molar mass averages were estimated using PEG standards (molar mass 2 000–22 000 g mol^{-1}).

Static Light Scattering (SLS)

Static light scattering measurements were performed with a Sofica instrument, equipped with a He-Ne laser (vertically polarized, λ = 633 nm) in the angular range 30–150 °C. The processed data are represented (unless otherwise noted) as

$$Kc/\Delta R(0) = 1/M_w + 2A_2c \ , \qquad (1)$$

where M_w is the mass-average molar mass, K is the optical constant which includes the square of the refractive index increment, $\Delta R(0)$ is the excess Rayleigh ratio, proportional to the intensity of light scattered from the copolymer particles, extrapolated to zero angle of measurement, A_2 is the second virial coefficient, and c is the copolymer concentration in g ml^{-1}. Refractive index increment of copolymer solutions in water and methyl cellosolve, $(dn/dc)_\mu$, was measured with a Brice–Phoenix differential refractometer after equilibrium dialysis of copolymer solutions against corresponding solvents, as described elsewhere[40]. For the aqueous solutions of copolymers effective value of $(dn/dc)_\mu$ lay in the range 0.125–0.136. For solutions in methyl cellosolve $(dn/dc)_\mu$ were about 0.073 ± 0.002.

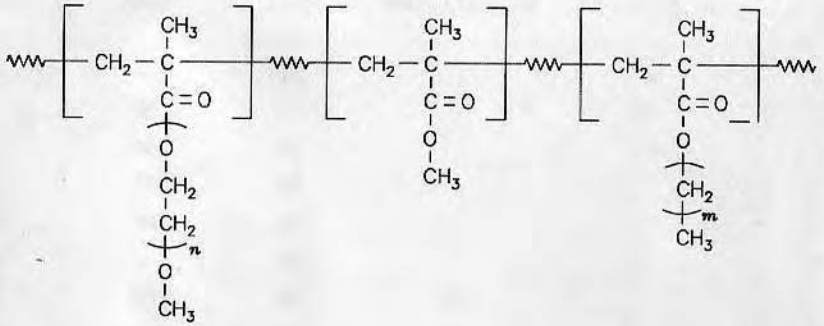

MPOEMA–1900 or MPOEMA–4000 | MMA | HMA (m = 5) or LMA (m = 11)

SCHEME 1

Dynamic Light Scattering (DLS)

olarized DLS measurements were made using the apparatus and technique described previously[41]. n argon ion laser (λ_0 = 514.5 nm) was the light source. An ALV 5000, multibit, multi-tau autoorrelator was operated with 32 simultaneous sampling times covering approximately 12 decades in elay time. The samples were thermostatted in a refractive index matching liquid (*m*-xylene).

Two different methods were used to analyze the multi-tau autocorrelation functions:

(*1*) The inverse Laplace transformation using the REPES method[42] of constrained regularization, hich is similar in many respects to the inversion routine[43] CONTIN, to obtain a distribution $\tau A(\tau)$ f decay timer τ, according to

$$g^2(t) - 1 = [\int_0^\infty A(\tau)\exp(-t/\tau)d\tau]^2 \ , \qquad (2)$$

here $g^2(t)$ is the measured normalized autocorrelation function of scattered light. REPES directly inimizes the sum of the squared differences between the experimental and calculated intensity time orrelation functions using nonlinear programming. This method uses an equidistant logarithmic grid ith fixed components (here a grid of 10 components per decade) and determines their amplitudes, $A(\tau)$.

(*2*) The forced fit of experimental correlation functions to functions calculated under the assumption that the distribution of the relaxation times can be described by the Pearson V distribution:

$$A(\tau) = \tau_0^p \tau^{-(p+1)} \exp(-\tau_0/\tau)/\Gamma(p) \ , \qquad (3)$$

here τ_0 determines the position of the distribution on the τ axis and p its width; Γ is the gamma nction. The results of iteration procedure are parameters of distribution τ_0 and p.

From characteristic decay times τ_i (peak positions of $\tau A(\tau)$) of dynamic modes (i = f, fast or s, ow), apparent diffusion coefficients, D_{ai}, were obtained from the equation

$$D_{ai}(q) = 1/\tau_i q^2 \ , \qquad (4)$$

here q is the length of scattering vector ($q = 4\pi n_0 \sin(\theta/2)/\lambda_0$), where n_0 is the refractive index of e solvent and λ_0 the wavelength of used light (514.5 nm). The diffusion coefficients, D_i, were obined by extrapolating D_{ai} to zero scattering angle and zero copolymer concentration.

RESULTS AND DISCUSSION

raft copolymers used in this study were prepared by radical copolymerization of hyrophobic monomers (MMA, HMA or LMA) with a hydrophilic macromonomer ω-methyl-ω-hydroxy-poly(oxyethylene) methacrylate). Consequently, the copolymer olecules under study have different chemical composition. The compositional hetegeneity is generally the higher, the larger the difference in copolymerization paraeters is. Both the conventional monomers and the macromonomers used in this study re methacrylates with various alkyl ester groups. As polar effects of alkyl ester parts

do not differ substantially and the lengths of macromonomer side chains used in this study should not have a pronounced effect on the macromonomer reactivity[44], the copolymerization parameters should be similar for all combinations of monomers used. The discussion of the structure–solution properties relationship in this paper is based on the composition of the monomer mixture. We are aware that the real copolymer composition is slightly different from the starting one used in Table I.

The solubility of AMA-*graft*-MPOE copolymers in water was found to be a function of molar content of conventional hydrophobic comonomers. While copolymers 1 and 2 with low content of HMA (0 and 20 mole %) were soluble in water, forming true solutions with a low content of large swollen aggregates (see Fig. 1), copolymers with higher contents of HMA or LMA were not dispersable in water. A special procedure had to be used to prepared them in the pseudomicellar form in water. Thus, the proper hydrophilic/hydrophobic balance in these copolymers seems be the decisive factor in determining their solution properties.

The solution properties of water-soluble AMA-*graft*-MPOE copolymers (1 and 2) are complex. This is demonstrated in Fig. 1, where the decay time distribution functions $\tau A(\tau)$, obtained by the inverse Laplace transformation of multisampling time correlation functions, are plotted for an aqueous solution of the copolymer 2. The decay time distribution functions are bimodal. The two well-separated bands are ascribed to the fast decay time, τ_f, and the slow decay time, τ_s. The dynamic processes (fast and slow), characterized by τ_f and τ_s, have diffusive character (reciprocal values of τ_f and τ_s are q^2-dependent). Hence, it was possible to introduce two diffusion coefficients, D_f and D_s. The existence of two diffusion coefficients in dilute solutions generally points to the occurrence of two types of scatterers in the system with different hydrodynamic radii. Since R_{hf} is small and practically the same for both discussed copolymers, the fast mode was ascribed to polymer coil diffusion. The fairly broad distribution of this mode

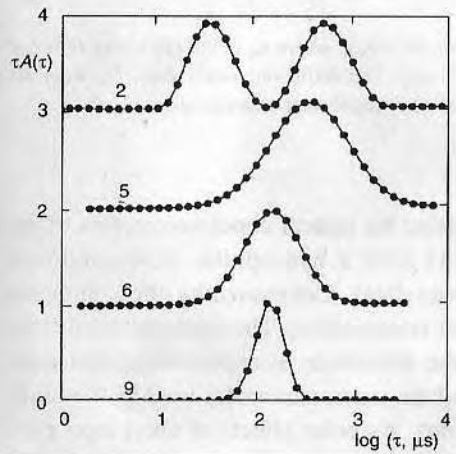

FIG. 1
Relaxation time distribution, $\tau A(\tau)$, from DLS data for the copolymers in water (for numbers of copolymers, see Table I)

reflects the polydispersity of a copolymer sample prepared by free radical copolymerization. Well-defined slow modes with a rather broad distribution can be related to diffusion of large scatterers which are probably formed by the association of copolymer molecules. Since the aggregates were found to be unstable at low concentrations (see below), the hydrodynamic radii of aggregates, R_{hs}, were calculated from the values of diffusion coefficients for infinite dilution (D_s) obtained by linear extrapolation of D_{as} (Eq. (4)) values for the higher concentration range only to $c = 0$ and they are shown in Table II.

In order to estimate the molar mass of aggregates, static light scattering measurement were performed. The total molar masses (M_{wt}) values shown in Table II were obtained by extrapolation of $Kc/\Delta R(0)$ values to $c = 0$ from the higher concentration range only. M_{wt} consists of the contribution of both aggregates, M_{wa}, and copolymer (unimer) molecules, M_{wu}

$$M_{wt} = w_a M_{wa} + w_u M_{wu} \,, \tag{5}$$

where w_a and w_u are the mass fractions of aggregates and unimer, respectively. Since we do not know the mass fraction of aggregates and copolymer molecules in solution, the molar mass of aggregates cannot be determined accurately. It can only be stated that

TABLE II
Characteristics of copolymers particles in water

Copolymer	$M_{wt} \cdot 10^{-5}$, g mol^{-1}	R_{hs}, nm	$\rho_a \cdot 10^4$, g ml^{-1}	$\Delta \log \tau$
1	3.3	68[a]	4.2[b]	–
2	8.6	109[c]	2.6[d]	–
3	2.0[e]	60	3.7[e]	0.6
4	64	65	92	0.45
5	8.3[e]	96	3.7[e]	0.42
6	8.0	21	330	0.32
7	2.9[e]	21	120[e]	0.30
8	3.5[e]	16.2	310[e]	0.17
9	6.6[e]	17.3	510[e]	0.16

M_{wt}, total mass-average molar mass (micelles + unimers); R_{hf}, hydrodynamic radius of unimers; R_{hs}, hydrodynamic radius of aggregates; ρ_a, the average segmental density in micelles ($\rho_a = 3M_{wt}/4\pi R_{hs}^3 N_A$); $\Delta \log \tau$, the halfwidth at the half height of the distribution of relaxation times.
[a] R_{hf} 4.0 nm; [b] ρ_u 0.12 g ml^{-1}; [c] R_{hf} 4.3 nm; [d] ρ_u 0.10 g ml^{-1}; [e] $\Delta R(0)/Kc$ for $c \approx 2 \cdot 10^{-3}$ g ml^{-1}.

the molar mass of aggregates, M_{wa} is actually higher than the experimental value of M_{wt}. In the case of copolymers 1 and 2, where the relative scattering amplitudes for fast (A_f) and slow (A_s) modes are comparable (Fig. 1), w_a should be several times lower than w_u.

Copolymers with higher contents of hydrophobic AMA comonomers (No. 3–9) were not easily soluble in water and a special dialysis procedure had to be used to dissolve them. The light scattering of aqueous solutions of these copolymers is dominated by

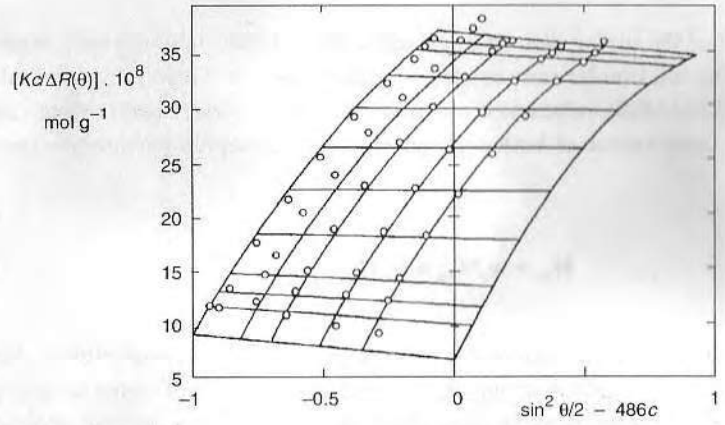

FIG. 2
Zimm plot for copolymer 4 in water; c is in g ml^{-1}

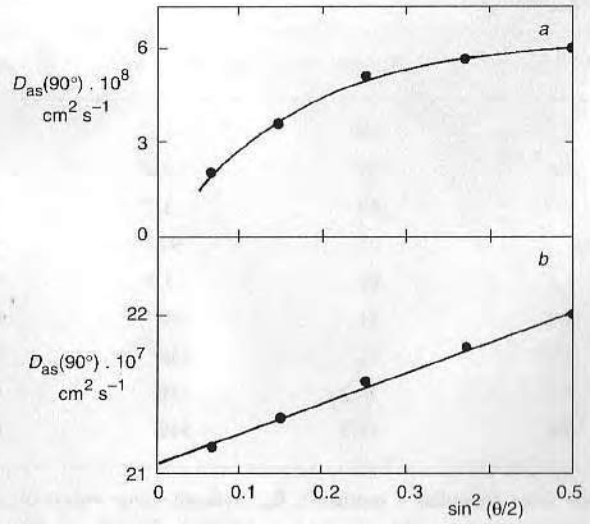

FIG. 3
Scattering angle dependence of the apparent diffusion coefficient of the slow mode, $D_{as}(90°)$, as obtained from DLS data for copolymers 4 (*a*) and 9 (*b*)

stable aggregates and the scattering of molecularly dissolved copolymer molecules was undetectable in DLS experiments. Therefore, the multisampling time correlation functions were analyzed by the forced fit (method 2) which provides more realistic information on the distribution widths of relaxation times, $\Delta \log \tau$. As demonstrated in Fig. 1, the distribution width decreases with increasing hydrophobicity of AMA units. Thus, copolymers containing LMA units have better defined aggregates than those containing comparable amounts of HMA (cf. copolymers 5 and 6 in Fig. 1). The use of the hydro-

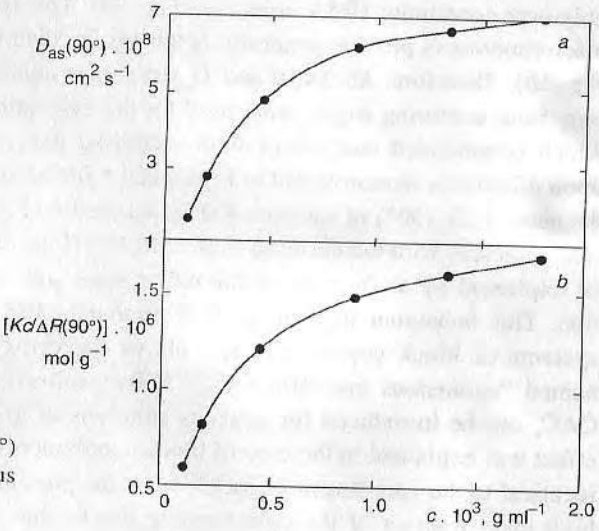

FIG. 4
Concentration dependence of $D_{as}(90°)$ (*a*) and $Kc/\Delta R(90°)$ (*b*) for aqueous solutions of copolymer 4

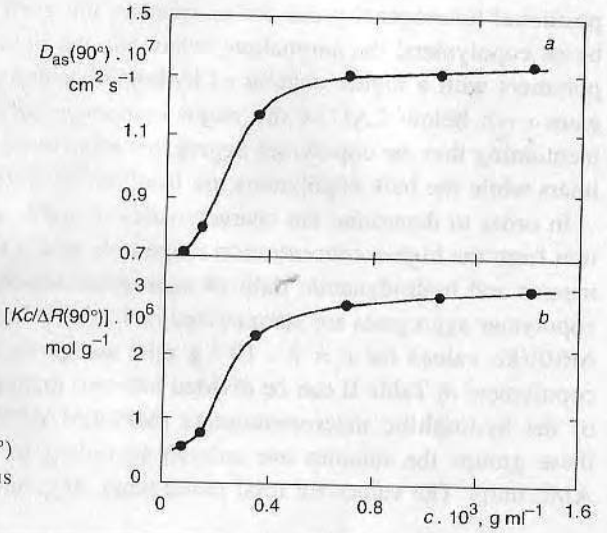

FIG. 5
Concentration dependence of $D_{as}(90°)$ (*a*) and $Kc/\Delta R(90°)$ (*b*) for aqueous solutions of copolymer 6

philic macromonomer with molar mass 4 000 unambiguously enhances the formation of small, well-defined particles (cf. copolymer 9 in Fig. 1). Thus, the hydrophilic/hydrophobic "polarity" of copolymers is a dominant factor in determining their aggregation (association) properties.

The very high polydispersity of aggregates complicates evaluation of light scattering data. Practically all $\sin^2(\theta/2)$-dependences of $Kc/\Delta R(\theta)$ (see Zimm plot in Fig. 2) have shown a deviation from linear dependences, a steep decrease at small scattering angles. Similar deviations were observed even in the plots of $D_{as}(\theta)$ versus $\sin^2(\theta/2)$ for copolymers containing HMA units (see Fig. 3*a*). The copolymers from MPOEMA-4000 macromonomers provide generally better results than those from MPOEMA-1900 (see Fig. 3*b*). Therefore, $Kc/\Delta R(0)$ and $D_{as}(0)$ values obtained by linear extrapolation from only back scattering angles were used for the evaluation of M_{wt} and R_{hs}. Another factor which complicated analysis of light scattering data was the instability of aggregates upon dilution as demonstrated in Figs 4 and 5 for copolymers 4 and 6, respectively. The decrease in $D_{as}(90°)$ of samples 4 (Fig. 4*a*) and 6 (Fig. 5*a*) with decreasing concentration coincides with the decrease in $Kc/\Delta R(90°)$ (Figs 4*b* and 5*b*). All these changes may be explained by an increase in the molar mass and size of the aggreagates upon dilution. This behaviour of aggregates is similar to the behaviour observed for micellar systems of block copolymers just above the critical micelle concentration, CMC, named "anomalous micellization"[45–47]. By analogy, critical aggregate concentration, CAC, can be introduced for aqueous solutions of graft copolymers under study. This effect was explained in the case of block copolymers by the presence of homopolymers identical to the core-forming block[47] or by the presence of copolymer molecules with a high mass fraction of the core-forming blocks due to compositional heterogeneity[45]. The latter explanation could be adopted for the system under study because large compositional heterogeneity can be assumed in the graft copolymers used. In analogy to block copolymers, the anomalous behaviour can be ascribed to a fraction of graft copolymers with a higher content of hydrophobic units which would form large aggregates even below CAC of the major component of the graft copolymer. It is worth mentioning that the copolymer aggregates seem to be in dynamic equilibrium with unimers while the bulk copolymers are insoluble in water.

In order to determine the characteristics of stable aggregates only, linear extrapolation from the higher concentration range only to $c = 0$ was again made to obtain molar masses and hydrodynamic radii of aggregates which, along with other parameters of copolymer aggregates are summarized in Table II. In extremely complicated cases only $\Delta R(0)/Kc$ values for $c = 2 \cdot 10^{-3}$ g ml^{-1} are given for the sake of comparison. The copolymers in Table II can be divided into two main groups according to molar masses of the hydrophilic macromonomers (MPOEMA-1900 and MPOEMA-4000); within these groups the samples are ordered according to the increasing hydrophobicity of AML units. The values for total molar mass, M_{wt}, and segmental density, ρ_a, increased

with the increasing content of HMA in graft copolymers with MPOEMA-1900 (copolymers 2, 3, 4, 5) indicating a higher tendency to aggregate formation. Contrary to this, the hydrodynamic radius, R_{hs}, changes only slightly. The graft copolymers of LMA with both the macromonomers (copolymers 6, 8 and 9) provide compact, dense and stable microparticles. Thus, besides very thin large polydispersed particles with $\rho_a \ll \rho_u$ (copolymers 1–5), small dense particles with $\rho_a \approx \rho_u$ are also formed from copolymers with the highest "polarity" (copolymers 6–9). It seems that these significant differences in properties of aggregates reflect their different structures. It is difficult to imagine that the structure of large aggregates is similar to that of normal micelles with the hydrophobic parts located in the spherical cores and hydrophilic POE chains in the shells. We propose the concept of a random association via attractive forces between hydrophobic HMA side chains, leading to a formation of aggregates through interpolymeric multiplets[48]. The existence of small interpolymeric multiplets was revealed several times by fluorescence spectroscopy[49,50] and light scattering methods[51,52] in aqueous solutions of hydrophilic copolymers containing hydrophobic side chains. As regards the small and compact particles ($R_{hs} \approx 20$ nm), we propose for them a quasimicellar structure with HMA or LMA hydrophobic side chains in geometrically unspecified cores and POE chains protecting the hydrophobic cores from further aggregation or even precipitation. Such a structure was recently proposed for hydrophobic/hydrophilic graft copolymers[36,37]. Because of the complexity of the graft copolymer system, only a qualitative verification of some theoretical implications has been possible on the basis of theoretical considerations. The theory predicts that the association number of micelles and, consequently, their molar mass increase with increasing length of the hydrophobic chains. This prediction could not be corroborated in our experimental results. Rather

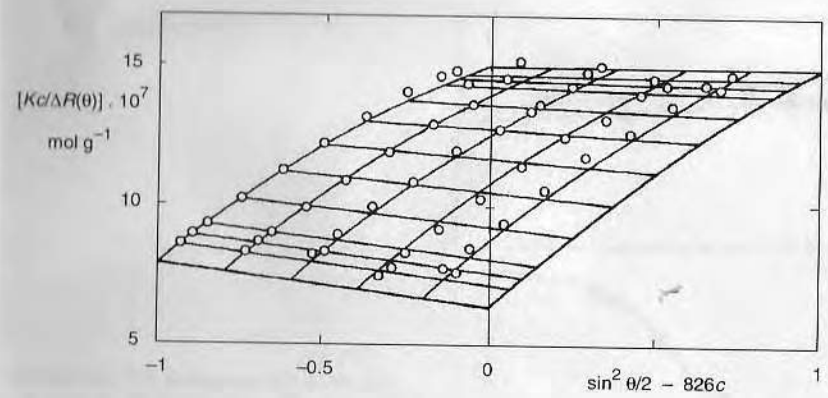

FIG. 6
Zimm plot for copolymer 4 in methyl cellosolve; c is in g ml^{-1}

than an increase of aggregate M_{wt} with a change in the number of carbon atoms in the hydrophobic side from five for HMA to eleven for LMA, a decrease in aggregate sizes due to the growing density of aggregates was observed (cf. characteristics of the copolymer 4 with 6, and 7 with 8). Unfortunately, the effect of copolymer composition has not been theoretically discussed yet.

The above experimental observation gave rise to a question whether the aggregates were formed during the preparation (stepwise dialysis). In order to elucidate this problem, solution properties of graft copolymers were also measured in methyl cellosolve.

TABLE III
Characteristics of copolymers particles in methyl cellosolve

Copolymer	$(dn/dc)_\mu$	$M_{wt} \cdot 10^{-5}$ g mol^{-1}	R_g, nm	R_{hs}, nm	$\rho_a \cdot 10^3$ g ml^{-1}	$\Delta\log\tau$
3	0.071	3.5	35	40	2.2	0.35
4	0.073	6.1	63	53	1.7	0.38
5	0.072	8.0	138	155	0.085	0.44
6	0.072	5.1	39	31	7.0	0.38
7	0.078	1.4	37	29	2.4	0.43
8	0.075	1.4	36	14.4	19	0.37
9	0.074	9.0	195	14.7	110	0.23

For the meaning of symbols, see Table II.

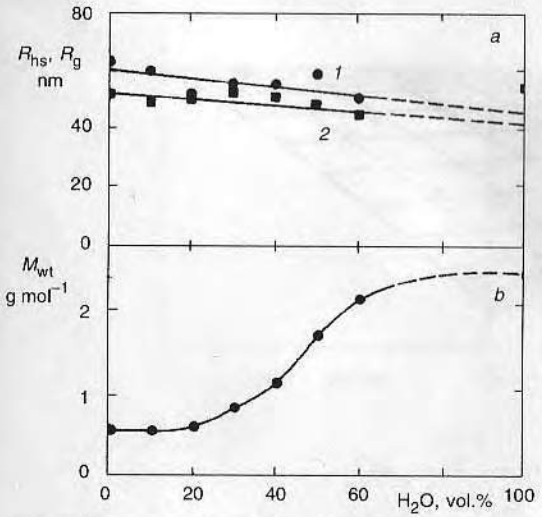

FIG. 7
Plot of *a* the geometric (*1*) and hydrodynamic (*2*) radii and *b* the total mass-average molar mass (M_{wt}) as a function of water/methyl cellosolve mixture composition

Contrary to aqueous solutions, the scatterers are better defined in methyl cellosolve solutions so that the usual Zimm plot analysis could be successfully used. This is demonstrated in Fig. 6 where the Zimm plot is shown for copolymer 4. The characteristics of scatterers are given in Table III. Since R_{hs} values in Table III are more than one order of magnitude higher than those of R_{hf} for unimer molecules in Table II, its appears that the light scattering experiments are again dominated by light scattering of loosely aggregated copolymer molecules. Comparing particle characteristics in Tables II and III it is evident that M_{wt} values for particles in methyl cellosolve are systematically smaller than those in water, whereas the particle sizes remain essentially the same. This means that the average segmental density in methyl cellosolve is smaller than in water. It can be assumed that the formation of denser and heavier aggregates takes place somewhere in water/methyl cellosolve mixtures during the dialysis procedure. Therefore, we started a detailed investigation of solution properties of the copolymers in water/methyl cellosolve mixtures. It was found that the copolymers are soluble in the mixed solvent system up to the 60 vol.% water content. As demonstrated in Fig. 7 for copolymer 4, M_{wt} increases in the mixed solvents between 20 and 60 vol.% of water and R_{hs} is practically constant as expected. The copolymers are not soluble in the mixtures with 70–100 vol.% of water. Parameters of aggregates in the mixture with 60 vol.% of water and in pure water are practically the same (Fig. 7) which means that no significant changes of particles take place in the course of dialysis in the latter region of mixed solvent. The same results were obtained with all the samples under study.

CONCLUSION

Aqueous solutions of graft copolymers containing variable amounts of hydrophilic (oxyethylene) and hydrophobic (alkyl methacrylate) units have been studied by static and dynamic light scattering. Generally, these copolymers were not soluble or dispersable in water but could be transferred into water from aqueous methyl cellosolve by a stepwise dialysis. Experimental results gave evidence of rather polydisperse multimolecular "pseudomicelles" which, unlike "regular" micelles of block copolymers with a concentric core/shell structure, have a very low segmental density.

This research was supported in part by the U.S.A.–Czech Scientific Program Project 93003, by the Grant No. 203/93/1058 of the Grant Agency of the Czech Republic and by the Grant No. 450416 of the Grant Agency of the Academy of Sciences of the Czech Republic.

REFERENCES

1. Tuzar Z., Kratochvíl P.: Adv. Colloid Interface Sci. *6*, 201 (1976).
2. Tuzar Z., Kratochvíl P. in: *Surface and Colloid Science* (E. Matijevic, Ed.), p. 1. Plenum Press New York 1993.

3. de Gennes P. G. in: *Solid State Physics* (J. Liebert, Ed.), Suppl. 14, p. 1. Academic Press, New York 1978.
4. Noolandi J., Hong M. H.: Macromolecules *16*, 1443 (1983).
5. Leibler L., Orland H., Wheeler J. C.: J. Chem. Phys. *79*, 3550 (1983).
6. Nagarajan R., Ganesh K.: J. Chem. Phys. *90*, 5843 (1989).
7. Munch M. R., Gasr A. P.: Macromolecules *21*, 1360 (1988).
8. Halperin A.: Macromolecules *20*, 2943 (1987).
9. Riess G., Rogez D.: Polym. Prepr. *23*(2), 19 (1982).
10. Zhou Z., Chu B.: Macromolecules *21*, 2548 (1988).
11. Tuzar Z., Webber S. E., Ramireddy C., Munk P.: Polym. Prepr. *31*(1), 525 (1991).
12. Cao T., Munk P., Ramireddy C., Tuzar Z., Webber S. E.: Macromolecules *24*, 6300 (1991).
13. Kiserow D., Procházka K., Ramireddy C., Tuzar Z., Munk P., Webber S. E.: Macromolecules *25*, 461 (1992).
14. Procházka K., Kiserow D., Ramireddy C., Tuzar Z., Munk P., Webber S. E.: Macromolecules *25*, 454 (1992).
15. Xu R., Winnik M. A., Riess G., Chu B., Croucher M. D.: Macromolecules *25*, 644 (1992).
16. Kotaoka K.: J. Macromol. Sci., Pure Appl. Chem. A *31*, 1759 (1994).
17. Battaerd H. A. J., Treager G. W.: *Graft Copolymers.* Wiley-Interscience, New York 1967.
18. Bekturov E. A., Bakauova Z. Kh.: *Synthetic Water-Soluble Polymers in Solution.* Hüthig and Wepf, Basel 1986.
19. Strauss U. P., Jackson E. G.: J. Polym. Sci. *5*, 649 (1951).
20. Luhmann B., Finkelmann H., Rehage G.: Angew. Makromol. Chem. *123*, 217 (1984).
21. Shih L. B., Shen E. Y., Chen S. H.: Macromolecules *21*, 1387 (1988).
22. Schulz D. N., Kaladas J. J., Maurer J., Bock J., Pace S. J., Schulz W. W.: Polymer *28*, 2110 (1987).
23. Valint P. L., jr., Bock J.: Macromolecules *21*, 175 (1988).
24. Pietschmann N., Brezesinski G., Tschierske C., Zaschke H., Kuschel F.: Liq. Cryst. *5*, 1697 (1989).
25. Lee J. H., Kopečková P., Kopeček J., Andrade J. D.: Biomaterials *11*, 455 (1990).
26. Lee J. H., Kopeček J., Andrade J. D.: J. Biomed. Mater. Res. *23*, 351 (1989).
27. *Polymers in Aqueous Media: Performance through Association.* Adv. Chem. Ser. *223* (1989).
28. McCormick C. L., Bock J., Schulz D. N. in: *Encyklopedia of Polymer Science and Engineering*, 2nd ed. (H. F. Mark, N. M. Bikales, C. G. Overberger, G. Menges and J. I. Kroschwitz, Eds), Vol. 17, p. 730. Wiley-Interscience, New York 1989.
29. Anron P., Koberle P., Laschewsky A.: Makromol. Chem. *194*, 1 (1993).
30. Nakagawa T., Inove H.: Kolloid-Z. Z. Polym. *195*, 93 (1964).
31. Dubin P. L., Strauss U. P. in: *Polyelectrolytes and Their Applications* (A. Rembaum and E. Selegny, Eds). D. Reidel, Dordrecht 1975.
32. Barbieri B. W., Strauss U. P.: Macromolecules *18*, 411 (1985).
33. Kammer V., Elias H. G.: Kolloid-Z. Z. Polym. *250*, 344 (1972).
34. Nagai K., Elias H. G.: Makromol. Chem. *188*, 1095 (1987).
35. Chen D. Y., Thomas J. K.: Macromolecules *24*, 2212 (1991).
36. Hamad E., Qutubuddin S.: Macromolecules *23*, 4185 (1990).
37. Hamad E., Qutubuddin S.: J. Chem. Phys. *96*, 6222 (1992).
38. Zdanowicz V. S., Strauss U. P.: Macromolecules *26*, 4770 (1993).
39. Kabanov A. V., Batrakova E. V., Melik-Nubarov N. S., Fedoseev N. A., Dorodnich T. Yu., Alakhov V. Yu., Chekhonin V. P., Nazarova I. R., Kabanov V. A.: J. Controlled Release *22*, 141 (1992).

Kop-1

New Polymeric Mater., Vol. 1, No. 4, pp. 289–297 (1990)

The influence of poly(ethylene oxide) spacers on the covalent and non-specific binding of immunoglobulin G to silica surfaces

P. KOPEČKOVÁ, J. KOPEČEK and J. D. ANDRADE

Department of Bioengineering, University of Utah, Salt Lake City, Utah 84112, USA

Accepted in revised form 14 September 1989

Abstract—Porous silica beads coated with 3-aminopropyl triethoxy silane (APS) were modified with excess glutaraldehyde followed by reaction with an excess of one of the following compounds: 1,2-diaminoethane; α,ω-diaminopoly(ethylene oxide), $M_r = 1000$; α,ω-diaminopoly(ethylene oxide), $M_r = 5000$. By this procedure beads were prepared which contained spacers terminated in primary amino groups. The influence of the spacer structure on the non-specific sorption of ^{125}I-labeled human immunoglobulin G was studied. Whereas the amount of IgG bound to beads modified with 1,2-diaminoethane was comparable to the adsorption on APS modified beads, the non-specific adsorption decreased when PEO spacers were introduced. PEO_{5000} was more effective in decreasing the non-specific sorption of IgG than PEO_{1000}.

The beads containing spacers terminated in amino groups were modified with glutaraldehyde again and ^{125}I-labeled IgG was bound covalently. The amount of IgG bound was independent of the structure of the spacer. Desorption studies indicated that under the conditions used for covalent binding the non-specific binding was minimal. The time dependence of both types of binding on beads containing the PEO_{5000} spacer was determined.

Keywords: IgG immobilization; PEO spacers; silica substrates; non-specific IgG binding.

1. INTRODUCTION

Research interests in solid-phase immunoassays have dramatically increased in the last decade. More recently, considerable research efforts have been devoted to the development of fiber-optic immunosensors. It was shown that an electromagnetic field generated at a silica–liquid interface by total internal reflection can be used to excite fluorescence of molecules present at the interface [1–3]. Thus silica is a particularly promising material for the development of immunosensors. There are several reports of antibody (Ab) immobilization to silica surfaces [4, 5]. However, the problem is to immobilize the Ab such that it is efficient and accessible to the antigen (Ag). There is another important requirement in the development of immunosensors for monitoring biological fluids. If the immobilized Ab is coated or covered with a layer of non-specifically bound protein, fibrin or thrombus, then the sensor ceases to function [6]. In other words it is necessary to minimize the non-specific adsorption of proteins to the immunosensor's surface. It was previously demonstrated that poly(ethylene oxide) surfaces exhibit low protein adsorption and cell adhesion characteristics, probably due to their very high chain mobility and only modest hydrogen bonding tendencies [7, 8].

The main objective of this paper was to study the influence of spacers on covalent and non-specific binding of IgG to silica surfaces. To be able to determine quantitatively the surface modification and IgG binding, porous silica beads (high surface area) were used in this study. APS modified beads were treated with glutaraldehyde followed by reaction

with an excess of α,ω-amino terminated compounds of various length. The relationship between the length of the spacer and the amount of covalent and non-specific binding of human IgG was determined.

2. MATERIALS AND METHODS

2.1. Chemicals

Porous silica beads, 3-aminopropyl triethoxy silane (APS) coated, 30–40 Mesh, 375 Å pore size, were from Fluka. They contained 14 nmol/mg of amino groups, specific area 33 m^2/g. Glutaraldehyde, 25% solution in water, E.M. Grade was from Polysciences. Diamines: NH_2–PEO_{5000}–NH_2 50% solution in water and NH_2–PEO_{1000}–NH_2 were a kind gift from Dr. S. Nagaoka (Toray Industries, Inc., Kanagawa, Japan); 1,2-diaminoethane from Fluka was freshly distilled before use. ^{125}I-Sodium iodide in dilute sodium hydroxide solution, free from reducing agents, was from Amersham, 100 mCi/ml. Immunoglobulin G, human, lyophilized was from Sigma.

2.2. Methods

2.2.1. Aldehyde beads –CH=O (2). 1 g of APS coated beads (1), containing 14 nmol NH_2/mg, were reacted with 20 ml 2.5% glutaraldehyde in borate buffer, pH 8.6. The reaction mixture was gently shaken overnight at room temperature, then many times washed with water, ethanol, ether and dried. No NH_2 groups on beads were detectable by a qualitative test using trinitrobenzenesulfonic acid [9]. The beads remained colorless. The original APS coated beads gave an intense yellow color.

2.2.2. Amino beads –$(CH_2)_2$–NH_2 (3), –PEO_{1000}–NH_2 (4), –PEO_{5000}–NH_2 (5). 1 g of aldehyde beads (2) were treated with large excess of the solution of the respective diamine: 10 ml 25% NH_2–PEO_{5000}–NH_2 or 5 ml 10% NH_2–PEO_{1000}–NH_2 or 5 ml 5% 1,2-diaminoethane in sodium carbonate/bicarbonate buffer pH 9.5. Beads were gently shaken overnight and washed thoroughly as described above. The azomethine bond formed was reduced by reaction with 50 mg $NaBH_4$ in 3 ml carbonate/bicarbonate buffer pH 9.0. After proper washing and drying the content of NH_2 was determined as described in 2.3. No aldehyde groups on beads were detectable after diamine treatment by the reaction with dinitrophenylhydrazine [10].

2.2.3. Modification of spacer containing beads—synthesis of –$(CH_2)_2$–CH=O (6), –PEO_{1000}–CH=O (7), and –PEO_{5000}–CH=O (8). 1 g of NH_2 beads (3), (4), (5) respectively, containing approx. 10 nmol NH_2/mg were treated with 20 ml 2.5% glutaraldehyde by the same procedure as described above.

2.2.4. ^{125}I labeling of IgG. Human immunoglobulin G was radioiodinated with ^{125}I-iodine using the chloramine-T method previously described [11]. Unbound iodine was removed by centrifugation using Sephadex G-25 grade coarse resin (Pharmacia) minicolumns. The purity of preparation was checked before use by determining the radioactivity profile on a Sephadex G-25 (PD-10) column. The amount of free iodine was always less than 5%. Radioactivity measurements were performed in plastic vials in a Beckman Radioisotope Detector (Model 170) by counting each sample for 1 min.

2.2.5. Covalent binding of ^{125}I-IgG to modified silica beads. General procedure: 75 mg (about 10^{-6} mol –CH=O groups) of beads (2, 6, 7 or 8) in 0.25 ml PBS buffer pH 7.4 were mixed with 0.25 ml of stock solution containing 2.5 mg (17 nmol) of ^{125}I–IgG. The stock solution was prepared by mixing 25 mg cold IgG in 2.5 ml PBS buffer and 5 μl of the solution of labeled IgG. The activity of the stock solution was about 40 000 cpm per 1 ml. The binding reaction proceeded in tubes with agitation for three hours (or different time intervals with beads 8) at room temperature. The beads were then washed with PBS buffer untill their radioactivity did not change during three succesive washings.

2.2.6. Non-specific sorption of ^{125}I-IgG to silica beads. The same procedure as described for covalent binding was used.

2.2.7. Release of ^{125}I-IgG from beads. The stability of IgG bound on beads was followed in PBS buffer pH 7.4 and 1 M phosphate buffer pH 9.0. 75 mg of beads with ^{125}I-IgG bound were mixed with 2 ml of buffer and the radioactivity of the supernatant was measured at time intervals always before adding the fresh buffer.

2.3. Analysis of beads

2.3.1. Determination of NH_2 groups. The amount of amino groups on the beads was determined using *N*-succinimidyl-3-(2-pyridyldithio)propionate (SPDP) [12]. The beads were treated with an excess of SPDP. The unreacted reagent was removed by washing, followed by the reduction of acylated beads by dithiothreitol resulting in the release of pyridine-2-thione. The concentration of the latter was determined spectrophotometrically at 343 nm ($\varepsilon = 8080\,l\,mol^{-1}\,cm^{-1}$).

2.3.2. Surface area determination. The porosity of beads was characterized by the specific area measured by the dynamic desorption of nitrogen on a Quantasorb apparatus (Quantachrome Corp.). The specific surface of original APS coated beads was 33.4 m^2/g. All modified beads had specific surface in the range from 29.2 to 31.0 m^2/g.

3. RESULTS

The modification of porous silica beads is schematically shown on Fig. 1. The APS-coated beads (1) contained 14 nmol/ml of NH_2 groups. After reaction with a large excess of glutaraldehyde, practically all amino groups were converted to aldehyde groups (beads 2). The latter were modified with a large excess of diamines: 1,2-diaminoethane; H_2N–PEO_{1000}–NH_2; H_2N–PEO_{5000}–NH_2, respectively). The resulting beads (3, 4 and 5) contained 9–10 nmol/mg of terminal NH_2 groups (Table 1). After reaction with an excess of glutaraldehyde beads 6, 7 and 8 were prepared, which contained terminal –CH=O groups. The surface area of the beads did not essentially change during these polymer-analogous transformations (Table 2).

The non-specific adsorption of ^{125}I-IgG was studied on amino-terminated beads (1, 3, 4 and 5). After incubating the beads for 3 h with labeled IgG the amount of non-specifically adsorbed glycoprotein was dependent on the structure of the spacer (Table 1). The amount of adsorbed IgG on beads (1) and (3) was practically identical, indicating that an ethylenediamine spacer had no influence on the adsorption. Introduction of

)-NH_2 (1) Original beads, APS coated

↓ excess of O=CH-$(CH_2)_3$-CH=O

)-CH=O (2)

↓ 1. diamine in excess: NH_2-$(CH_2)_2$-NH_2 or NH_2-PEO_{1000}-NH_2 or NH_2-PEO_{5000}-NH_2

↓ 2. $NaBH_4$ reduction

)-$(CH_2)_2$-NH_2 (3)
)-----PEO_{1000}-NH_2 (4)
)-----PEO_{5000}-NH_2 (5)

↓ glutaraldehyde in excess

)-$(CH_2)_2$·CH=O (6)
)-----PEO_{1000}·CH=O (7)
)-----PEO_{5000}·CH=O (8)

Figure 1. Modification of porous silica beads.

Table 1.
Non-specific binding of ^{125}I-IgG on amine beads[a]

Bead no.	Structure of spacer arm	Density of NH_2 groups		IgG bound		
		nmol/mg	nmol/m²	% radio-activity[b]	nmol/mg	nmol/m²
1	$-NH_2$	14	420	59	0.13	3.9
3	$-(CH_2)_2NH_2$	9.8	330	57	0.12	4.0
4	$-PEO_{1000}-NH_2$	9.2	310	26	0.058	1.9
5	$-PEO_{5000}-NH_2$	9.8	330	19	0.043	1.4

[a]In each experiment 2.5 mg IgG in 0.5 ml PBS buffer pH 7.4 was treated with 75 mg of beads for 3 h.
[b]Total radioactivity was 10000 cpm.

Table 2.
Specific surface area of beads

Bead no	Structure of spacer arm	Specific surface m²/g
1	$-NH_2$	33.4
4	$-PEO_{1000}-NH_2$	29.4
5	$-PEO_{5000}-NH_2$	31.0
8	$-PEO_{5000}-CH=O$	30.6

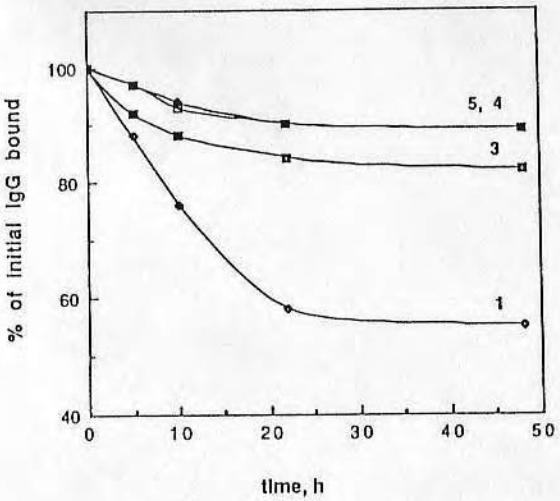

Figure 2. Desorption of non-specifically bound ^{125}I-IgG. Desorption of IgG was followed from $-PEO_{5000}-NH_2$ (5); $-PEO_{1000}-NH_2$ (4); $-(CH_2)_2-NH_2$ (3); and $-NH_2$ (1) beads in 1 M phosphate buffer, pH 9.0. The amount of IgG released was calculated from radioactivity of the supernatant and expressed as a percentage of radioactivity initially bound on the beads.

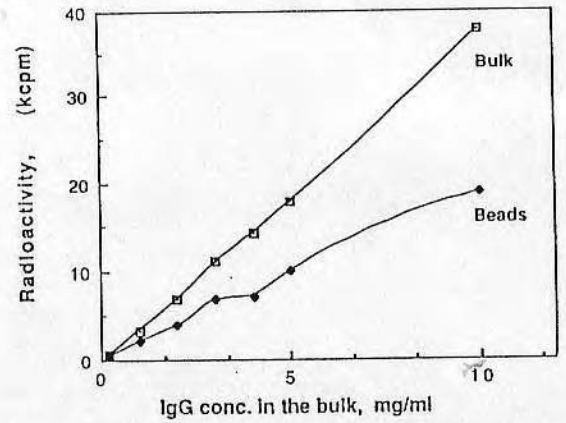

Figure 3. Relationship between the concentration of ^{125}IgG in the reaction mixture and the amount covalently bound to silica beads. IgG was immobilized on $-PEO_{5000}-CH=O$ (8) beads in individual tubes one for each concentration, in PBS buffer pH 7.4 for 3 h. The upper line shows the starting radioactivity in the bulk, the lower curve shows the respective radioactivity bound on the beads.

PEO spacers decreased the non-specific adsorption of IgG (Table 1). PEO_{5000} was more effective in the repulsion of glycoprotein compared to PEO_{1000}. The stability of association of IgG with the beads was also studied (Fig. 2). On the relative basis the stability was the lowest on beads (1), higher on beads containing spacers. It appeared that beads with PEO spacers (4 and 5) retained the glycoprotein slightly stronger compared to beads (3) (Fig. 2).

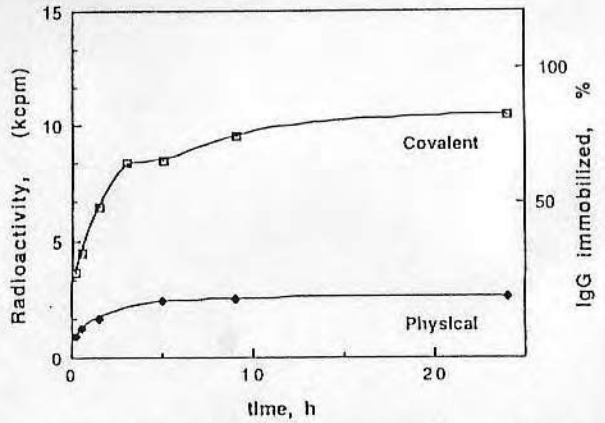

Figure 4. Time course of ^{125}I-IgG immobilization. The upper curve shows the amount of IgG covalently immobilized on $-PEO_{5000}-CH=O$ (8) beads, the lower curve shows non-specifically bound IgG on $-PEO_{5000}-NH_2$ (5) beads. IgG was immobilized on beads in individual tubes (one for each interval) in PBS buffer, pH 7.4. The starting radioactivity of IgG solution in all tubes varied between 12 000 and 13 000 cpm. For details see experimental.

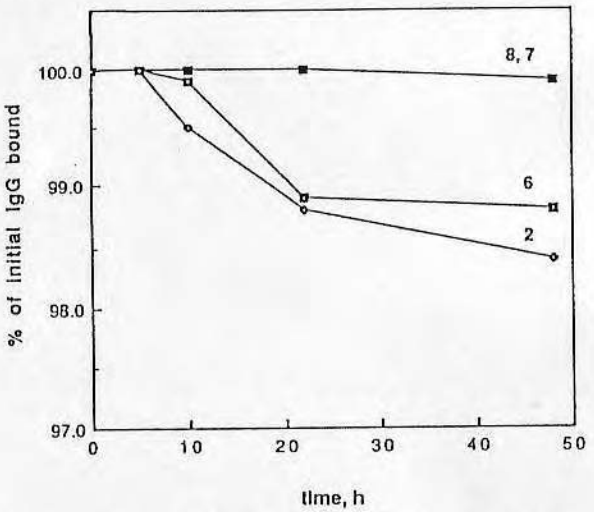

Figure 5. Stability of covalently bound ^{125}I-IgG. Stability of IgG bound was studied on $-PEO_{5000}-CH=O$ (8); $-PEO_{1000}-CH=O$ (7); $-(CH_2)_2-\cdots CH=O$ (6); and $-CH=O$ (2) beads in 1 M phosphate buffer, pH 9.0. The amount of IgG released was calculated from radioactivity of the supernatant and expressed as a percentage of radioactivity initially bound to the beads.

Covalent binding of ^{125}I-IgG was studied with $-CH=O$ terminated beads (2, 6, 7 and 8). The influence of the structure of spacer was evaluated (Table 3). It appears that there was no essential difference in the amount of IgG bound. The amount of IgG bound was proportional to the concentration of IgG in the reaction solution (Fig. 3). Both the amount of covalent binding of IgG to beads (8) and the amount of non-specific adsorption of IgG to beads (5) was time dependent (Fig. 4).

The covalent bond between IgG and the beads was stable in spite of the fact that no reduction of the azomethine bond was performed. During 40 h of incubation in buffer (pH 9) practically no release of IgG was observed from beads with different spacers (Fig. 5).

4. DISCUSSION

Coupling of bioactive molecules to solid supports must involve mild chemical reactions to retain the biological activity of the conjugate. The simplest procedure for producing surface bound conjugates consists of contacting a solution of a bioactive molecule with a reactive group generated on a solid support.

In this work APS-coated porous silica was used. It has a high enough surface area to permit an exact analysis of surface bound groups. Primary amino groups on its surface can be easily converted to aldehyde groups by reaction with glutaraldehyde. This reaction was performed at pH 8.6 to avoid an extensive polymerization of glutaraldehyde on the surface resulting from aldol condensation [13]. The subsequent reaction (Fig. 1) was the attachment of α,ω-diamino compounds by one end. It is known [14] that to avoid cycle (loop) formation it is necessary to use large excess (about 100 fold) of the diamine compound during the reaction. The amount of spacers bound via one end was 9–10 nmol/mg, i.e. about 70% compared to the initial value on APS coated beads (1).

Proteins adsorb to almost all surfaces during the first minutes of blood exposure [15]. PEO modified surfaces appear to be protein resistant probably due to its low interfacial free energy with water, unique solution properties and molecular conformation in aqueous solution, hydrophilicity, high surface mobility and steric stabilization effects [8, 16, 17]. Recently, we have shown that polyethylene surfaces treated with either PEO-containing nonionic polymeric surfactants [18] or tailor-made copolymers of alkyl methacrylates with PEO macromonomers [19] are effective in decreasing the adsorption of proteins. In the latter case it was observed that an increase of the PEO length rendered the modified surface more effective in protein repulsion.

The adsorption of ^{125}I-IgG on beads (1, 3, 4 and 5) has shown a similar pattern. The amount of IgG adsorbed decreased when PEO spacers were bound to the silica surface (beads 4 and 5). The short 1,2-diaminoethane spacer was not efficient in decreasing the non-specific adsorption of IgG in accordance with results of Sato *et al.* [21], whereas the PEO spacers were effective. These results indicate that PEO surfaces in water are particularly effective in exhibiting rapid motions [20] and a large excluded volume, thereby actively minimizing the adsorption of proteins [22]. We are aware that the improved protein repulsion from silica surfaces modified with PEO_{5000} may result from combination of two factors: better repulsion properties of PEO chains of higher molecular weight and of hindered diffusion of IgG into pores after PEO modification. However, the 'free' diameter of pores after modification with PEO_{5000} (end to end distance in free solution is about 45 Å) would be $375-(2\times 45)=285$ Å. Taking into account the size of the IgG molecule (about 100 Å) it can be assumed that better repulsion of IgG by PEO_{5000} is the more important factor.

The covalent binding of IgG was performed via aldehyde groups generated at the ends of spacers (Fig. 1, beads 6, 7 and 8) and on beads (2) (without spacer). The amount of IgG bound (Table 3) was similar in all cases indicating that the decisive factor in this binding reaction is the ratio of reactive groups. The IgG molecule contains about 90 amino groups. To avoid IgG aggregation we have used maximally a 10% wt. solution.

Table 3.
Covalent binding of ^{125}I-IgG on aldehyde beads[a]

Bead no.	Structure of spacer arm	IgG bound		
		% radioactivity[b]	nmol/mg	nmol/m^2
2	$-CH=O$	67	0.15	4.5
6	$-(CH_2)_2-CH=O$	74	0.16	5.3
7	$-PEO_{1000}-CH=O$	68	0.15	5.0
8	$-PEO_{5000}-CH=O$	60	0.13	4.3

[a]In each experiment 2.5 mg IgG in 0.5 ml PBS buffer pH 7.4 reacted with 75 mg of beads for 3 h.
[b]Total radioactivity added was 10 000 cpm.

The chemistry described here offers a simple way of binding of biomolecules to silica surfaces. No spacial orientation of the IgG molecule on the surface is necessary for the binding reaction to proceed. However, the orientation of the bound IgG will be of importance in determining its binding activity. It is known that the specific activity of immobilized biomolecules is a function of bonds per macromolecule [23, 24] and of the density of ligands on the surface [25]. The spacing of the antibody on the surface influences its binding constant [26]. Lochmüller *et al.* [27] observed that ligands on silica gel surface are not equally distributed but rather are clustered into regions of high density. Performing a series of chemical reactions on the surface will most probably increase the non-uniform distribution of ligands. The yield of chemical reactions depends on the concentration of reaction components. It is more probable that a successful collision will occur in the regions of high density of ligands. Thus on the modified surfaces there will be a nonuniform distribution of biomolecules (antibodies). For the development of biosensors it is important that areas with low density of antibodies are at least partially covered with PEO molecules preventing non-specific sorption of competing proteins. This study suggests that by varying the concentration of reactants in individual steps of surface modification it may be possible to optimize the methods of binding to match the needs of particular biomolecules and to decrease the amount of non-specific sorption.

Acknowledgments
This study was supported by the Center of Biopolymers at Interfaces. We thank to Drs. J. N. Lin and T. Oolman for valuable discussions, Mrs. E. Votavová (Institute of Macromolecular Chemistry, CSAS, Prague) for the determination of the porosity of beads and to Dr. S. Nagaoka (Toray Industries, Inc., Kanagawa, Japan) for the kind gift of α,ω-diaminopoly(ethylene oxide)s.

REFERENCES

1. T. Hirschfeld, U.S. Patent 4,447,546.
2. R. M. Sutherland, C. Dahne, J. F. Place and A. R. Ringrose, *J. Immunol. Methods* 74, 253 (1984).
3. J. D. Andrade, R. A. van Wanegen, D. E. Gregonis, K. Newby and J. N. Lin, *IEEE Trans. Electron Devices* ED-32, 1175 (1985).
4. J. N. Lin, J. Herron, J. D. Andrade and M. Brizgys, *IEEE Trans. Biomed. Eng.* 35, 466 (1988).
5. J. N. Lin, J. D. Andrade and I. N. Change, *J. Immunol. Methods*, in press.
6. J. D. Andrade, J. Herron, J. N. Lin, H. Yen, J. Kopeček and P. Kopečková, *Biomaterials* 9, 76 (1988).
7. T. H. Chiu, E. Nyilas and L. R. Turcotte, *Trans. Am. Soc. Artif. Inter. Organs* 24, 389 (1978).

8. S. Nagaoka, Y. Mori, H. Takiuchi, K. Yokota, H. Tanzawa and S. Nishiumi, in: *Polymers as Biomaterials*, p. 361, S. W. Shalaby, A. S. Hofman, B. D. Ratner and T. A. Horbett (Eds.). Plenum Press, New York (1984).
9. G. Antoni, R. Presentini and P. Neri, *Anal. Biochem.* 129, 60 (1983).
10. F. T. Weiss, in: *Determination of Organic Compounds*, p. 92, P. J. Elving and I. M. Kolthof (Eds.). Wiley, New York (1970).
11. H. Y. K. Chuang, W. F. King and R. G. Mason, *J. Lab. Clin. Med.* 92, 483 (1978).
12. T. T. Ngo, *J. Biochem. Biophys. Methods* 12, 349 (1986).
13. P. Monsan, *J. Mol. Catalysis* 3, 371 (1977/1978).
14. J. Kopeček, *Makromol. Chem.* 178, 2169 (1977).
15. L. Vroman, *Blood*. Natural History Press, Doubleday, New York, 1967.
16. E. W. Merrill and E. W. Salzman, *ASAIOJ.* 6, 60 (1983).
17. D. Knoll and J. Hermans, *J. Biol. Chem.* 258, 5710 (1983).
18. J. H. Lee, J. Kopeček and J. D. Andrade, *J. Biomed. Mater. Res.* 23, 351 (1989).
19. J. H. Lee, P. Kopečková, J. Kopeček and J. D. Andrade, *Biomaterials*, in press.
20. J. D. Andrade, S. Nagaoka, S. Cooper, T. Okano and S. W. Kim, *ASAIO J.* 10, 75 (1987).
21. H. Sato, T. Kidaka and M. Hori, *J. Biomed. Mater. Res.* 20, 853 (1986).
22. W. R. Gombotz, A. S. Hoffman, J. M. Harris, B. Hovanes, G. H. Wang and A. Safranj, *Proc. IUPAC Int. Symp. "Molecular Design of Functional Polymers", Seoul, Korea, June 1989.*
23. A. C. Koch-Schmidt and K. Mosbach, *Biochemistry* 16, 2105 (1977).
24. G. Manecke and H. G. Vogt, *Makromol. Chem.* 177, 725 (1976).
25. M. E. Landgrebe, D. Wu and R. R. Walters, *Anal. Chem.* 58, 1607 (1986).
26. B. L. Liu and J. S. Schultz, *IEEE Trans. Biomed. Eng.* BME-33, 133 (1986).
27. C. H. Lochmüller, A. S. Colborn, M. L. Hunnicutt and J. M. Harris, *Anal. Chem.* 55, 1344 (1983).

Targetable Photoactivatable Drugs. 1. Synthesis of Water-Soluble Galactosamine Containing Polymeric Carriers of Chlorin e_6 and Their Photodynamic Effect on PLC Cells *in vitro*

N.L. Krinick[1], B. Říhová[2], K. Ulbrich[3], J.D. Andrade[1], J. Kopeček[1,3]*

[1]Department of Bioengineering, University of Utah, Salt Lake City, Utah 84112, USA
[2]Institute of Microbiology, Czechoslovak Academy of Sciences, 14220 Prague 4, Czechoslovakia
[3]Institute of Macromolecular Chemistry, Czechoslovak Academy of Sciences, 16206 Prague 6, Czechoslovakia

ABSTRACT

A copolymer of N-(2-hydroxypropyl)methacrylamide (HPMA) and N-methacryloylglycine p-nitrophenyl ester (MA-Gly-ONp) was synthesized by radical precipitation copolymerization. Galactosamine was coupled to the polymer by reaction with the active ester side chains. The remaining p-nitrophenyl groups were converted to amine functionalities via a polymeranalogous reaction with an excess of ethylene diamine. Chlorin e_6 was activated using a mixed anhydride method and subsequently bound to the modified side chains of the polymer. The photodynamic activity of the conjugate with galactosamine as the targeting moiety was tested *in vitro* on a human hepatoma cell line: PLC/PRF/5 (Alexander cells). It appears that the conjugate enters the cell interior by receptor mediated pinocytosis via the asialoglycoprotein receptors present on the surface of the PLC cells. Photoactivation of the chlorin containing conjugate with red light proved cytotoxic to the cells. Structure tests comparing the HPMA copolymer-galactosamine-chlorin e_6 conjugate and a nontargetable HPMA copolymer-chlorin e_6 conjugate, with comparable chlorin e_6 content, indicate that the targeted conjugate is more biologically active.

1. INTRODUCTION

In general, a photosensitizer is a molecule that when subjected to light of a characteristic wavelength will be converted to a high energy triplet state. The triplet state molecule is capable of giving up its energy to molecular oxygen, converting it to a high energy singlet state. In biological systems, this singlet oxygen may then participate in a number of "photodynamic" reactions resulting in the damage of certain cell organelles and eventual cell death.[1] The effect of photosensitized oxidation on a number of biomolecules which contribute to cell destruction have been examined.[2] It is possible to exploit the photodynamic properties of porphyrins (class of photosensitizers) to cause the destruction of a variety of cancer cells.

It is widely known that some porphyrins have localizing abilities and preferential uptake by tumor tissue. There is, however, nonspecific uptake by normal tissue. This is not a problem when the direct targeting of light to the uptake site is possible, but, in most cases, this is not feasible. Also, a problem is the ultrasensitivity to light of normal tissue after administering a dosage of drug effective in killing a tumor due to the retention of the porphyrin in the system for at least 30 days.[3] Therefore, it would be beneficial to develop a system of targeting porphyrins to the desired site, and as much as possible, limit photodynamic activity to the target tissue. Synthetic polymers have been used as drug carriers because they can be chemically modified and "tailor-made" for specific purposes.[4] An appropriate choice of the polymer to be used as a drug carrier is imperative. The polymer must remain in the body long enough to carry the porphyrin to the tumor site, but, then it must be eliminated from the body. The molecular weight and the biodegradability of the polymer determine its fate.[5] HPMA copolymers are appropriate for these purposes and have been extensively studied as carriers of other types of anticancer drugs.[4] The backbone of the HPMA copolymers are nonbiodegradable, but, have been shown to elicit minimal immunogenicity,[6] and are eliminated from the body by the kidneys depending on their molecular weights and molecular weight distributions.[7,8] Binding carbohydrate functionalities to target HPMA drug carriers to specific cells has been demonstrated.[9] It has been proven that soluble

* To whom correspondence should be addressed.

synthetic copolymers of HPMA with galactosamine terminated side chains are accumulated in hepatocytes in the liver of rats.[10] The uptake of polymers via receptor mediated pinocytosis by the asialoglycoprotein receptors in the hepatocyte plasma membrane is dependent on the galactosamine content of the polymers.[10] It was also found[7,11] that these systems incorporated with enzymatically cleavable side chains are effective in delivering and releasing pharmacological agents into the lysosomes of these cells.

Theoretically, it is possible to design HPMA copolymers as carriers of porphyrins with galactosamine terminated side chains to target this complex to cells that express asialoglycoprotein receptors.[12] Then, by receptor mediated pinocytosis, the conjugate can enter the cell and via a transport mechanism may be able to enter the cell lysosome.[13] Even if some nonspecific binding of the conjugate occurs, the porphyrin remains in its inactive form unless subjected to light. Therefore, the inherent localizing ability of the porphyrin does not have to be relied upon, and the porphyrin can be chosen based on its photodynamic properties.[14] Chlorin e_6 is activated by red light with a maximum at 662 nm (DMF). Light at this wavelength yields deeper tissue penetration than light at shorter wavelengths.[15] In this paper, we have synthesized an HPMA copolymer-galactosamine-chlorin e_6 conjugate and have studied its photodynamic effect on PLC cells *in vitro*.

2. MATERIALS AND METHODS

2.1 Synthesis of monomers:

N-(2-hydroxypropyl)methacrylamide (HPMA) was prepared as previously described.[16] N-methacryloylglycine p-nitrophenyl ester (MA-Gly-ONp) monomer was prepared as follows: N-Methacryloylglycine (MA-Gly-OH) was synthesized by dissolving glycine (20 g, 0.266 moles) in 66.9 ml of 4N NaOH. A hydroquinone inhibitor was added to prevent polymerization. The mixture was cooled to 0°C. Slowly, 66.9 ml of 4N NaOH and methacryloylchloride (25.8 ml, 0.266 moles) were added dropwise to the mixture, simultaneously, under vigorous stirring, maintaining a temperature of 0°C. The reaction proceeded for 1 hour more at room temperature. Concentrated HCl was added to adjust pH to 2. The mixture was extracted 4 times with ethylacetate, collecting the organic layer. The solution was dried with Na_2SO_4 and then filtered. The mixture was evaporated until crystals appeared, which were recrystallized with EtOH/hexane. The melting point of the product was 106-108°C.

MA-Gly-ONp was prepared by first dissolving MA-Gly-OH (6.5 g, 0.045 moles) in 37 ml tetrahydrofuran (THF) and cooled to -20°C. Dicyclohexylcarbodiimide (DCC) (10.31 g, 0.050 moles) was dissolved in 11 ml THF. The DCC solution was slowly dropped into the reaction mixture, under vigorous stirring, maintaining the temperature at -20°C. p-Nitrophenol (6.95 g, 0.050 moles) was dissolved in 18 ml THF and dropped slowly into the reaction mixture, maintaining the temperature at -20°C. The reaction proceeded 3 hours at -20°C. Acetic acid was added to remove any unreacted DCC. The dicyclohexylurea (DCU) side product produced in the reaction was filtered off. The product was evaporated to dryness. The product was crystallized in ethylacetate/ether and recrystallized in ethanol/ether. The melting point of the product was 101°C.[17]

2.2 Synthesis of Copolymer Ia-reactive copolymer precursor, (Scheme A):

Mole ratio HPMA:MA-Gly-ONp 87.5:12.5. HPMA (5.14 g, 35.9 mmole), MA-Gly-ONp (1.355 g, 5.13 mmole), and azoisobutyronitrile (AIBN) (0.312 g) were dissolved in 56.7 ml acetone. The polymerization proceeded in a sealed ampule for 24 hours in a 50°C water bath. The copolymer precipitate was filtered and washed with acetone. The copolymer was dissolved in methanol and reprecipitated into a twenty-fold excess of acetone. The mole percentage of active ester in the copolymer was determined to be 8.4 mole percent by UV spectra (λ_{max}=274 nm; ε_{DMSO}=0.95E4 l/mole·cm). The molecular weight of copolymer Ia (M_W=18,700; M_W/M_n=1.3) was estimated, after aminolysis with 1-amino-2-propanol, from GPC analysis on a Sepharose 4B/6B (1:1) column (90x1.6 cm) calibrated with fractions of polyHPMA (buffer 0.5 M NaCl+0.05 M TRIS pH 7.5).

2.3 Synthesis of Copolymer III-targetable HPMA copolymer-galactosamine-chlorin e_6 conjugate, (Scheme B):

Synthesis of Copolymer II:

Copolymer Ia (60 mg, 0.03 mmoles ONp) was dissolved in 0.45 ml DMSO. Galactosamine hydrochloride (4.25 mg, 0.02 mmole) (Fluka Chemical Corp., Ronkonkoma, NY) was added. Triethylamine (2.75 µl, 0.02 mmole) was subsequently added. The reaction proceeded overnight at room temperature. Under vigorous stirring, the polymer

solution was dropped into ethylene diamine (0.217 ml, 3.23 mmole) and reacted 20 minutes at room temperature. Copolymer II was precipitated into acetone, filtered, washed with acetone and ether, and dessicated. The NH_2 content was determined to be 4.4 mole percent by the ninhydrin method.[18]

Chlorin e_6 Activation: Chlorin e_6 activation was carried out similarly to the procedure used by Oseroff et al.[14] Triethylamine (5.13 µl, 0.037 mmole) was added to a mixture of chlorin e_6 (21.4 mg, 0.034 mmole) (Porphyrin Products, Logan Utah), in 0.42 ml DMF. The mixture was cooled to -15°C. Ethylchloroformate (3.19 µl, 0.034 mmole) was added and the reaction proceeded for 30 minutes at -15°C. TLC analysis was performed to confirm chlorin e_6 activation.

Binding of activated chlorin e_6: Copolymer II (41 mg, 0.01 mmoles NH_2 groups) was dissolved in 0.54 ml DMF and added to the activated chlorin e_6 mixture. The reaction proceeded for 1 hour at -15°C and 3 hours more at room temperature. The mixture was evaporated to dryness, dissolved in methanol, and precipitated into a twenty-fold excess of acetone. The polymer was filtered, washed with acetone and ether, and dessicated. Unreacted chlorin e_6 was separated from the bound chlorin e_6 on an LH-20 column (4x40 cm) in methanol. The polymer fraction was collected and evaporated to dryness. The residue was dissolved in distilled water, frozen, and lyophilized. The mole percentage of bound chlorin e_6 was determined by UV spectra (λ_{max}=662; ε_{DMF}=53,000 l/mole·cm) to be 3.6 mole percent and the polymer contained 3.75 mole percent of galactosamine. The galactosamine content of the copolymer was evaluated by first hydrolyzing the copolymer in 4N HCl at 100°C for 4 hours in a sealed ampule. An amino acid analyzer was used to determine the sugar content.[19,20]

2.4 Synthesis of Copolymer V-nontargetable HPMA copolymer-chlorin e_6 conjugate, (Scheme C):

Synthesis of Copolymer Ib-reactive copolymer precursor, (Scheme A):

The reactive copolymer of HPMA and MA-Gly-ONp (Copolymer Ib) was synthesized as described above. Mole ratio HPMA : MA-Gly-ONp 93 : 7. Copolymer Ib contained 4.3 mole percent of reactive side chains.

Aminolysis of Copolymer Ib with an excess of ethylene diamine (Copolymer IV):

Copolymer Ib (2 g, 0.57 mmoles ONp groups) was dissolved in 8 ml DMSO. Under vigorous stirring, the copolymer solution was dropped into ethylene diamine (7.77 ml, 115 mmole). The reaction mixture was stoppered and was stirred for 1 hour at room temperature. The excess ethylene diamine was rotoevaporated. The remaining solution was precipitated into a twenty-fold excess of acetone. Copolymer IV was filtered and washed with acetone and ether, and then dessicated. The NH_2 content was determined to be 3.8 mole percent by the ninhydrin method.[18]

Binding of activated chlorin e_6: Chlorin e_6 was activated as described above. Copolymer IV (0.179 g, 0.05 mmoles NH_2 groups) was dissolved in 1.8 ml DMF and added to the activated chlorin e_6 mixture. The reaction proceeded for 1 hour at -15°C and 4 additional hours at room temperature. Excess DMF was evaporated and Copolymer V was precipitated into a twenty-fold excess of acetone. Unreacted chlorin e_6 was separated from the bound chlorin e_6 on an LH-20 column (2x40 cm) in methanol. The polymer fraction was collected and evaporated to dryness. The residue was dissolved in distilled water, frozen, and lyophilized. The mole percentage of bound chlorin e_6 was determined by UV spectra (λ_{max}=662 nm; ε_{DMF}=53,000 l/mole·cm) to be 3.6 mole percent.

2.5 Synthesis of Copolymer VI-targetable HPMA copolymer-galactosamine conjugate control, (Scheme D):

Copolymer Ia (0.05 g, 0.03 mmoles ONp groups) was dissolved in 0.375 ml DMSO. Galactosamine hydrochloride (3.54 mg, 0.016 mmole) was added, with subsequent addition of triethylamine (2.29 µl, 0.016 mmole). The polymeranalogous reaction proceeded overnight at room temperature. 1-Amino-2-propanol (2.03 µl, 0.026 mmole) was added. The reaction proceeded for 15 minutes at room temperature. The copolymer product was precipitated into a twenty-fold excess of acetone, filtered, washed with acetone and ether, and dessicated. The content of galactosamine in the copolymer was evaluated by first hydrolyzing the copolymer in 4N HCl at 100°C for 4 hours in a sealed ampule. An amino acid analyzer was used to determine the sugar content (3.80 mole percent).[19,20]

3. *IN VITRO* PHOTOLYSIS

The human PLC/PRF/5 hepatoma cell line was a kind gift of Dr. L. Stancek, Institute of Preventive Medicine, Bratislava, Czechoslovakia. PLC cells were grown in complete minimum essential medium (MEM) without protein in Roux flasks in a 5% CO_2, 37°C incubator. Cell viability was checked under a microscope. Ninety six well culture plates were seeded with 10^5 cells/well in 100 µl of MEM containing penicillin and streptomycin. PLC cultures used two days after innoculation gave the best results. It seems that this is sufficient time to permit regeneration of cell surface markers removed by trypsinization in the transfer of cells from Roux flasks to culture plates. 100 µl of samples dissolved in MEM [or dissolved in DMSO and diluted with MEM for free chlorin (final DMSO concentration: 0.01-5.0% v/v)] were added to each well and the plates were incubated for 1 hour (5% CO_2, 37°C or 4°C). After the incubation period, the plates were centrifuged for 5 minutes at 1200 rpm at 15°C, and the supernatant was removed. Cells were washed two times with cold PBS. Next, 100 µl of complete MEM with 10% (bovine calf serum) BCS were added to each well. The plates were irradiated in a CO_2 environment at 37°C for 7.5 or 24 hours, 25.5 cm from an approximately 0.77 mW/cm^2 light source. An Ennmat slide projector functioned as the light source equipped with a water layer filter between the light source and the cells to prevent a temperature increase, and a red filter to provide light at a maximum of 660 nm. After irradiation, the plates were incubated for 18 hours (5% CO_2, 37°C) to be certain that any photodynamic damage to the cells was irreversible. Simultaneously, control plates were kept in the dark at 37°C in a CO_2 environment.

4. Evaluation of Cell Viability

The MTT colorimetric assay was used to determine cell viability.[21] This method is based on MTT reduction by cell dehydrogenases producing a blue formazan product. It tests only living cells because the tetrazolium ring is cleaved only by active mitochondria. After the 18 hour incubation period, 20 µl of MTT (5 mg/ml PBS), (3-(4,5-dimethylthiazol-2-yl)-2,5-diphenyl tetrazolium bromide (Sigma), were added to each well. After 4 hours of incubation (5% CO_2, 37°C), 100 µl of 10% SDS in 0.01N HCl were added to each well to dissolve the blue crystals. Plates were incubated (5% CO_2, 37°C) overnight after which the absorbance at 570 nm was measured on a multiwell scanning spectrophotometer (ELISA reader). In this way, the relative number of living cells was determined.

5. RESULTS

An HPMA copolymer-galactosamine-chlorin e_6 conjugate (Copolymer III) was synthesized containing approximately 3.6 mole percent of chlorin e_6 and 3.75 mole percent of galactosamine. The UV spectra of the bound chlorin e_6 remained virtually unchanged compared to that of the free chlorin e_6 (fig.1). Human PLC cells were incubated for 1 hour (5% CO_2, 37°C or 4°C) and irradiated with 660 nm light for 7.5 or 24 hour time periods.

The results of four photodynamic experiments performed can be found in Figures 2-5. On the vertical axis of the graphs, the absorbance read at 570 nm is indicated, which is proportional to the relative percentage of live cells, for various samples. The samples are referenced by their chlorin e_6 concentrations (µg/ml) in the culture plate wells. Both irradiated and nonirradiated (control) results are displayed. All four of the experiments represented are, in fact, structure tests. In the experiments represented by Figures 2, 4 and 5 cells were incubated at 37°C. In the experiment with its results displayed in Figure 3, cells were incubated at 4°C for 1 hour. All experiments except that represented by Figure 2, in which samples were irradiated 24 hours, were irradiated for 7.5 hours. The cells used for experiments with results shown in figures 4 and 5 used cell cultures two days postinnoculation, while experiments represented by Figures 2 and 3 used 1 and 3 day cell cultures, respectively. In Figures 2 and 3, free chlorin e_6, nontargetable Copolymer V, and targetable conjugate (Copolymer III) are compared. As shown, free chlorin e_6 at the two highest concentrations used (64 and 13 µg/ml) were toxic, even in the dark. Targetable and nontargetable chlorin e_6 containing copolymers were toxic when exposed to light and nontoxic when kept in the dark. The targetable conjugate (Copolymer III) appears to be more biologically active compared with the nontargetable Copolymer V for the two highest concentrations of chlorin e_6 used, as pictured in Figure 3.

In Figure 4, targetable (Copolymer III) and nontargetable (Copolymer V) conjugates are compared, again with the same results as in Figures 2 and 3. In addition, the nontargetable conjugate (Copolymer V) plus free N-acetyl galactosamine (to mimic bound galactosamine) was compared with the other two samples. There is virtually no difference between the results obtained for this mixed sample and that of the nontargetable copolymer (Copolymer V).

As in the other experiments, Figure 5 compares the effect of free chlorin e_6 , nontargetable (Copolymer V) and targetable (Copolymer III) conjugates, and in addition, a drug-free galactosamine copolymer control (Copolymer VI) plus free chlorin e_6. The galactosamine content of the drug-free polymer was approximately equivalent to that of the two concentrations of conjugate bearing the same amount of chlorin e_6 as the amount of free chlorin e_6 added (1.3 and 0.13 μg/ml). The results of this experiment show nearly the same effect as that of chlorin e_6 alone at the concentrations used. The presence of the copolymer did not seem to alter chlorin e_6 activity.

The appropriate control experiments (not shown) were performed: samples of DMSO in equivalent amounts used for chlorin e_6 dissolution, and a polymer containing approximately the same content of galactosamine as bound to the conjugate (Copolymer VI). DMSO and the drug-free galactosamine containing copolymer showed no effect on cell viability at the concentrations tested.

6. DISCUSSION

As has been shown previously, *in vitro*, galactosamine targeted HPMA copolymers are internalized by cells with receptors that have affinity for galactosamine.[10] This has also been demonstrated *in vivo* by injecting rats intravenously with HPMA copolymers bearing galactosamine residues, and measuring the uptake of copolymer in the liver. The copolymer was found associated with the hepatocytes.[10] The mechanism is probably via receptor mediated pinocytosis. Duncan et al.[10] have also shown that there is accumulation of the HPMA copolymers with galactosamine terminated side chains in the secondary lysosomes of hepatocytes with time. By incubating Hep G2 cells (human hepatoma cell line expressing approximately 225,000 asialoglycoprotein receptors per cell) at 4°C for 1 hour with ^{125}I-asialoorosomucoid (ASOR), Schwartz, et al.[22] found that there was binding to the surface receptors with minimal degredation products (receptor or ligand) in the cell lysosome. After the 4°C incubation period, there was internalization of receptor-ligand complex followed by transport to the cell lysosome at 37°C. Materials that enter the cell lysosome come in contact with various acids (pH 4 to 5) as well as lysosomal digestive enzymes. This is an extremely harsh environment and can decompose many natural macromolecules, including components of the cell itself.[23] In our case, after incubating PLC cells with targetable (Copolymer III) and nontargetable (Copolymer V) conjugate at both 4°C and 37°C, photolysis at 37°C caused cell destruction. Since irradiation at 37°C was for a comparatively much longer time period (7.5 hours) than the 1 hour incubation at 4°C (Figure 3), it seems that the incubation temperature had little to do with the ultimate effects of photolysis. (Compare Figure 3 with Figures 4 and 5 in which other physical parameters are equivalent). It is likely that the targetable conjugate (Copolymer III) entered the cell interior by receptor mediated pinocytosis followed by entry into the lysosomal compartment independent of incubation temperature. This is probably true because binding of targeted conjugate to the cell surface can take place at 4°C. Over the long irradiation period at 37°C the conjugate should have sufficient time to internalize. Upon photolysis, a combined mechanism of cell destruction is possible: the photodynamic activity of the chlorin e_6 possibly lyses the cell lysosome thereby releasing lysosomal enzymes, also leading to cell death.[23] Although the difference in incubation temperature showed no difference on the effect of photolysis of the chlorin e_6 copolymer conjugates on PLC cells, mechanistic differences in cell entry of these substances would be likely. These effects should be more apparent if both incubation and irradiation procedures were performed at 4°C. In this way, surface effects vs. effects in the cell interior due to photolysis could be studied. Questions of this type (mechanism of cell destruction) are under study. It must be stressed that the experiments presented in this paper are preliminary. The goal was only to compare the effects of targetable vs. nontargetable copolymer chlorin e_6 conjugates upon photolysis on PLC cells *in vitro*.

All experiments demonstrated an increasing degree of cell kill with increasing chlorin e_6 concentration whether the chlorin e_6 was free or in a bound state. In terms of cytotoxicity, it was found that it was possible to expose PLC cells in the dark to a higher concentration of chlorin e_6 when it was bound to a copolymer than the free drug. This difference could be a result of two factors. For one, small molecules enter the cell cytosol by diffusion through the plasma membrane. This process is faster than either fluid phase pinocytosis (likely mechanism for Copolymer V) or

receptor mediated pinocytosis (likely mechanism for Copolymer III), which results in a higher concentration of chlorin e_6 inside the cell in a shorter time period. The mere presence of a high level of chlorin e_6 inside the cell could be toxic to the cell. Another possibility is through hydrophobic effects. Chlorin e_6 is an extremely hydrophobic molecule and due to surface effects on the cell membrane may prevent the cell from carrying on its normal metabolic functions. Binding the hydrophobic drug to the hydrophilic copolymer may in some way mask the hydrophobic effects of the chlorin e_6.

It appears in Figure 2 that the Copolymer V is more effective than in the other figures. This is most likely because of the 24 hour irradiation period (6.7E4 $mW \cdot s/cm^2$) as compared with the 7.5 hour intervals (2.1E4 $mW \cdot s/cm^2$). Fluid phase pinocytosis is a slow process and the longer time would aid the entry of the nontargetable conjugate (Copolymer V) into the cell. Also, it is already proven that an increase in the time of irradiation leads to an increase in cell kill.[14]

The results presented herein are promising for future experimentation. The fact that the galactosamine containing conjugate (Copolymer III) showed more biological activity than the nontargetable complex (Copolymer V) is encouraging. PLC cells have a relatively low content of asialoglycoprotein receptors compared with other cell lines, such as the Hep G2 hepatoma cell line. In the future, it would be worthwhile to synthesize conjugates as described in this paper and study their photodynamic effects on cells expressing a higher quantity of asialoglycoprotein receptors than do PLC cells. Competition studies between N-acetyl galactosamine and polymer conjugates bearing the galactosamine targeting moiety would be valuable in providing information on the receptor mediated function of endocytosis. *In vivo* targeting is possible, as the biocompatibility of this kind of copolymer has been proven, yet the photodynamic effects of these types of conjugates will not be ascertained unless a suitable light source is available.

In this study, the targetability of an HPMA copolymer-chlorin e_6 conjugate was proven. Therefore, it would be of interest to synthesize conjugates of the type described above (Copolymer III) with targeting moieties other than galactosamine to target porphyrins to other cell types. We have shown in the past that HPMA copolymer-anti Thy 1.2 antibody-daunomycin conjugates can be targeted to T lymphocytes.[24] Conjugates of HPMA copolymer-anti Thy 1.2 antibody-chlorin e_6 have already been synthesized, and their biological evaluation is in progress.

7. ACKNOWLEDGMENTS

We would like to thank Drs. T. Hasan (Harvard Medical School), E. Brynda and P. Kopečková (Institute of Macromolecular Chemistry, Prague, Czechoslovakia) for helpful discussions, Mr. H. Yen (University of Utah, Salt Lake City, Utah) for general laboratory assistance, and to Mrs. H. Semorádová (Institute of Microbiology, Prague, Czechoslovakia) for assistance with the biological experimentation.

REFERENCES

1. J.D. Spikes, "Photosensitization," *in* The Science of Photobiology, K.C. Smith (Ed.) Plenum Press, NY, NY, 1977, 87-112.

2. R.C. Straight and J.D. Spikes, "Photosensitized oxidation of biomolecules," *in* Singlet O_2, A.A. Frimer (Ed.) CRC Press, Boca Raton, FL, 1985, IV, 91-143.

3. T. Dougherty, "Photoradiation therapy for cutaneous and subcutaneous malignancies," J. Invest. Derm. 77, 122-124 (1981).

4. J. Kopeček, "Synthesis of tailor-made soluble polymeric drug carriers" *in* Recent Advances in Drug Delivery Systems, J.M. Anderson and S.W. Kim (Eds.) Plenum Press, NY, NY, 1984, 41-62.

5. R. Duncan, and J. Kopeček, "Soluble synthetic polymers as potential drug carriers," Adv. Polym. Sci. 57, 51-101 (1984).

6. B. Říhová, J. Kopeček, K. Ulbrich, M. Pospíšil and P. Mančal, "Effect of the chemical structure of N-(2-hydroxypropyl)methacrylamide copolymers on their ability to induce antibody formation in inbred strains of mice," Biomaterials 5, 143-148 (1984)

7. J. Kopeček, "Controlled biodegradability of polymers-a key to drug delivery systems," Biomaterials 5, 19-27 (1984).

8. L. Seymour, R. Duncan, J. Strohalm and J. Kopeček, "Effect of molecular weight (M_w) of N-(2-hydroxypropyl)methacrylamide copolymers on body distribution and rate of excretion after subcutaneous, intraperitoneal, and intravenous administration to rats," J. Biomed. Mater. Res. 21, 1341-1358 (1987).

9. R. Duncan, J. Kopeček, P. Rejmanová, and J.B. Lloyd, "Targeting of N-(2-hydroxypropyl)methacrylamide copolymers to liver by incorporation of galactose residues," Biochim. Biophys. Acta 755, 518-521 (1983).

10. R. Duncan, L. Seymour, L. Scarlett, J.B. Lloyd, P. Rejmanová and J. Kopeček, "Fate of N-(2-hydroxypropyl)methacrylamide copolymers with pendent galactosamine residues after intravenous administration to rats," Biochim. Biophys. Acta 880, 62-71 (1986).

11. R. Duncan, H.C. Cable, J.B. Lloyd, P. Rejmanová and J. Kopeček, "Polymers containing enzymatically degradable bonds. 7. Design of oligopeptide side chains in poly[N-(2-hydroxypropyl)methacrylamide] copolymers to promote efficient degradation by lysosomal enzymes," Makromol. Chem. 184, 1997-2008 (1983).

12. G. Ashwell and J. Hartford, "Carbohydrate-specific receptors of the liver," Ann. Rev. Biochem. 51, 531-554 (1982).

13. W. Dunn, A. Hubbard, and N. Aronson Jr., "Low temperature selectivity inhibits fusion between pinocytic vesicles and lysosomes during heterophagy of ^{125}I-asialofetuin by the perfused rat liver," J. Biol. Chem. 255, 5971-5978 (1980).

14. A. Oseroff, D. Ohuoha, T. Hasan, J. Bommer, and M. Yarmush, "Antibody targeted photolysis: Selective photodestruction of human T-cell leukemia cells using monoclonal antibody-chlorin e_6 conjugates," Proc. Nat'l. Acad. Sci. USA, 83, 8744-8748 (1986).

15. W. Nourse, R. Parkhurst, W. Skinner and R. Jordan, "Photodynamic toxicity of porphyrins and chlorins for a human tumor cell line: Combined light and concentration dose responses for the retained fraction," Biochim. Biophys. Res. Commun. 151, 506-511 (1988).

16. J. Strohalm and J. Kopeček, "Poly[N-(2-hydroxypropyl)methacrylamide]. 4. Radical precipitation polymerization. Angew. Makromol. Chem. 70, 109-118 (1978).

17. P. Rejmanová, J. Labský and J. Kopeček, "Aminolysis of monomeric and polymeric 4-nitrophenyl esters of N-methacryloylamino acids," Makromol. Chem. 178, 2159-2168 (1977).

18. S. Moore and W. Stein, "Photometric ninhydrin method for use in the chromatography of amino acids," J. Biol. Chem. 176, 367-377 (1948).

19. T.H. Plummer Jr., "A simplified method for determination of amino sugars in glycoproteins," Anal. Biochem. 73, 532-536 (1976).

20. P.W. Cheng and T.F. Boat, "An improved method for the determination of galactosaminitol, glucosaminitol, glucosamine and galactosamine on an amino acid analyzer," Anal. Biochem. 85, 276-282 (1978).

21. T. Mosmann, "Rapid colorimetric assay for cellular growth and survival: Application to proliferation and cytotoxicity assays," J. Immunol. 65, 55-63 (1983).

22. A. Schwartz, S. Gridovich and H. Lodish, "Kinetics of internalization and recycling of the asialoglycoprotein receptor in a human hepatoma cell line," J.Biol. Chem. 257, 4230-4237 (1982).

23. C. De Duve, T. Barsy, B. Poole, A. Trouet, P. Tulkens and F. Van Hoof, "Lysosomotropic agents," Biochem. Pharmacol. 23, 2495-2531 (1974).

24. B. Říhová, P. Kopečková, J. Strohalm, P. Rossman, V. Větvička and J. Kopeček, "Antibody directed affinity therapy applied to the immune system: In vivo effectiveness and limited toxicity of daunomycin conjugates to HPMA copolymers and targeting antibody," Clin. Immunol. Immunopathol. 46, 100-114 (1988).

SCHEME A : Synthesis of the reactive copolymer precursors (Copolymer Ia, Ib).

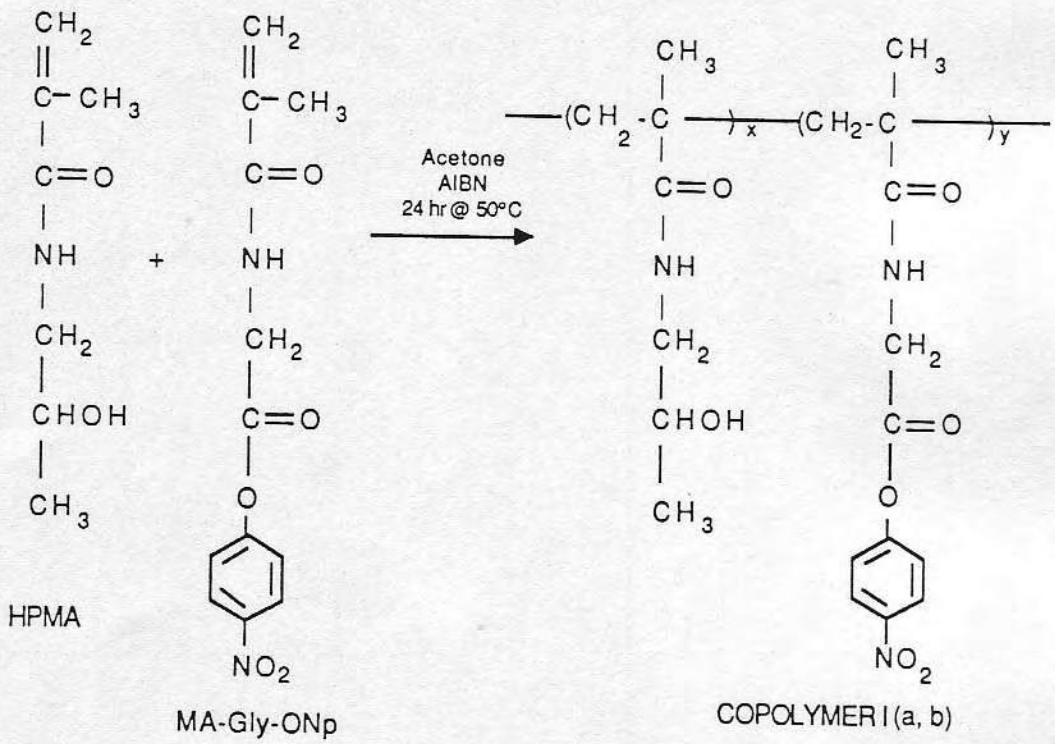

SCHEME B: Synthesis of the targetable HPMA copolymer-galactosamine-chlorin e_6 conjugate (Copolymer III).

Consecutive aminolysis of Copolymer Ia with galactosamine and ethylene diamine:

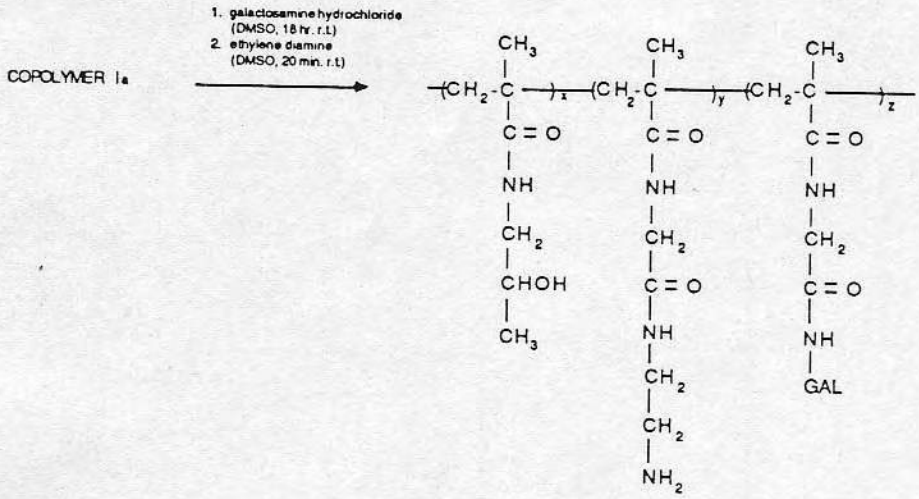

COPOLYMER II

Binding of chlorin e_6 to Copolymer II:

Chlorin e_6 activation:

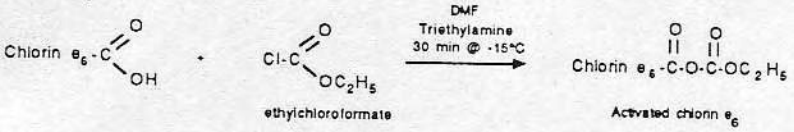

Binding of chlorin e_6 to Copolymer II:

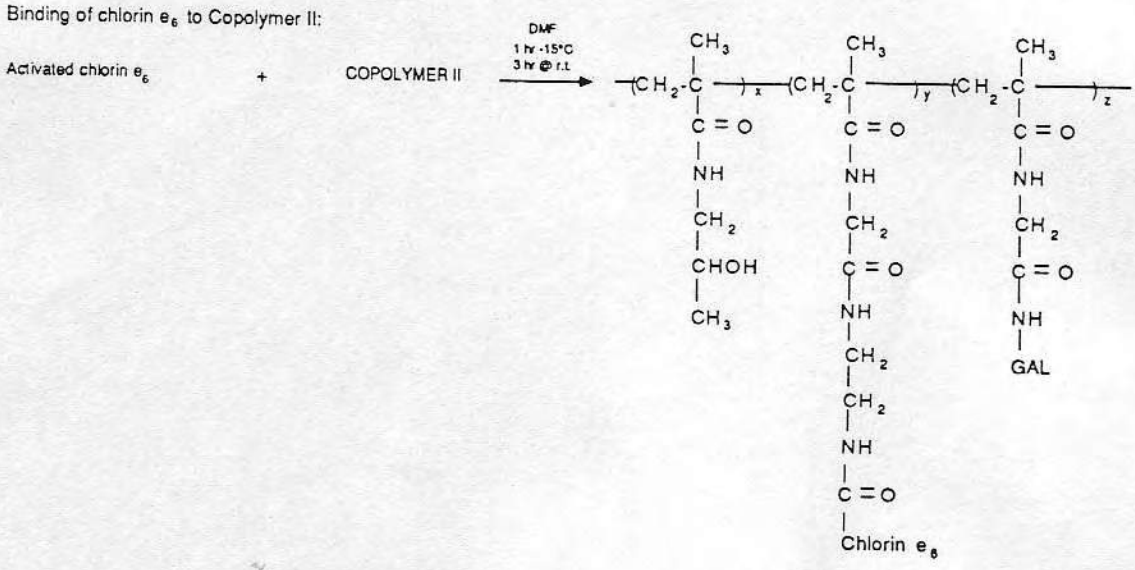

COPOLYMER III

SCHEME C: Synthesis of the nontargetable HPMA copolymer-chlorin e_6 conjugate (Copolymer V).

Aminolysis of Copolymer Ib with an excess of ethylene diamine:

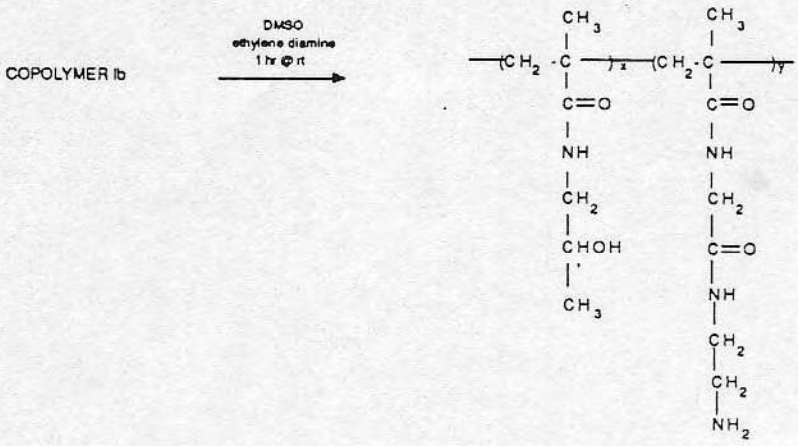

Binding of chlorin$_6$ to Copolymer IV

Chlorin e_6 activation:

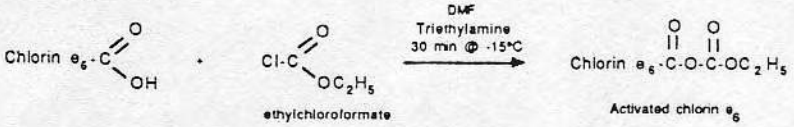

Binding of activated chlorin e_6 to Copolymer IV:

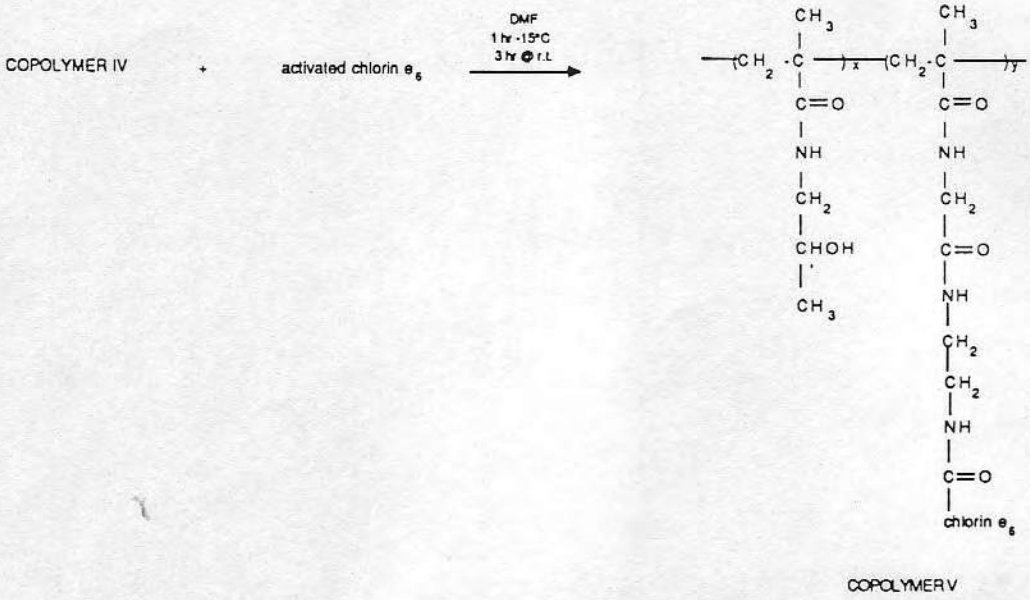

SCHEME D: Synthesis of the targetable HPMA copolymer-galactosamine conjugate control (Copolymer VI).

Consecutive aminolysis of Copolymer Ia with galactosamine and 1-amino-2-propanol:

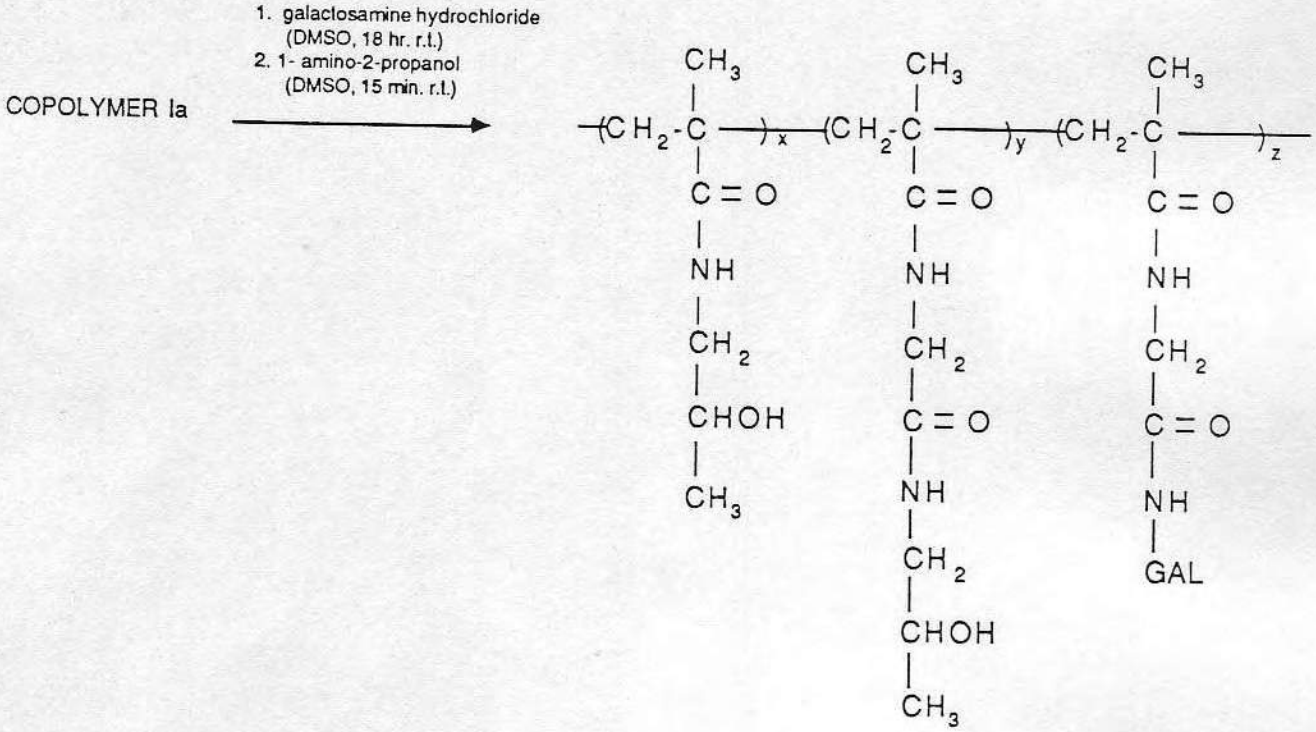

COPOLYMER VI

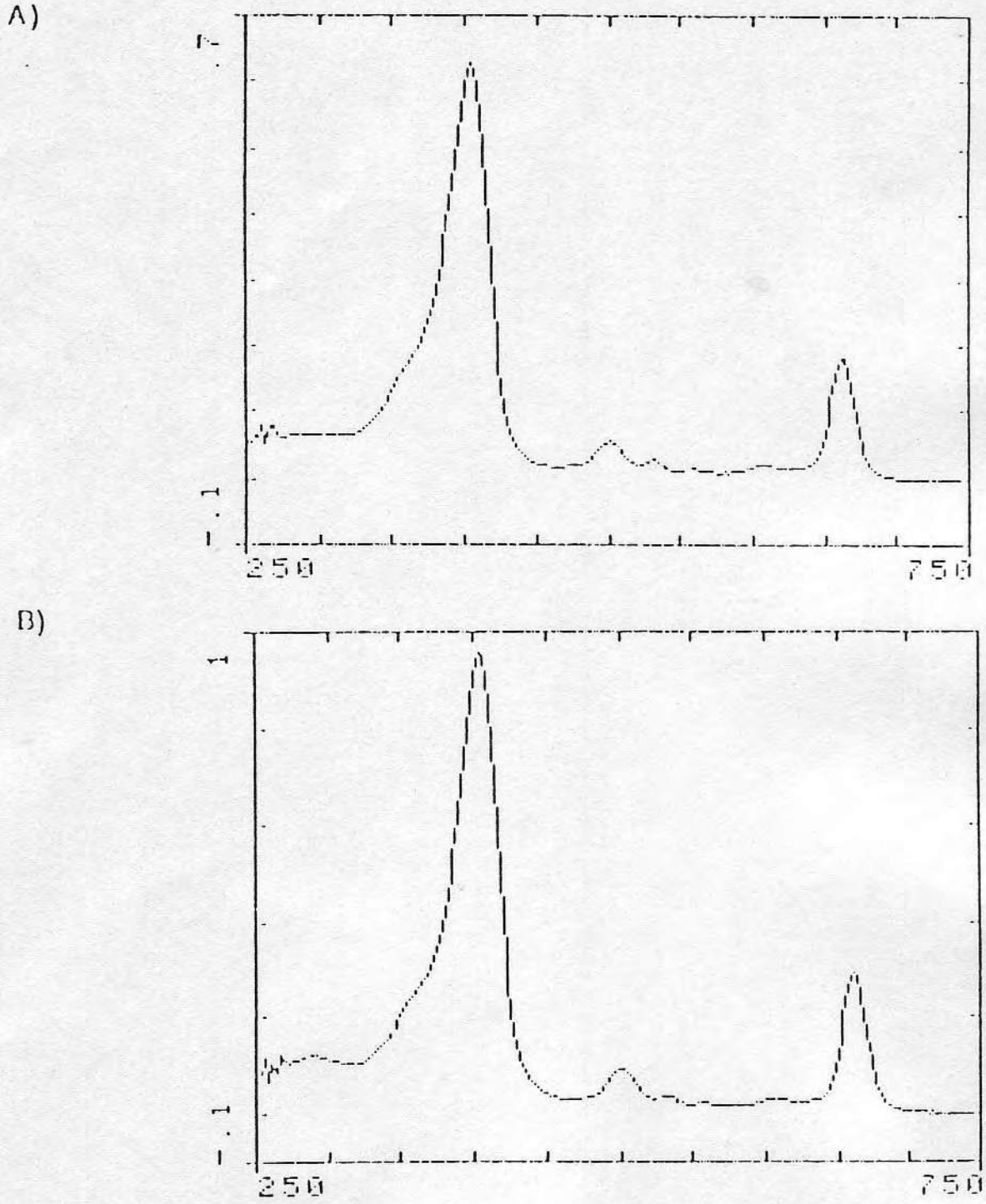

Figure 1. UV Spectra in DMF A) Chlorin e_6 B) Copolymer III (HPMA copolymer-galactosamine-chlorin e_6 conjugate).

Figures 2-5. Surviving PLC cells (represented by A_{570} which is proportional to the number of live cells, as determined by the MTT method). The data represent mean ± standard deviation (error bars) of 3-6 samples. Samples are free chlorin e_6 (chlorin or chlor), HPMA copolymer-galactosamine- chlorin e_6 conjugate (Copoly III), nontargetable HPMA copolymer conjugate (Copoly V), HPMA-galactosamine conjugate (Copolymer VI), and free N-acetyl galactosamine (gal). The numbers represent the concentration of chlorin e_6 (μg/ml) in culture plate wells.

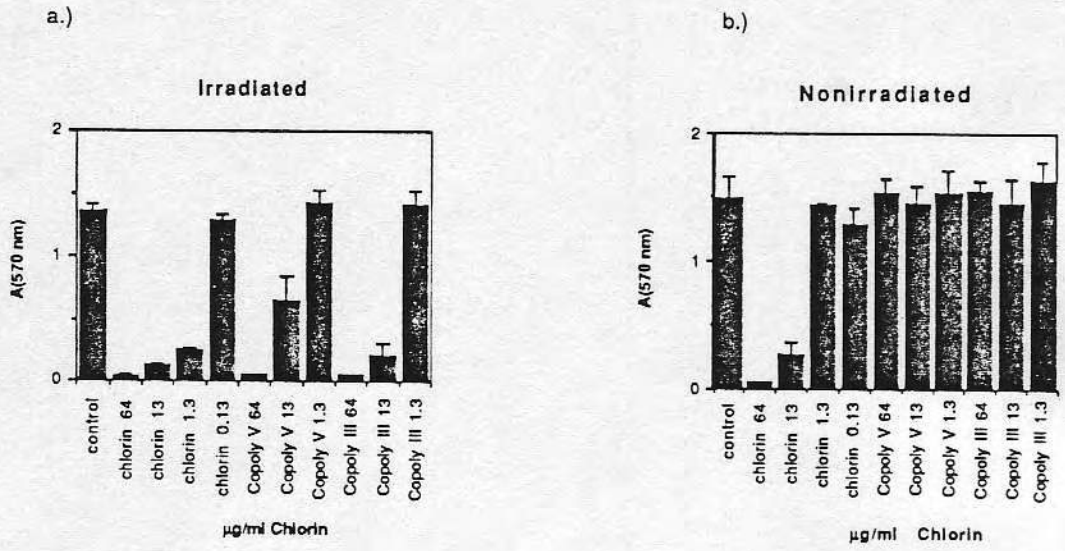

Figure 2. 1 hour incubation 37°C, 1 day culture, a.) 24 hour irradiation 37°C, b.) nonirradiated.

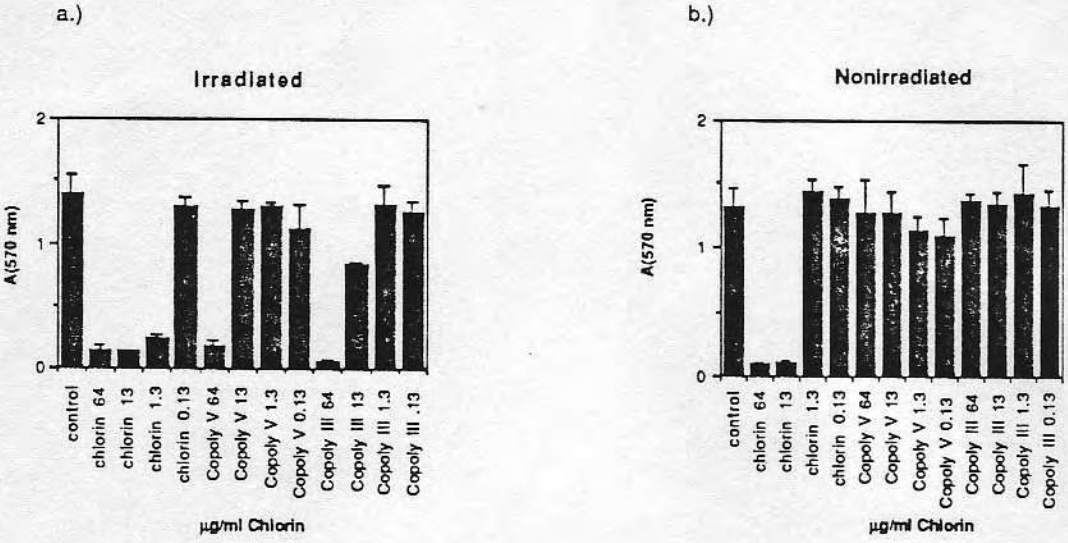

Figure 3. 1 hour incubation 4°C, 3 day culture, a.) 7.5 hour irradiation 37°C, b.) nonirradiated.

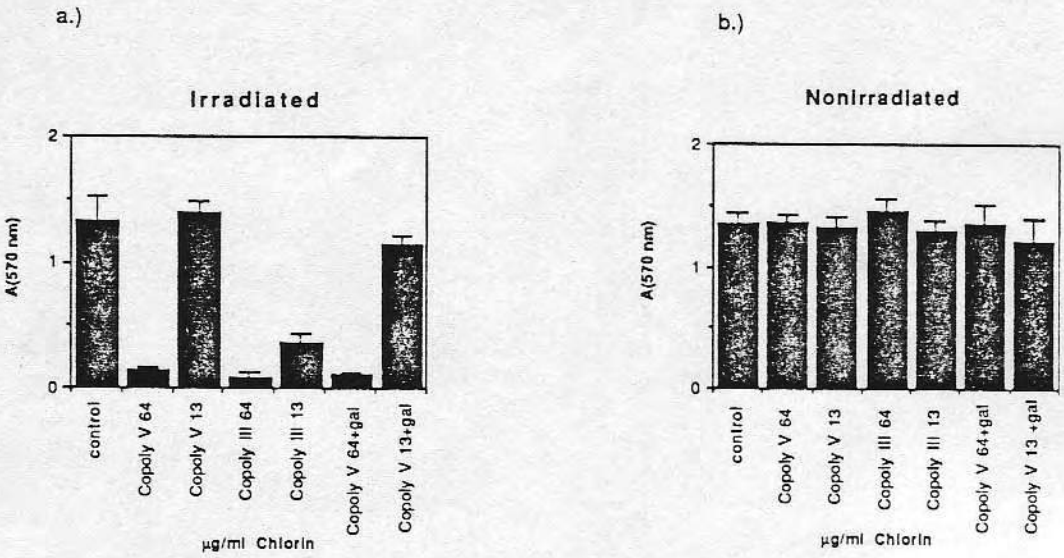

Figure 4. 1 hour incubation 37°C, 2 day culture, a.) 7.5 hour irradiation 37°C, b.) nonirradiated.

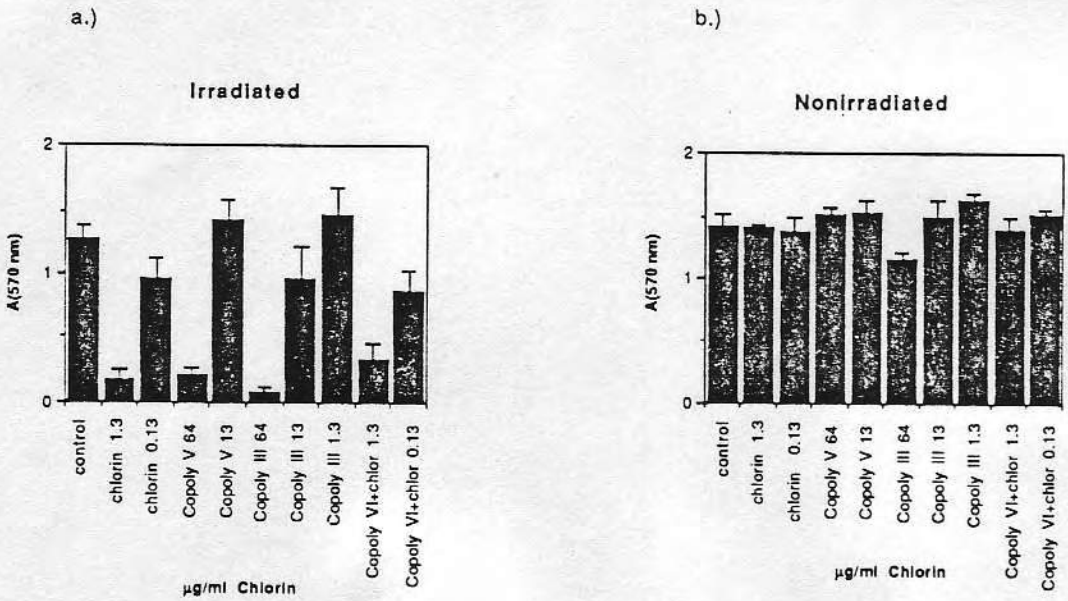

Figure 5. 1 hour incubation 37°C, 2 day culture, a.) 7.5 hour irradiation 37°C, b.) nonirradiated.

PROCEEDINGS

SPIE—The International Society for Optical Engineering

Advances in Photochemotherapy

Tayyaba Hasan
Chair/Editor

6–7 September 1988
Boston, Massachusetts

Sponsored by
SPIE—The International Society for Optical Engineering

Cooperating Organization
Center for Photochemical Sciences/Bowling Green State University

SPIE
P
PROCEEDINGS SERIES

Volume 997